Investigations on the role of the *IGF2* mRNA-binding protein p62 and the long non-coding RNA *H19* in cell culture and *in vivo* models of hepatocellular carcinoma

Dissertation

zur Erlangung des Grades

des Doktors der Naturwissenschaften

der Naturwissenschaftlich-Technischen Fakultät

der Universität des Saarlandes

von

Christina Stefanie Hubig

Saarbrücken

2018

Tag des Kolloquiums:	10.12.2018
Dekan:	Prof. Dr. Guido Kickelbick
Berichterstatter:	Prof. Dr. Alexandra K. Kiemer
	Prof. Dr. Claus-Michael Lehr
Vorsitz:	Prof. Dr. Marc Schneider
Akad. Mitarbeiter:	Dr. Sascha Tierling

Contents

Für meine Eltern

Evelyn und Jürgen Schultheiß

Abstract

Hepatocellular carcinoma (HCC) is the second most common cause of cancer-related death worldwide mainly due to late diagnosis and its highly resistant nature resulting in limited therapeutic options. HCC development and progression is characterized by a dysregulation of RNA-binding proteins (RBPs) and long non-coding RNAs (lncRNAs).

In a mouse model of diethylnitrosamine-induced hepatocarcinogenesis, the lncRNA *H19* showed tumor-suppressive and anti-proliferative actions, which were confirmed in human hepatoma cell lines. Since HCC evolves from an inflammatory environment, the anti-inflammatory action of *H19* found in our mouse model underlines its tumor-preventive action.

Chemoresistance is a major problem for the efficacy of systemic HCC therapy. *H19* was downregulated during chemoresistance due to altered methylation at the *H19* promoter and sensitized hepatoma cells towards chemotherapeutic drugs.

The expression of *H19* was induced by the transgenic expression of the RBP p62, which promoted genomic instability and thereby a more aggressive phenotype of HCC through a DLK1-RAC1-ROS axis. A *H19* knockout only slightly increased the tumor-promoting effect of p62.

Taken together, *H19* antagonized hepatocarcinogenesis by preventing three important hallmarks of cancer: proliferation, inflammation, and chemoresistance. The tumor-suppressive and chemosensitizing functions of *H19* could provide new opportunities to overcome chemoresistance and improve the options of HCC therapy.

Zusammenfassung

Das Hepatozelluläre Karzinom (HCC) ist aufgrund begrenzter Therapieoptionen, die hauptsächlich aus späten Diagnosen und ausgeprägter Chemoresistenz resultieren, weltweit die zweithäufigste krebsbedingte Todesursache. Eine Dysregulierung von mRNA-bindenden Proteinen (RBPs) und langen nicht-codierenden RNAs (lncRNAs) ist charakteristisch für die Entstehung und Progression des HCCs.

Im Mausmodell mit Diethylnitrosamin-induzierter Hepatokarzinogenese zeigte die lncRNA *H19* eine tumorunterdrückende und proliferationshemmende Wirkung, welche in humanen Hepatomzelllinien bestätigt werden konnte.

Da sich HCC aus einer entzündlichen Umgebung heraus entwickelt, untermauert die entzündungshemmende Wirkung von *H19* seine tumorpräventive Funktion.

H19 war aufgrund veränderter Promotor-Methylierung in der Chemoresistenz - dem Hauptproblem der systemischen HCC-Therapie - herabreguliert und erhöhte die Empfindlichkeit von Hepatomzelllinien gegenüber Chemotherapeutika.

Das RBP p62 induzierte die *H19*-Expression, förderte die genomische Instabilität über einen DLK1-RAC1-ROS-Weg und begünstigte dadurch die Entstehung eines aggressiven HCC-Phänotyps. Ein *H19*-Knockout erhöhte die tumorfördernde Wirkung von p62 nur gering.

H19 antagonisiert die Hepatokarzinogenese durch Unterdrückung von Proliferation, Entzündung und Chemoresistenz. Die tumorpräventive und chemosensibilisierende Wirkung von *H19* könnte neue Möglichkeiten zur Überwindung der Chemoresistenz und Verbesserung der HCC-Therapie eröffnen.

Introduction

1. Hepatocellular carcinoma

Cancer is the leading cause of death worldwide (World-Health-Organization, 2008). Whereas the mortality of most types of cancer is declining due to early diagnosis and highly efficient therapies, the mortality of liver cancer has still dramatically increased in men and women during the past 2 decades (Sia et al., 2017) (**Figure 1**). Regarding liver cancer patients in Germany, only 14% of male and 11% of female patients survive for more than 5 years (www.krebsdaten.de; Krebs in Deutschland für 2013/2014).

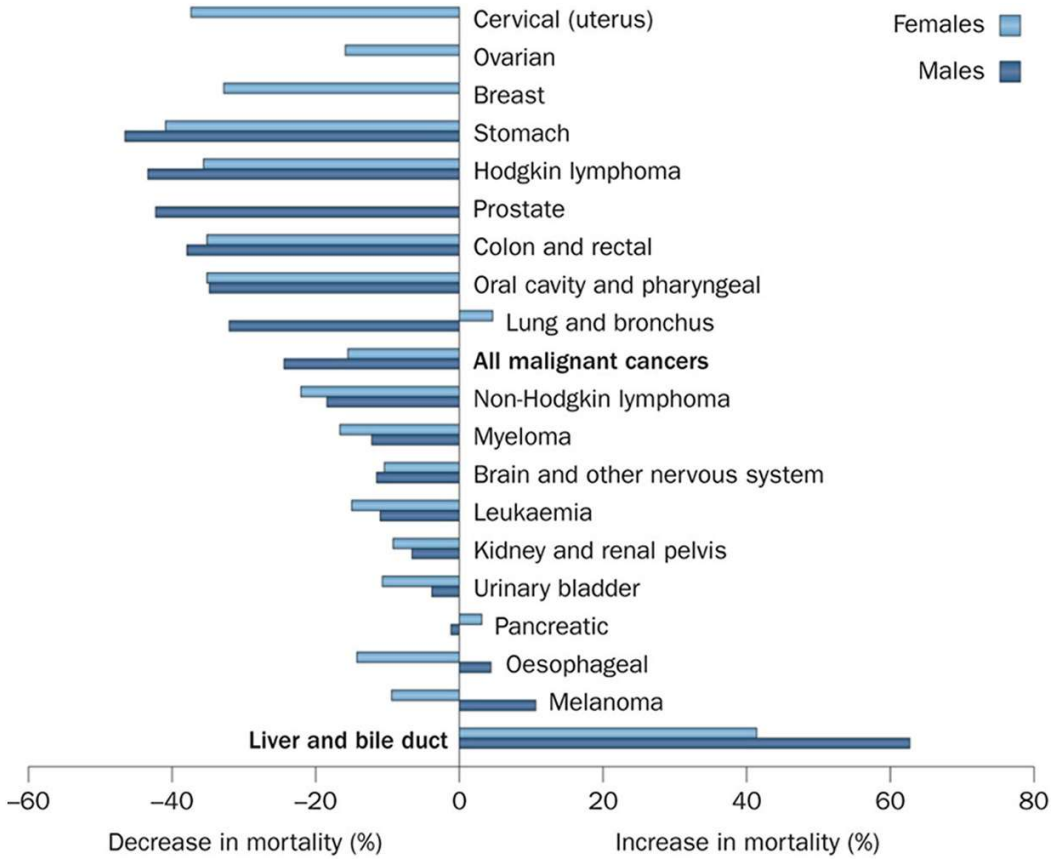

Figure 1: **Mortality trends of patients with different types of malignancies** in the United States from 1990 to 2009. From Sia et al., 2017.

With almost 800,000 new cases annually, hepatocellular carcinoma (HCC) is the predominant type of primary liver cancer (Llovet et al., 2016) and the second most common cause of cancer-related deaths worldwide (Stewart & Wild, 2014).

The cellular origin of HCC are hepatocytes, which constitute 60-80% of the liver mass (Sia et al., 2017). Due to chronic injury, hepatocytes develop genetic alterations and defective cell cycle regulation leading to promoted cellular growth and resisting cell death (El-Serag & Rudolph, 2007).

1.1 HCC: Risk factors

The risk factors for the development of HCC vary by region. In Africa and Asia, hepatitis B or hepatitis C virus infections and the consumption of aflatoxin B1-contaminated food are the main risk factors. In the Western world, chronic alcoholic fatty liver disease (AFLD) and non-alcoholic fatty liver disease (NAFLD) are the leading risk factors for HCC (El-Serag & Rudolph, 2007, Ozakyol, 2017). AFLD is triggered by heavy alcohol abuse for several years (Ozakyol, 2017) and NAFLD develops in consequence of insulin resistance, steatosis, oxidative stress, and inflammation (Petta & Craxi, 2010). Further risk factors for HCC development are cigarette consumption and the intake of oral contraceptives, which are also commonly used in Western countries (Bosch et al., 2004).

1.2 HCC: Therapy

Since 1999, HCC is classified by the Barcelona Clinic Liver Cancer (BCLC) staging system for the determination of the best treatment options (Llovet et al., 1999). Curative therapies, realized by resection of the tumor tissue or liver transplantation, are advised only in early HCC stages and realizable for only 10-30% of the patients (Lau & Lai, 2008). Palliative treatments for patients with intermediate or advanced HCC include the multikinase inhibitor sorafenib (standard first-line systemic therapy since 2008) and the anthracycline doxorubicin (used in combination with sorafenib) (EASL-Clinical-Practice-Guidelines, 2018, Raymond et al., 2012, Wörns et al., 2009). Sorafenib inhibits tumor cell proliferation and angiogenesis, and induces apoptosis by targeting serine/threonine and tyrosine kinases (Liu et al., 2006, Wilhelm et al., 2004). Doxorubicin exerts its cytotoxicity by intercalation into DNA and thereby deactivating topoisomerase II through strong binding (Cutts et al., 2005).

The highly resistant nature of HCC presents a major hindrance to the efficacy of systemic treatments. Factors mediating chemoresistance of HCC are p53 mutations, overexpression of topoisomerase IIa, and enhanced cellular efflux by drug transporters, e.g. the multi-drug resistance protein 1 (MDR1) (Hussain et al., 2007, Park et al., 1994, Watanuki et al., 2002).

Due to the rising incidence and lack of suitable therapies, the investigation of underlying mechanisms in the development and resistance of hepatocellular carcinoma is of utmost importance.

2. Long non-coding RNAs

While only 1.2% of the transcribed human genome encodes proteins (IHGS-Consortium, 2004, Ransohoff et al., 2018), the remaining part is transcribed into a group of non-coding RNAs (ncRNAs) (Djebali et al., 2012) consisting of long non-coding RNAs (lncRNAs), ribosomal RNAs (rRNAs), transfer RNAs (tRNAs), small nuclear RNAs (snRNAs), small nucleolar RNAs (snoRNAs), telomere-associated RNAs, microRNAs (miRNAs), small interfering RNAs (siRNAs), and Piwi-associated RNAs (piRNAs) (Blackburn & Collins, 2011, Czech & Hannon, 2011, Feuerhahn et al., 2010, Henras et al., 2004, Kim et al., 2009, Okamura & Lai, 2008, Peculis, 2000, Siomi et al., 2011, Xiao et al., 2002) (**Figure 2**).

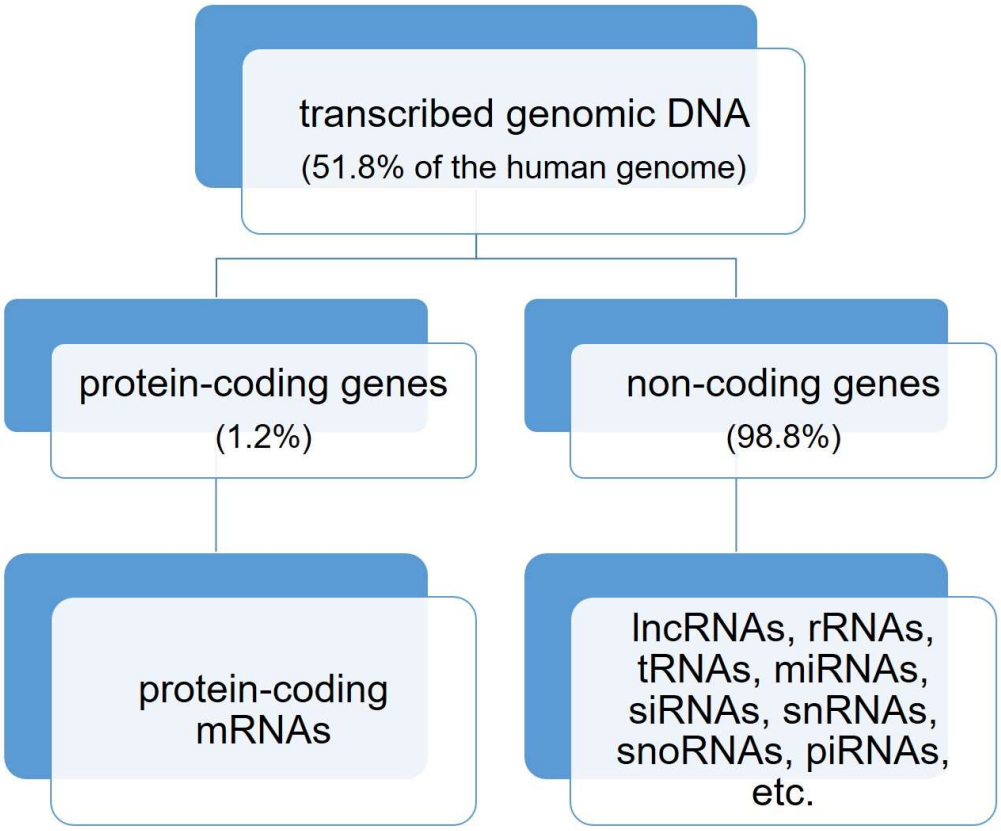

Figure 2: **The human genome consisting of translated and non-translated genes.** Percentage values were taken from Ransohoff et al., 2018.

LncRNAs are defined as autonomously transcribed RNAs longer than 200 nucleotides with minimal coding potential (Ransohoff et al., 2018) that can be found in the nucleus as well as in the cytoplasm (Batista & Chang, 2013). They are able to bind DNA, proteins, or other RNAs (such as miRNAs) (Batista & Chang, 2013, Guttman & Rinn, 2012, Rinn & Chang, 2012). Thereby, almost all biological processes are affected by lncRNAs, for example, epigenetic silencing of gene expression, mRNA splicing, mRNA decay, and translation (Wapinski & Chang, 2011). By regulating e.g. apoptosis, proliferation, and angiogenesis, lncRNAs are important players in cancer development (Schmitt & Chang, 2016, Tsai et al., 2011).

2.1 The lncRNA *H19*

One example of cancer-associated lncRNAs is *H19*. The *H19* gene, located on chromosome 11p15.5 in the human system and on chromosome 7 in mice, is maternally imprinted (Rachmilewitz et al., 1992). The enhancer elements - binding and thereby activating the *H19* promoter - are also used by the *insulin-like growth factor 2 (IGF2)* gene. *IGF2* is located around 80 kb adjacent to *H19* and reciprocally expressed (Rachmilewitz et al., 1992). The *H19* gene contains 5 exons, seperated by 4 introns, and is transcribed by the RNA polymerase II. The transcript is spliced, polyadenylated, capped, and exported into the cytosol (Gabory et al., 2010). Although the expression of *H19* is dramatically repressed after birth except for skeletal muscles and the heart muscle (Gabory et al., 2010), a reactivation of the *H19* gene in different tumor types, including HCC, has been reported (Matouk et al., 2013, Raveh et al., 2015, Zhou et al., 2017).

The known functions of *H19* are, in part, mediated by the binding of proteins. Thereby, it interacts with transcription factors (Luo et al., 2013, Monnier et al., 2014), tumor-suppressors, e.g. p53 (Yang et al., 2012), and mRNA-binding proteins, such as IGF2 mRNA-binding protein 1 (IGF2BP1) and the K homology-type splicing regulatory protein (KSRP) (Giovarelli et al., 2014). *H19* can also act through microRNA-binding: the tumor-suppressive miRNAs *miR-200* and *let-7* are well described *H19* targets (Zhou et al., 2017). The role of *H19* in tumor progression is controversially discussed. Although most hallmarks of cancer - including proliferation, apoptosis, inflammation, metastasis, and

invasion (Hanahan & Weinberg, 2011) - have been linked to *H19*, it is not clear whether it acts as an oncogene or as a tumor-suppressor (Chen et al., 2016, Li et al., 2016, Ohtsuka et al., 2016, Raveh et al., 2015, Yang et al., 2012, Yoshimizu et al., 2008, Yu et al., 2013).

H19 is a precursor for the micro RNA *miR-675*, located in *H19*`s first exon (Cai & Cullen, 2007). Numerous targets of *miR-675* have been found, some of them with oncogenic and others with tumor-suppressive function. Examples for *miR-675* targets are the tumor-suppressor *retinoblastoma* (*Rb*) (Tsang et al., 2010), the anti-apoptotic *Fas-associated via death domain (FADD)* (Yan et al., 2017), and the proliferation- and migration-associated receptors *insulin-like growth factor 1 receptor (IGF1R)* (Keniry et al., 2012) and *vitamin D receptor (VDR)* (Chen et al., 2017). In addition, *miR-675* has been associated with epithelial to mesenchymal transition (EMT), and with its reverse process (Djebali et al.), which are important steps in invasion and metastasis (Raveh et al., 2015). Vennin et al. reported an enhanced tumorigenesis and metastasis of breast cancer cells due to *miR-675* by targeting the *ubiquitin ligase E3 family (c-Cbl and Cbl-b)* (Vennin et al., 2015). In contrast, *miR-675* represses metastasis of prostate cancer by binding the mRNA of transforming growth factor beta induced protein (TGFBI*)* (Zhu et al., 2014). Hence, the role of *miR-675* in cancer progression is also conflicting.

Though the *H19* RNA was classified as non-coding (Brannan et al., 1990), a 26 kDa protein derived from *H19* was described in 2012 (Gascoigne et al., 2012). The biological action of this protein has not been analyzed so far. Since Zeisel and Baumert predicted a biological function of such peptides derived from non-protein coding genes in HCC development (Zeisel & Baumert, 2016), functional implications of these peptides should be considered in the investigations of *H19* and its function.

3. The *insulin-like growth factor 2 (IGF2)* mRNA-binding protein p62

The human genome encodes for 1,542 mRNA-binding proteins (RBPs) (Gerstberger et al., 2014) with some of them linked to the major steps in cancer development and progression, such as proliferation, apoptosis, angiogenesis, metastasis, and inflammation (Wang et al., 2016a). RBPs post-transcriptionally regulate their target mRNAs by binding sequences mainly located in the untranslated region (Miki et al., 1994, Newman et al., 2015).

The *insulin-like growth factor 2 (IGF2)* mRNA-binding proteins (IMPs) belong to the cancer associated RBPs (Dai et al., 2017, Jeng et al., 2008). The IMP family consists of IMP-1, IMP-2, and IMP-3, which share two RNA recognition motifs and four hnRNP K homology domains.
IMPs target the 5‘-UTR of the *IGF2-leader 3* mRNA (Liao et al., 2005, Nielsen et al., 1999) and thereby affect its processing. IGF2 is an oncofetal growth factor protein, typically repressed after birth (Takeda et al., 1996) and reactivated in cancers including HCC (Lu et al., 2005), where it exerts anti-apoptotic action by binding the IGF1 receptor (Nielsen, 1992, Resnicoff et al., 1995).
Beside *IGF2*, thousands of other IMP-targets were described (Hafner et al., 2010). IMP-1 and IMP-3 protect lots of mRNAs - including oncogenes and stemness maintenance genes - from *let-7*-dependent silencing (Degrauwe et al., 2018).
IMP-1 binds and controls the transport of *actin beta* (Farina et al., 2003) and *E-cadherin* (Conway et al., 2016), which are implicated in the stabilization of cell-cell contacts and adhesions, and targets *BCL2* resulting in apoptosis protection (Conway et al., 2016). These data underline the importance of IMPs in cancer initiation and progression.

p62 (IMP2-2) - a splice variant of IMP-2 lacking exon 10 - was originally identified as an autoantigen in an HCC patient (Zhang et al., 1999). Therefore, the detection of anti-p62 autoantibodies was suggested as a biomarker in diagnostics and monitoring of cancer (Liu et al., 2013). Several studies describe an overexpression of p62 in human HCC tissues (Kessler et al., 2015, Kessler et al., 2013, Lu et al., 2001, Qian et al., 2005) and

its oncogenic potential was demonstrated in a transgenic mouse model (Kessler et al., 2015).

Since IMPs target the reciprocally imprinted lncRNA *H19* and participate its localization (Runge et al., 2000), a link between p62 and *H19* expression was hypothesized. Indeed, a liver-specific overexpression of p62 in transgenic mice caused *H19* overexpression (Tybl et al., 2011), but an interaction between p62 and *H19* affecting tumorigenesis remained unexplored so far.

4. Aim of the present work

Dysregulation of RBPs and lncRNAs are features of HCC development and progression. Uncovering their modes of action will help to improve the therapy of this highly resistant type of tumor.

The RBP p62 and *H19,* a lncRNA affected by p62, are associated with hepatocarcinogenesis. p62 is overexpressed in HCC and acts as tumor promoter but the underlying mechanism of its action is not completely clarified so far. The role of *H19* in tumor progression is controversially discussed.

The work schedule of this research project addresses questions about:

1) The tumor-promoting action of p62
2) The role of *H19* in the tumor-promoting action of p62
3) The role of *H19* in carcinogenesis and chemoresistance of HCC
4) *H19* as molecular sponge
5) The role of two proteins derived from the *H19* locus

Chapter 1

Investigations on the tumor-promoting effect of p62

Introduction

Hepatocellular carcinoma mostly evolves in an environment characterized by chronic inflammation (chronic hepatitis). In the majority of cases this hepatitis results from either virus infection or alcoholic fatty liver disease (AFLD) and non-alcoholic fatty liver disease (NAFLD) (Castello et al., 2010, Koyama & Brenner, 2017).

The mRNA-binding protein p62, identified in 1999 (Zhang et al., 1999), induces steatosis as a pre-stage of steatohepatitis (Tybl et al., 2011). The vulnerability of mice expressing the *p62* transgene to the development of steatohepatitis is increased (Simon et al., 2014a) and inflammatory processes are amplified (Kessler et al., 2014, Laggai et al., 2014, Simon et al., 2014a, Simon et al., 2014b). Furthermore, in *p62* transgenic mice genomic instability was induced and levels of thiobarbituric acid reactive substances (TBARS) - as indicators of oxidative stress - were elevated after short-term treatment with the carcinogen diethylnitrosamine (DEN) (Kessler et al., 2015). Oxidative stress is a feature of inflammation that is mediated by high levels of reactive oxygen species (ROS) (Block & Gorin, 2012). For HCC, an increase of ROS levels from early to advanced stages has been described (Lim et al., 2008). By promoting not only inflammation but also genomic instability, immortality, angiogenesis, and metastasis (Block & Gorin, 2012, Hanahan & Weinberg, 2011), ROS play an important role in carcinogenesis and tumor progression.

The generation of ROS can be induced by the small GTPase RAC1 (Fürst et al., 2005), the expression of which was also increased in livers of *p62* transgenic mice (Kessler et al., 2015). Furthermore, the elevated *Rac1* expression strongly correlates with the expression of the hepatic stem cell marker *delta-like 1 homolog* (*Dlk1)* in the *p62* transgenic mouse model as well as in human HCC (Kessler et al., 2015).

In this study, the relation between DLK1, RAC1, and ROS production was analyzed.

Results

Mechanism of p62-triggered ROS generation

To test the hypothesis that Dlk1 was responsible for the increased genomic instability found in livers of *p62* transgenic mice (Kessler et al., 2015), its effect on RAC1 activity and ROS generation was examined *in vitro* using HepG2 cells. The level of activated RAC1 protein in HepG2 cells was significantly elevated after treatment with DLK1 for 5 min as detected by pull-down assay (**Figure 1A, B**). Cells treated with DLK1 revealed increased ROS production (**Figure 1C**), which was completely abrogated by pre-incubation with the RAC1 inhibitor NSC23766 (**Figure 1D**). These data supported the hypothesis that DLK1 triggered ROS generation through RAC1.

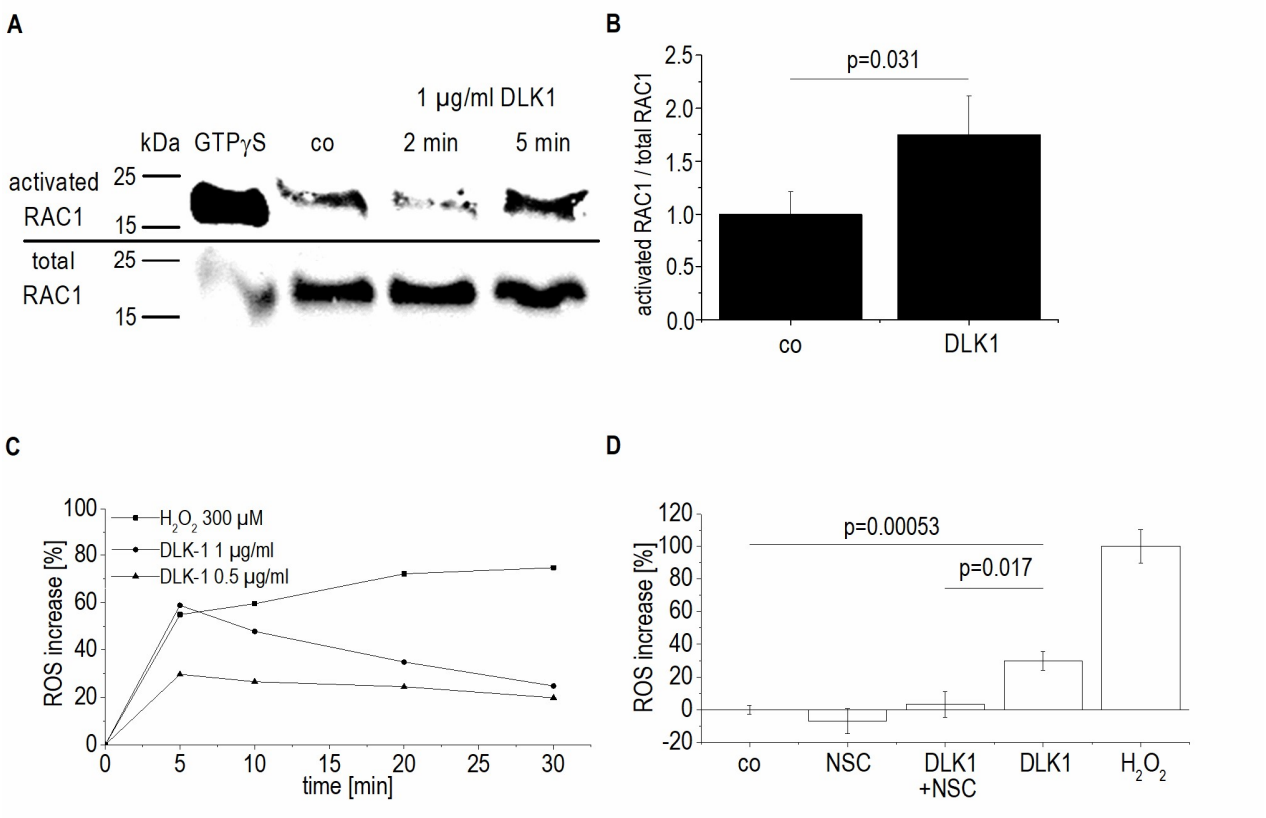

Figure 1: **DLK1-RAC1 driven ROS generation.** (**A**) Representative pull-down assay with activated RAC1 and total RAC1 in untreated HepG2 cells (co) and after treatment with 1 µg/ml DLK1 protein for 2 and 5 min. (**B**) Levels of activated RAC1 in untreated HepG2 cells (co) and after treatment with 1 µg/ml DLK1 protein for 5 min (DLK1) normalized to total RAC1 (n=4, singles and duplicates). (**C, D**) ROS increase [%]: (**C**) in HepG2 cells after treatment with 0.5 µg/ml DLK1, 1 µg/ml DLK1, or 300 µM H_2O_2 (positiv control) for 0-30 min normalized to untreated HepG2 cells (n=1, quintuplicates). (**D**) after treatment with DLK1, RAC1 inhibitor NSC23766 (NSC), or both (DLK1 + NSC), normalized to untreated HepG2 cells; H_2O_2-induced ROS formation was set as 100% (n=2, quintuplicates). The p values were calculated by two-sample t-test or ANOVA combined with Bonferroni *post hoc* test.

Discussion

The IMP p62 is overexpressed in different types of cancer including HCC (Dai et al., 2017). In glioblastoma, p62 preserves stem cells and promotes their tumor-initiating capacity (Degrauwe et al., 2016). Cancer stem cells have also been identified in HCCs (Cho & Clarke, 2008) and are linked to poor prognosis (Guo et al., 2014).
In this study a correlation between *p62* and the hepatic stem cell marker *Dlk1* was found. The expression of *DLK1* is under epigenetic control and dysregulated in HCC (Huang et al., 2007). It corresponds with poor patient survival and was suggested as prognostic factor of liver cancer (Jin et al., 2008). Regarding the function of DLK1, an induction of RAC1 by DLK1 had been found in mouse embryonic fibroblasts (Wang et al., 2010). Our data confirmed this DLK1-caused induction of RAC1 in the hepatoma cell line HepG2.
RAC1 is highly overexpressed in HCC (Kessler et al., 2015) and correlates with HCC metastasis by upregulation of the transcriptional activation of the vascular endothelial growth factor (Lee et al., 2006). Activated RAC1 induces ROS generation (Fürst et al., 2005). In HepG2 cells, elevated ROS levels due to increased RAC1 activity was determined. Increased ROS generation results in genomic instability (Block & Gorin, 2012), which was also found in tumors of *p62* transgenic mice with elevated *Rac1* expression (Kessler et al., 2015). Interestingly, in gallbladder cancer, *p62* also correlates with *Rac1* expression and the same Rac1-ROS mechanism was suggested (Kessler et al., 2017).
Taken together, the tumor-promoting action of p62 is, in part, mediated by oxidant actions. The underlying mechanism includes the DLK1-facilitated induction of RAC1 as an enhancer of ROS generation. The genomic instability - as a consequence of increased ROS generation - is linked to an aggressive tumor phenotype in the *p62* transgenic mouse model (Kessler et al., 2015).

These data were published in: Kessler S. M., Laggai S., Barghash A., **Schultheiss C. S.**, Lederer E., Artl M., Helms V., Haybaeck J., and Kiemer A. K. (2015) IMP2/p62 induces genomic instability and an aggressive hepatocellular carcinoma phenotype. *Cell Death and Disease,* 6(10), e1894.

Chapter 2

The role of *H19* in the tumor-promoting action of p62

Introduction

Hepatocarcinogenesis is a multistep process that requires a specific microenvironment often charecterized by chronic inflammation, changes in the cellular matrix, and altered cell signaling (Sia et al., 2017). Beside hepatocytes as cells of origin, different cell types are involved in HCC progression, e.g. immune cells administrating an altered immune response and activated stellate cells secreting collagen leading to fibrosis (Eng & Friedman, 2000, Hanahan & Weinberg, 2011). Hence, analysis of single cell lines is not sufficient for the investigation of HCC pathogenesis and several mouse models - class-divided into chemically induced models, xenograft models, and genetically modified models - are in use (Heindryckx et al., 2009).

The genetically modified models are composed of mice expressing hepatitis B/C virus genes, lacking tumor-suppressor genes, or overexpressing oncogenes, e.g. Myc, β-catenin, or p62 (Heindryckx et al., 2009, Kessler et al., 2015, Yan et al., 2018).

p62 has an important role in HCC initiation and progression by affecting inflammation and genomic instability (Kessler et al., 2015). The *p62* transgenic mouse model has been used for the functional analysis of p62 and contributed to the current knowledge on this mRNA binding protein (Kessler et al., 2015, Kessler et al., 2013, Laggai et al., 2014, Simon et al., 2014a, Simon et al., 2014b, Tybl et al., 2011). A complex mechanism enables the liver-specific expression of human p62 in the *p62* transgenic mice: *p62* expression is under control of the transrepressive responsive element cytomegaly virus promoter (TRE-CMV_{min} promoter) that can be activated by a transactivator (TA). To induce *p62* expression, mice need to be crossed with transgenic mice carrying a TA, the expression of which is controlled by a liver-enriched activator protein promoter (LAP promoter) (*LT2* mice). In the obtained *p62* positive and *LT2* positive mice, the TA is liver-specifically expressed and activates the TRE-CMV_{min} promoter resulting in the expression of human *p62* (Tybl et al., 2011).

p62 has been described to promote steatosis, steatohepatitis, fibrosis, and DEN-induced hepatocarcinogenesis (Kessler et al., 2015, Laggai et al., 2014, Simon et al., 2014a, Tybl et al., 2011). However, *p62* transgenic mice do not spontaneously develop tumors. Therefore, a chemically induced mouse model was used to trigger hepatocarcinogenesis, i.e. the carcinogen DEN model, which leads to DNA damage and induction of oxidative

stress (Heindryckx et al., 2009). Previous analyses of the *p62* transgenic mouse model revealed a significanly upregulated hepatic expression of the lncRNA *H19* (Tybl et al., 2011). *H19* is involved in tumorigenesis, but its function is a subject of controversy (Chen et al., 2016, Li et al., 2016, Ohtsuka et al., 2016, Raveh et al., 2015, Yang et al., 2012, Yoshimizu et al., 2008, Yu et al., 2013). Interestingly, the extent of *H19* overexpression was lower in tumor-bearing livers of *p62* transgenic mice treated with the carcinogen DEN (Laggai, 2014). These findings led us to the hypothesis that *H19* has tumor-suppressive functions.

Two different *H19* knockout mouse models are known from the literature: the *H19*Δ13 and the *H19*Δ3 model. The *H19*Δ13 mice carry a 13 kb deletion encompassing the *H19* gene and its upstream region containing sequences for the control of *H19* and *Igf2* expression. This results in lack of *H19*, but biallelic *Igf2* expression (Leighton et al., 1995). Since *Igf2* also promotes carcinogenesis (Lu et al., 2005, Nielsen, 1992, Resnicoff et al., 1995), this mouse model is not suitable to exclusively analyse the function of *H19*. In our study, the *H19*Δ3 mice, which carry a 3 kb deletion of *H19* and show only slightly increased *Igf2* expression (Ripoche et al., 1997), were investigated. The *H19*Δ3 mice were crossed with *p62* transgenic mice to clarify whether *H19* exerts tumor-suppressive action in the *p62* transgenic mouse model.

Results

To elucidate the function of *H19* in the *p62* transgenic mouse model, *p62* transgenic mice (Tybl et al., 2011) were crossed with *H19* deficient mice (Gabory et al., 2010, Ripoche et al., 1997) and treated with DEN to trigger HCC development.

H19 ko/*p62* tg mice: body and liver weight

H19 ko mice and the respective wild-types differed in body weight (**Figure 1A, B**). The highest body weights were detected for *H19* ko/*p62* tg mice. The body weight of *H19* ko/*p62* tg mice was significantly higher compared to *H19* wt/*p62* tg mice in both sexes and treatment groups. In female mice, the same weight-increasing effect of *H19* knockout was detected without the *p62* transgenic background (**Figure 1A, B**). Considering all genotypes, sexes, and treatments, mice containing the *H19* knockout revealed on average a 11.5% higher body weight compared to *H19* wild-type mice.

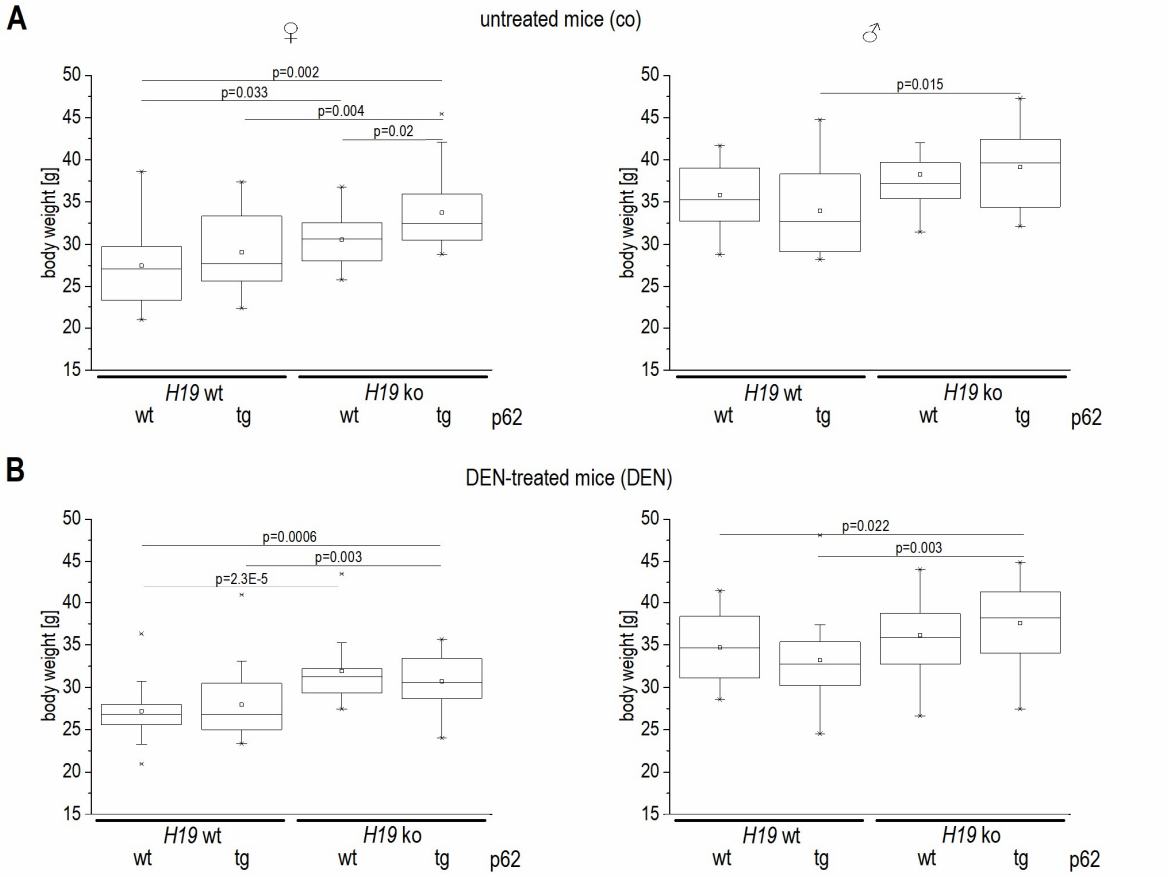

Figure 1: **Body weight** of female (left panels) and male (right panels) (**A**) untreated (co) and (**B**) DEN-treated (DEN) mice (co n=10-23, DEN n=20-25). The p values were calculated by Mann-Whitney *U* test or ANOVA combined with Bonferroni *post hoc* test.

Similar trends were found for the liver weights: the highest liver weights were detected for *H19* ko/*p62* tg mice and the liver weights of *H19* ko/*p62* tg mice were significantly higher compared to *H19* wt/*p62* tg mice (**Figure 2A, B**).

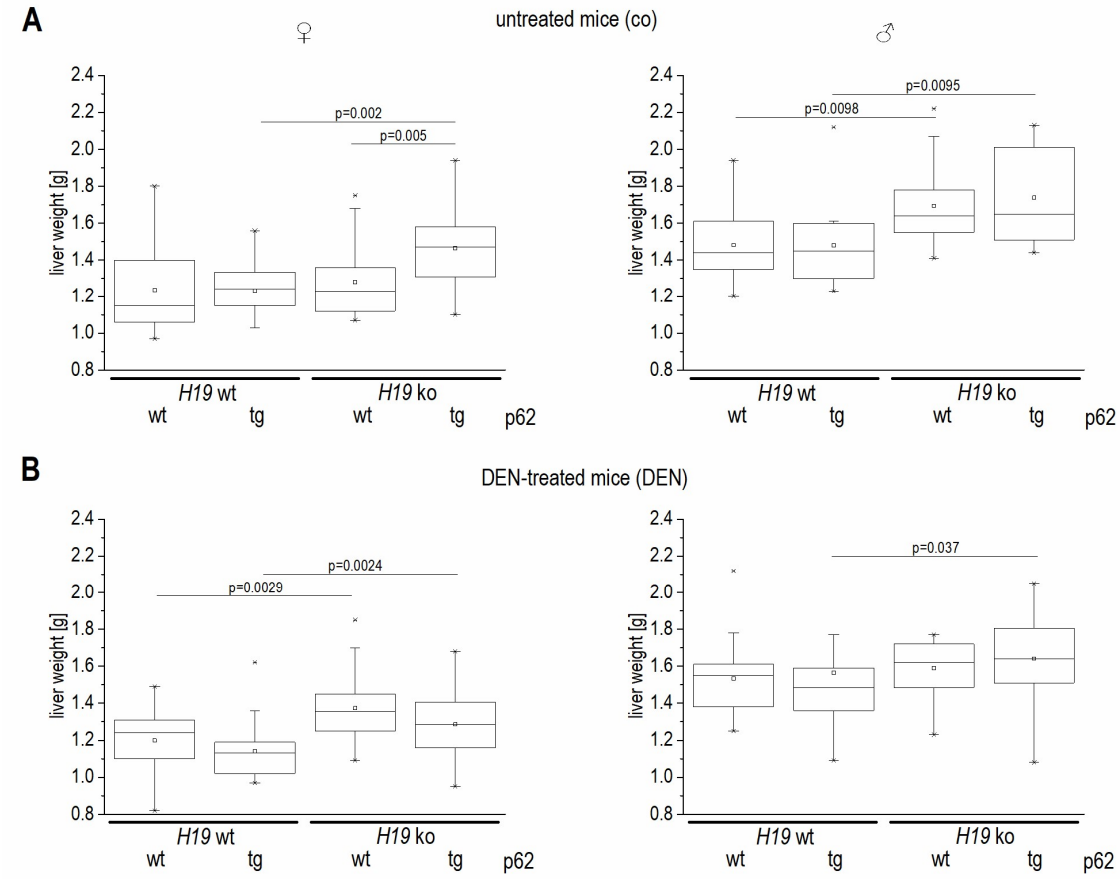

Figure 2: **Liver weight** of female (left panels) and male (right panels) (**A**) untreated (co) and (**B**) DEN-treated (DEN) mice (co n=10-23, DEN n=20-25). The p values were calculated by Mann-Whitney *U* test or ANOVA combined with Bonferroni *post hoc* test.

Hence, the liver to body weight ratio revealed no significant alterations, neither for untreated nor for DEN-treated mice (**Figure 3A, B**).

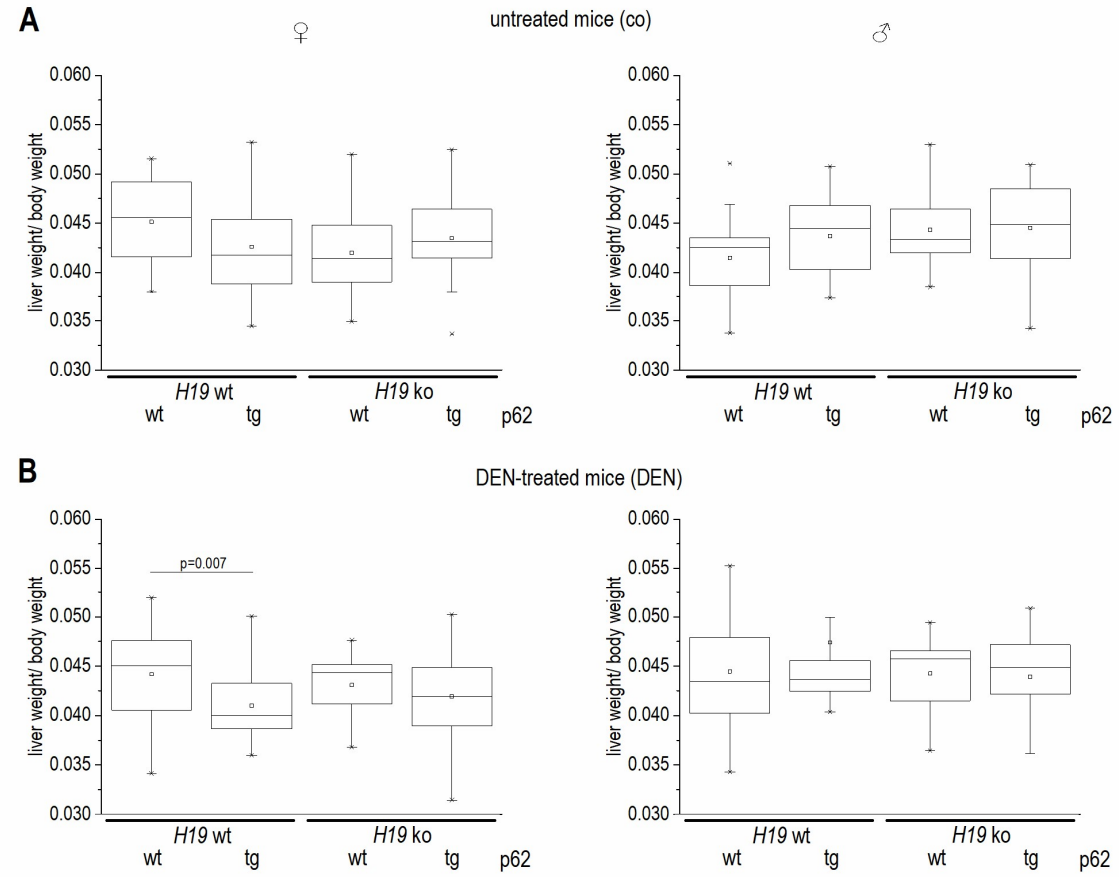

Figure 3: **Liver to body weight ratio** of female (left panels) and male (right panels) (**A**) untreated (co) and (**B**) DEN-treated (DEN) mice (co n=10-23, DEN n=20-25). The p values were calculated by Mann-Whitney *U* test or ANOVA combined with Bonferroni *post hoc* test.

H19 ko/*p62* tg mice: gene expression

To verify the effect of p62 on *H19* expression in the *H19* ko/*p62* tg mouse model, qPCR experiments were performed. As expected (Tybl et al., 2011), *p62* transgenic animals exhibited increased *H19* expression in case of the *H19* wild-type background. Furthermore, *H19* expression was significantly upregulated after DEN treatment in *H19* wt/*p62* wt animals (**Figure 4A**).

Igf2 expression was increased in *p62* transgenic compared to *p62* wild-type female mice, while the transgenic *p62* expression did not affect *Igf2* expression in male mice (**Figure 4B**). Female mice containing the *H19* knockout revealed significantly increased *Igf2* expression after DEN treatment. The same tendency was found for male mice (**Figure**

4B). In comparison to respective wild-type mice, the *H19* knockout did not affect *Igf2* expression except for male untreated *p62* transgenic mice.

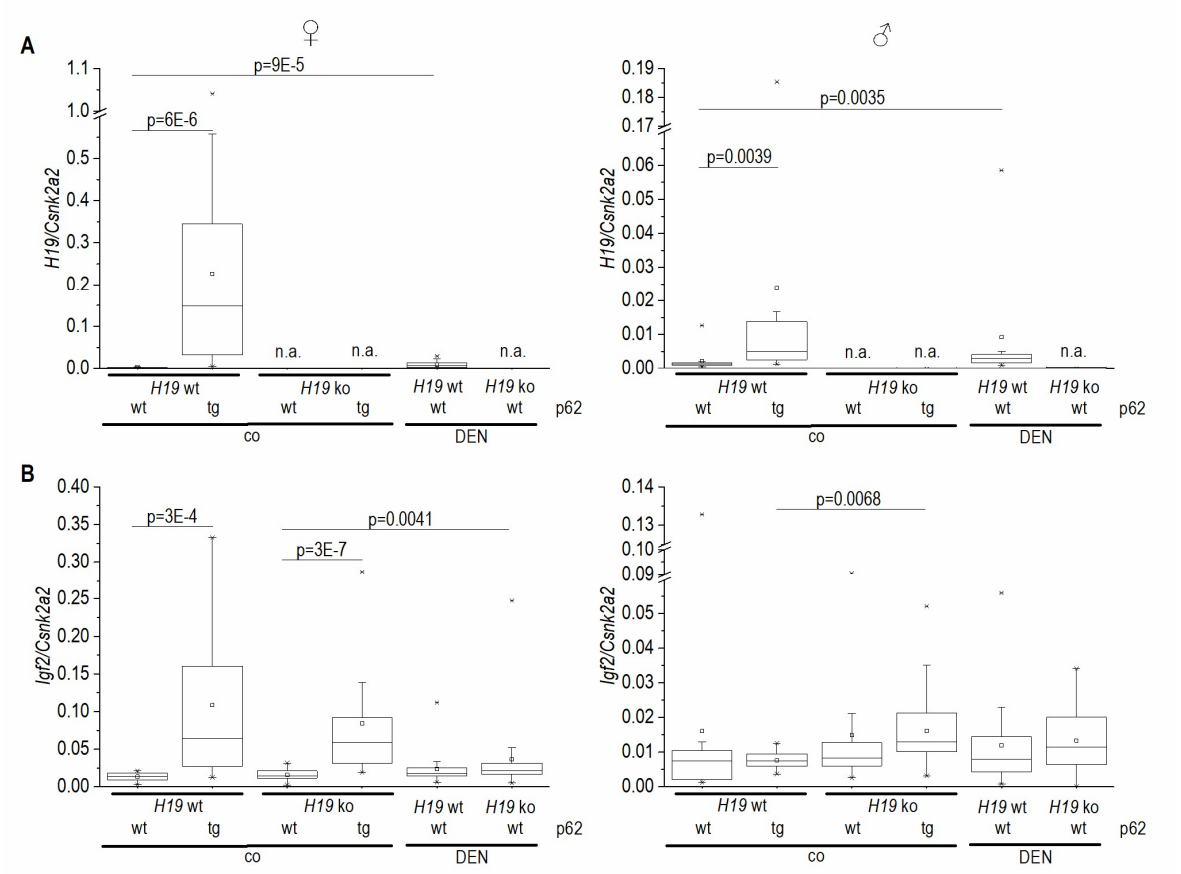

Figure 4: (**A**) ***H19* and** (**B**) ***Igf2* expression** in livers of female (left panels) and male (right panels) untreated and DEN-treated mice determined by qPCR (co n=10-23, DEN n=20-25). n.a. = not available. The p values were calculated by Mann-Whitney *U* test.

H19 ko/*p62* tg mice: steatosis and fibrosis

Steatosis is the first hit of liver disease (Day & James, 1998) and its development is promoted by transgenic p62 expression in mice (Tybl et al., 2011). Histological analyses of hematoxylin-eosin (H&E) stained liver sections revealed that none of the female mice and only 2 male *H19* ko/*p62* tg control mice, one *H19* wt/*p62* wt male DEN-treated mouse, and one *H19* ko/*p62* wt male control mouse developed macrovesicular hepatic steatosis (**Figure 5**).

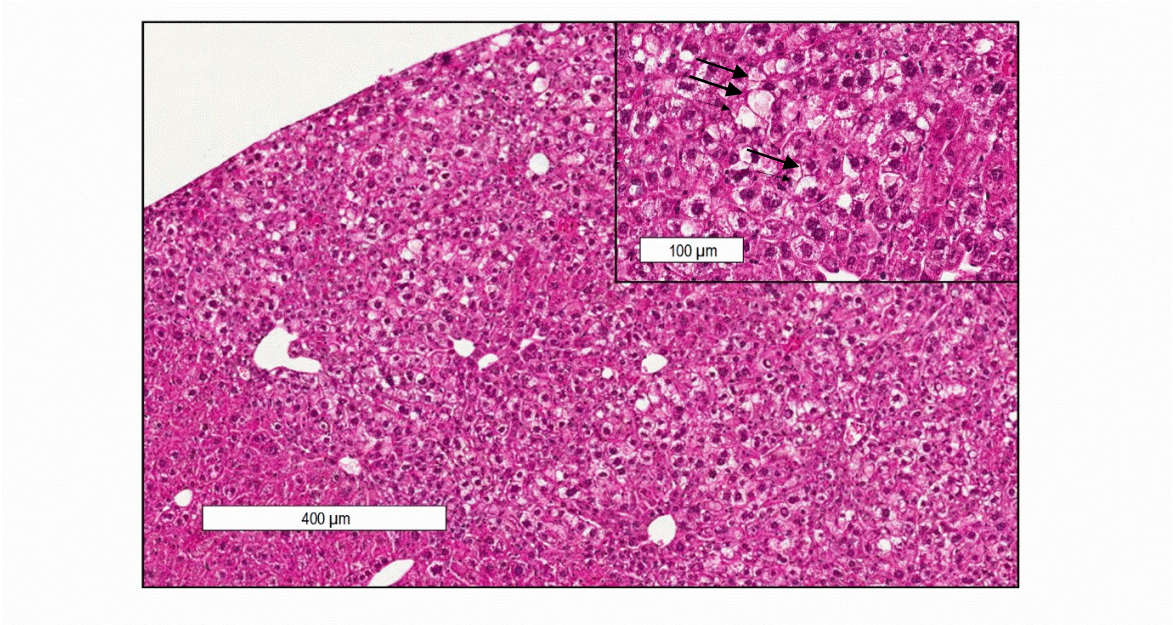

Figure 5: **Steatosis development.** H&E staining of a male DEN-treated *H19* wt/*p62* tg mouse is shown (the arrows indicate lipid accumulation).

Fibrosis characterized by collagen accumulation is present in most types of chronic liver disease in humans (Friedman, 2003). Fibrosis development in the *H19* wt/*p62* tg mouse model was analyzed by Sirius Red staining. Neither male nor female mice showed hepatic fibrosis (**Figure 6**).

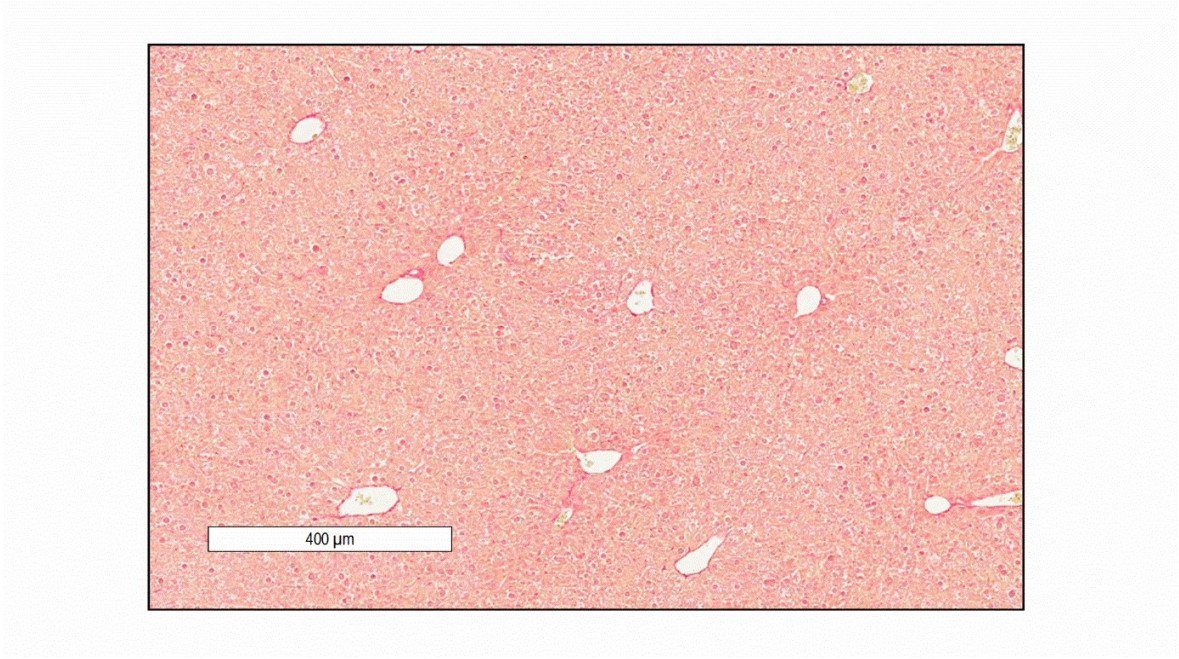

Figure 6: **Fibrosis detection.** Representative Sirius Red staining is shown.

H19 ko/*p62* tg mice: tumor induction and characterization

To clarify whether *H19* has tumor-suppressive effects in the *p62* transgenic mouse model, tumor development was investigated.

First, the tumor promoting action of p62 as shown by Kessler et al. 2015 in DBA2J/C57BL/6J mice was confirmed in mice on a 129sv/DBA2J/C57BL/6J background (Kessler et al., 2015): more tumors were found in male DEN-treated than female DEN-treated mice (**Figure 7A**). This is due to inhibitory effects of estrogens and stimulating effects of androgens on hepatocarcinogenesis (Nakatani et al., 2001, Naugler et al., 2007). No tumors were found in untreated mice. *H19* ko/*p62* wt mice developed significantly more tumors than *H19* wt/*p62* wt mice in both sexes. This tumor-suppressive effect of *H19* was not significant for mice with transgenic *p62* expression (female p=0.70, male p=0.81) (**Figure 7A**).

Small cell changes (SCCs) and large cell changes (LCCs) are dysplastic lesions found in the process of liver carcinogenesis (Park, 2011). Tumors of *H19* ko/*p62* wt mice displayed significantly more SCCs than tumors of *H19* wt/*p62* wt mice. Mice with transgenic *p62* expression showed also significantly more SCCs when they were *H19* deficient (female p=0.62, male p<1E-8). Most SCCs were detected in tumors of male *H19* ko/*p62* tg mice, which also exhibited LCCs (**Figure 7B**).

Taken together, the combination of *p62* overexpression and lack of *H19* did not significantly increase the number of tumors, but increased the dysplasia of tumor cells.

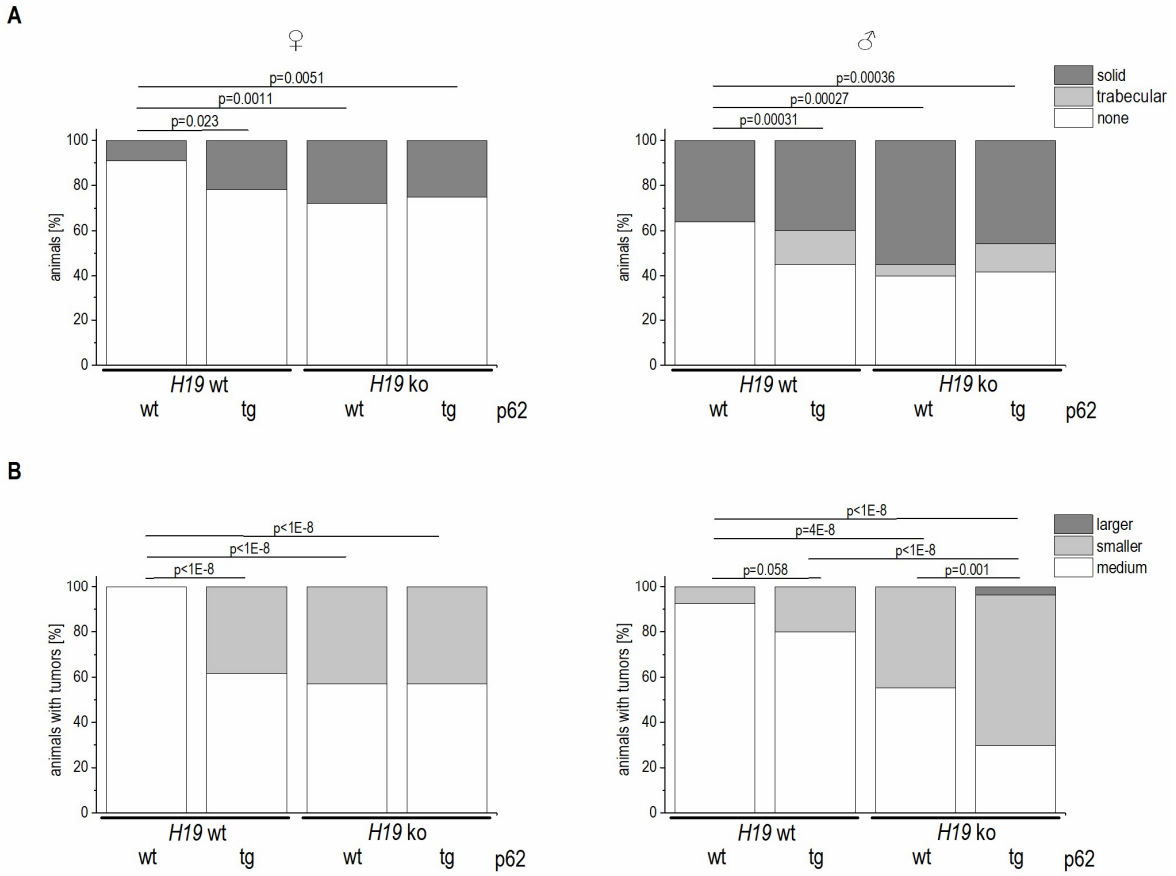

Figure 7: **Tumor development and characterization** in female (left panels) and male (right panels) DEN-treated mice. (**A**) Tumor development and (**B**) predominant cell size in tumors of DEN-treated female and male mice (co n=10-23, DEN n=20-25). The p values were calculated by Chi-square test.

Immunohistological stainings of all liver tumors revealed the expression of the tumor specific surface antigen Gp73 (**Figure 8A**). The early HCC marker glutamine synthetase (GS) was not expressed except for one male *H19* wt/*p62* tg and one male *H19* ko/*p62* tg mouse (**Figure 8B**).

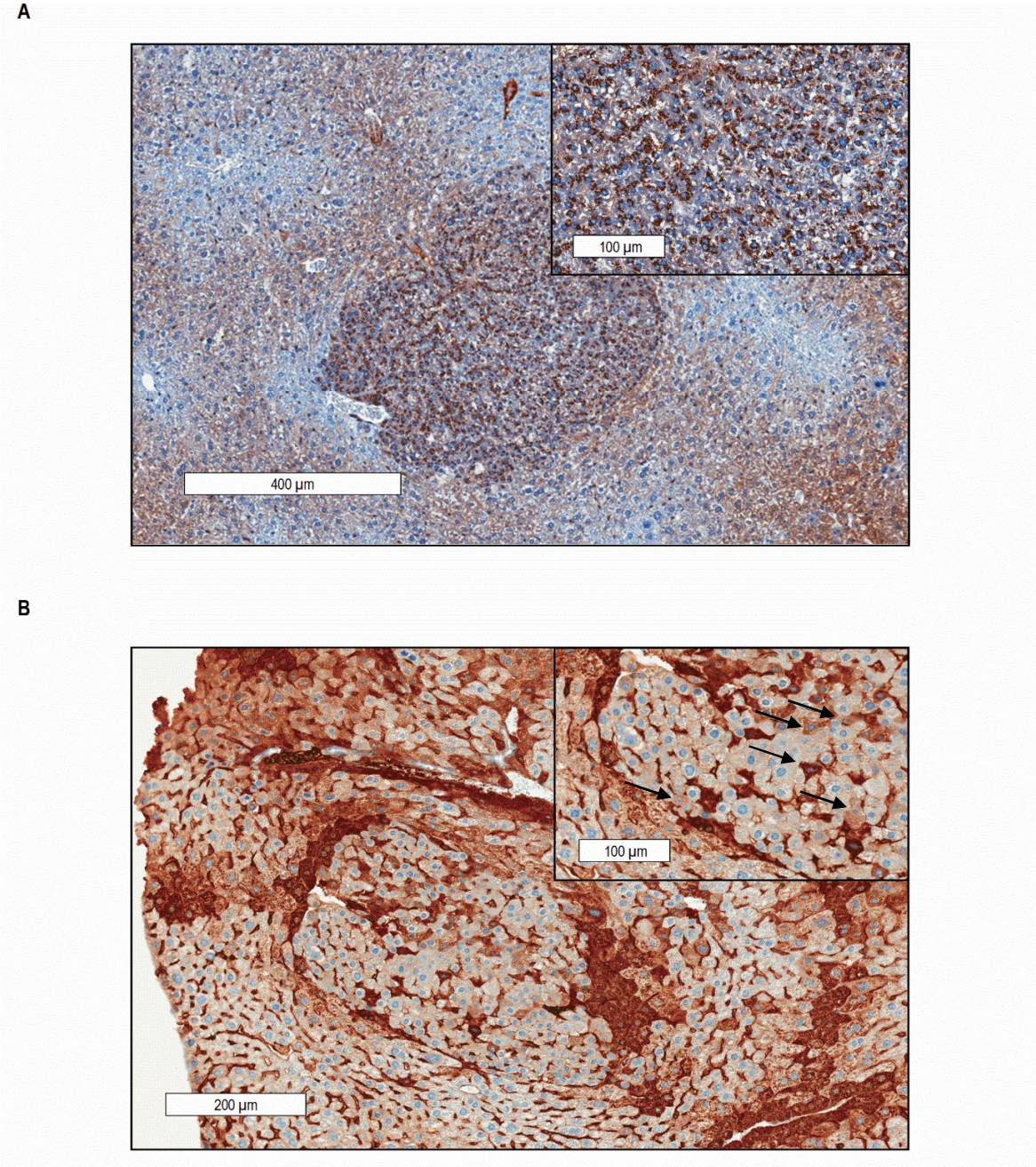

Figure 8: **Immunohistological staining of HCC markers.** Representative (**A**) Gp73 and (**B**) GS stains (the arrows indicate GS positive brown stained cells) are shown.

Further, tumors of male DEN-treated mice were analyzed with respect to the expression of the proliferation marker Ki67. Significantly more tumors of *H19* ko mice expressed Ki67 compared to *H19* wt mice either with or without the *p62* transgenic background (**Figure 9A, B**).

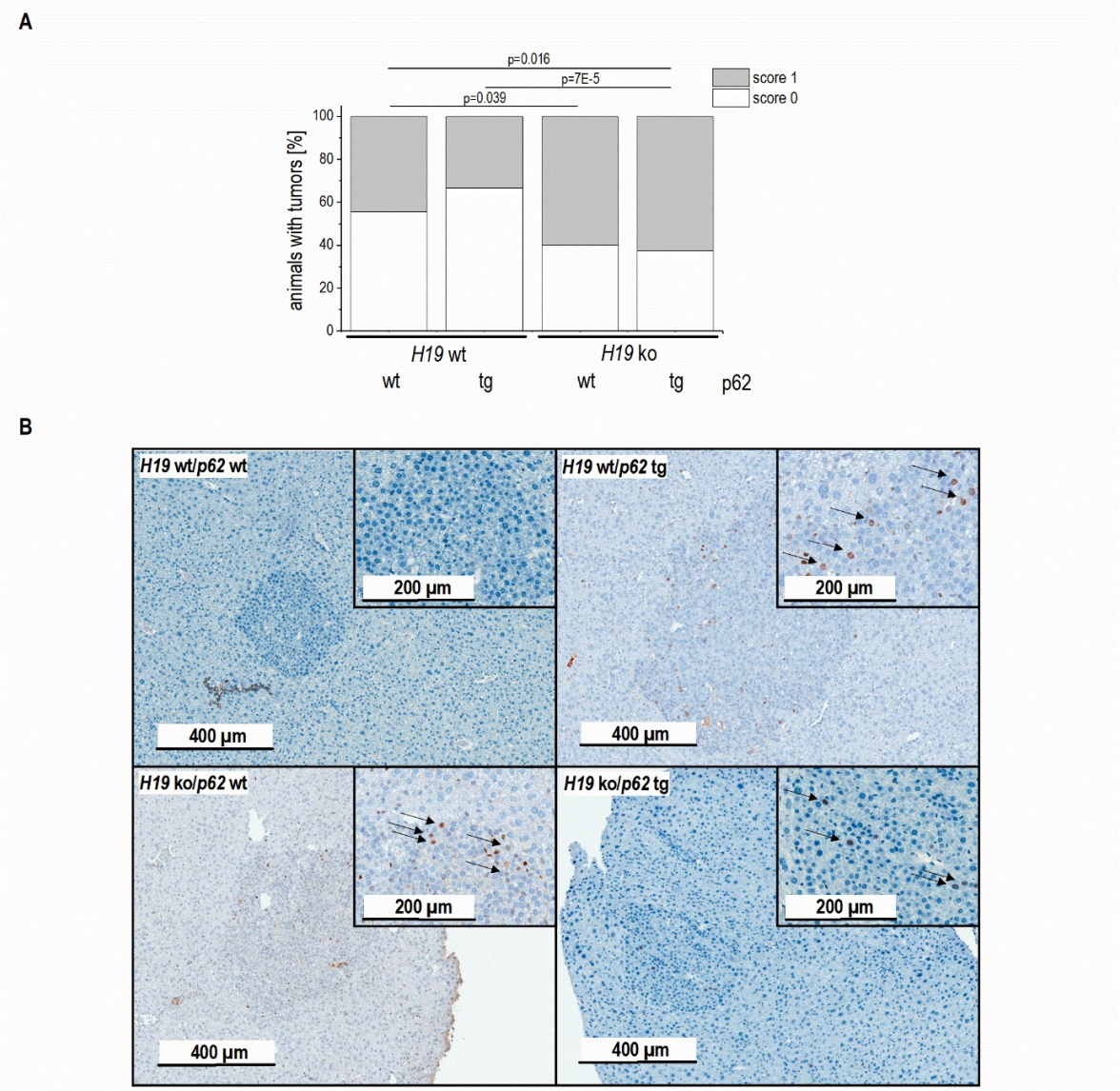

Figure 9: (**A**) **Expression of the proliferation marker Ki67 in tumors of male DEN-treated mice** (score 0: no proliferating cells detectable; score 1: less than 1% proliferating cells). The p values were calculated by Chi-square test. (**B**) Representative immunohistological staining of Ki67 (the arrows indicate Ki67 positive brown stained nuclei) (*H19* wt/*p62* wt n=9, *H19* wt/*p62* tg n=9, *H19* ko/*p62* wt n=10, *H19* ko/*p62* tg n=8).

In summary, the hypothesized synergistic effects of transgenic *p62* and lack of *H19* expression with respect to tumor development were not significant. These data suggest that *H19* did not protect from the formation of tumors in *p62* transgenic mice. However, the *H19* knockout promoted tumor progression as well as tumor cell dysplasia and proliferation in *p62* wild-type mice.

H19 ko/*p62* tg mice: apoptosis

The defective apoptosis pathway has been associated with the promotion stage of HCC (Guicciardi & Gores, 2005). An anti-apoptotic action of p62 in hepatoma cells treated with chemotherapeutics has been reported (Kessler et al., 2013). The role of *H19* in apoptosis is conflicting: *H19* knockout has been associated with reduced apoptosis in choriocarcinoma (Yu et al., 2013) as well as increased apoptosis in gastric cancer (Yang et al., 2012).

The amount of apoptotic cells in *p62* transgenic and *H19* knockout mouse livers was analyzed by histological examination. An anti-apoptotic effect of p62 could not be determined. In fact, mice with transgenic *p62* expression exhibited a higher amount of apoptotic cells (**Figure 10A, B**). *H19* knockouts showed higher apoptosis induction in livers of untreated *p62* wild-type mice (**Figure 10A**). The amount of apoptotic cells was not altered in livers of female DEN-treated mice, whereas in livers of male DEN-treated mice the *H19* knockout significantly induced apoptosis (**Figure 10B**). These data rather suggest an anti-apoptotic effect of *H19* in our model.

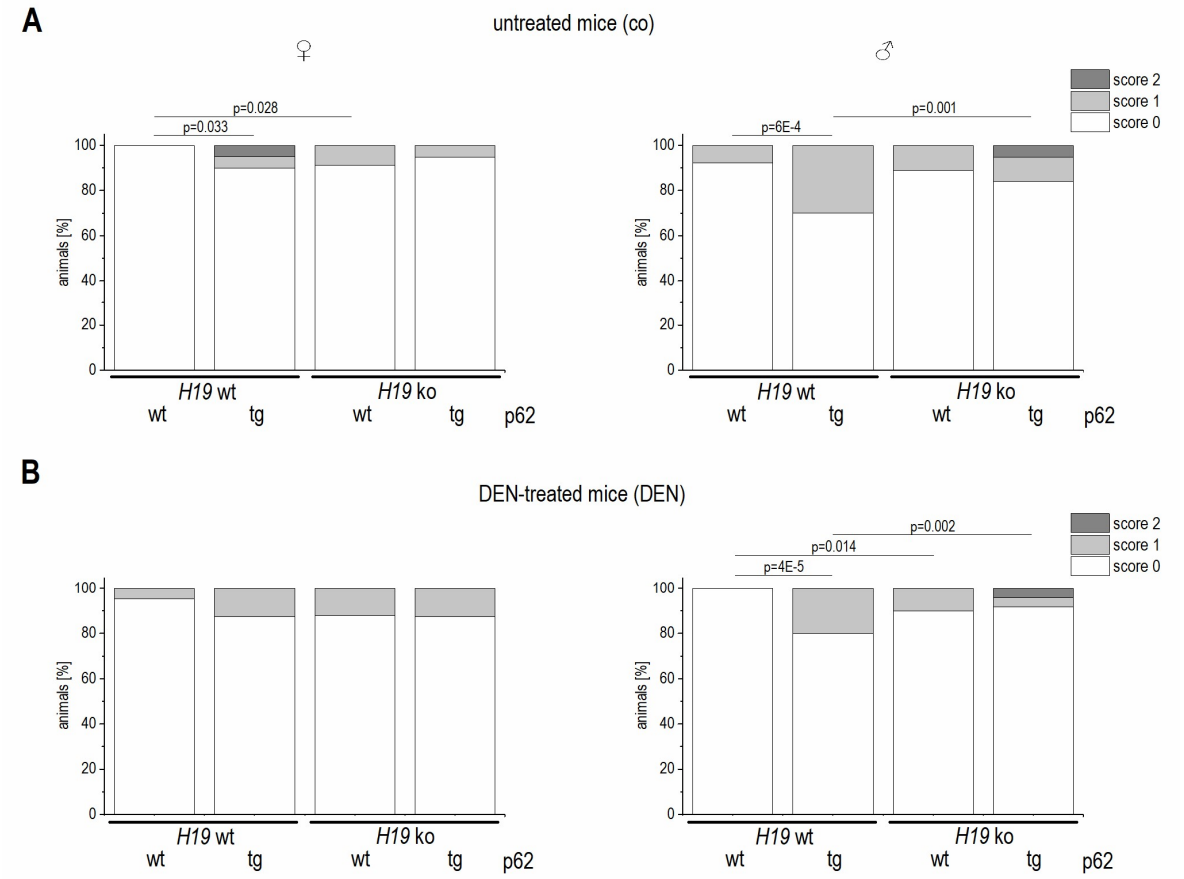

Figure 10: **Apoptosis induction** in livers of female (left panels) and male (right panels) (**A**) untreated (co) and (**B**) DEN-treated (DEN) mice (co n=10-23, DEN n=20-25) (score 0: no apoptotic cells found; score 1: less than 2 apoptotic cells in a 200x magnification; score 2: 2-4 apoptotic cells in a 200x magnification). The p values were calculated by Chi-square test.

H19 ko/*p62* tg mice: inflammation

Since inflammation is an important hallmark of cancer (Hanahan & Weinberg, 2011) and the role of *H19* in this process is controversially discussed (Chen et al., 2016, Li et al., 2016), the effect of *H19* knockout on inflammation was analyzed by histological examination.

In general, livers of female mice showed more lymphocytic and granulocytic infiltrates compared to livers of male mice (**Figure 11A, B; 12A, B**).

In the group of untreated mice *H19* knockout caused a significantly higher amount of inflammatory infiltrates (**Figure 11A, 12A, 13**). In female mice, also transgenic *p62* expression increased inflammation. Hence, the highest degree of inflammatory infiltrates was detected in female *H19* ko/*p62* tg mice (**Figure 11A, 12A**).

H19 knockout did not clearly affect inflammation in livers of DEN-treated mice (**Figure 11B, 12B**).

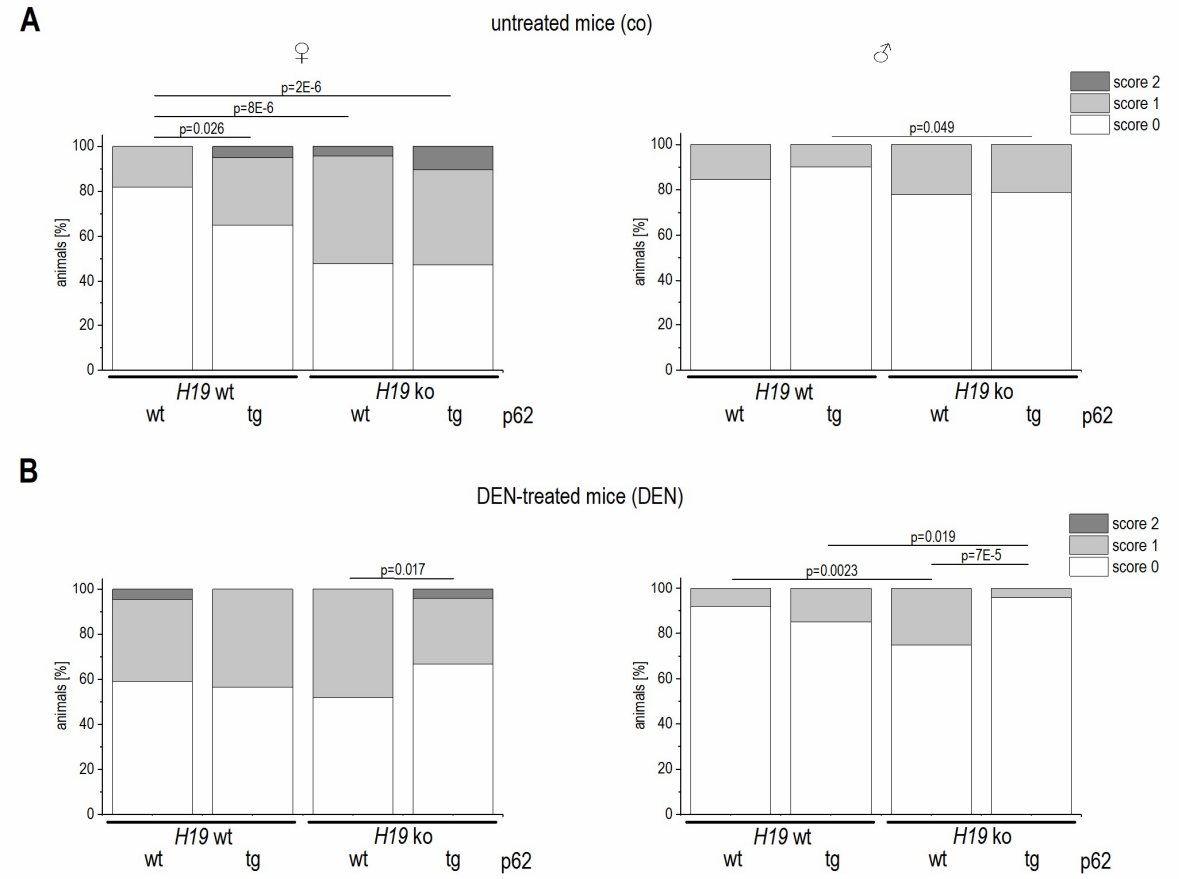

Figure 11: **Lobular lymphocytic inflammation** in livers of female (left panels) and male (right panels) (**A**) untreated (co) and (**B**) DEN-treated (DEN) mice (score 1: less than 2 lymphocytic cells in a 200x magnification; score 2: 2-4 lymphocytic cells in a 200x magnification) (co n=10-23, DEN n=20-25). The p values were calculated by Chi-square test.

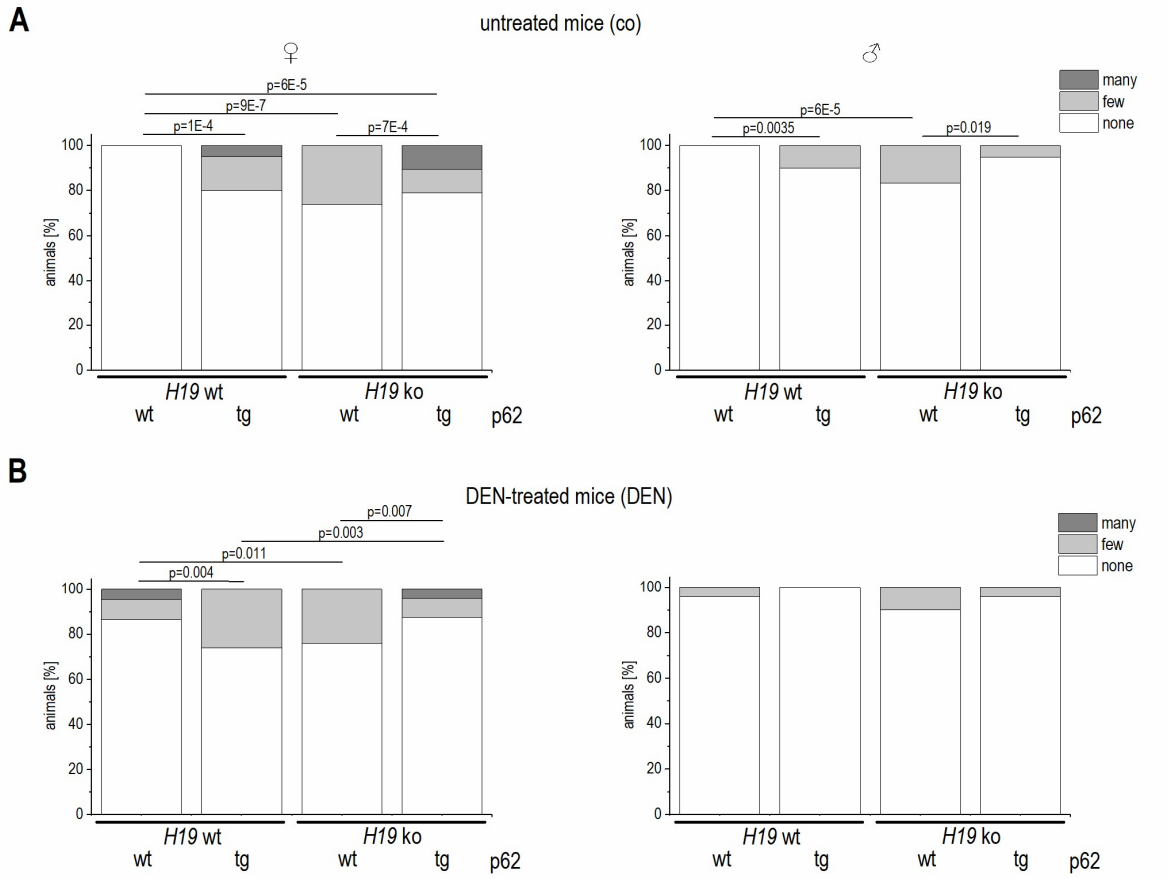

Figure 12: **Lobular granulocytic inflammation** in livers of female (left panels) and male (right panels) (**A**) untreated (co) and (**B**) DEN-treated (DEN) mice (few = 1-5 neutrophil granulocytes per inflammatory infiltrate; many = more than 5 neutrophil granulocytes per inflammatory infiltrate) (co n=10-23, DEN n=20-25). The p values were calculated by Chi-square test.

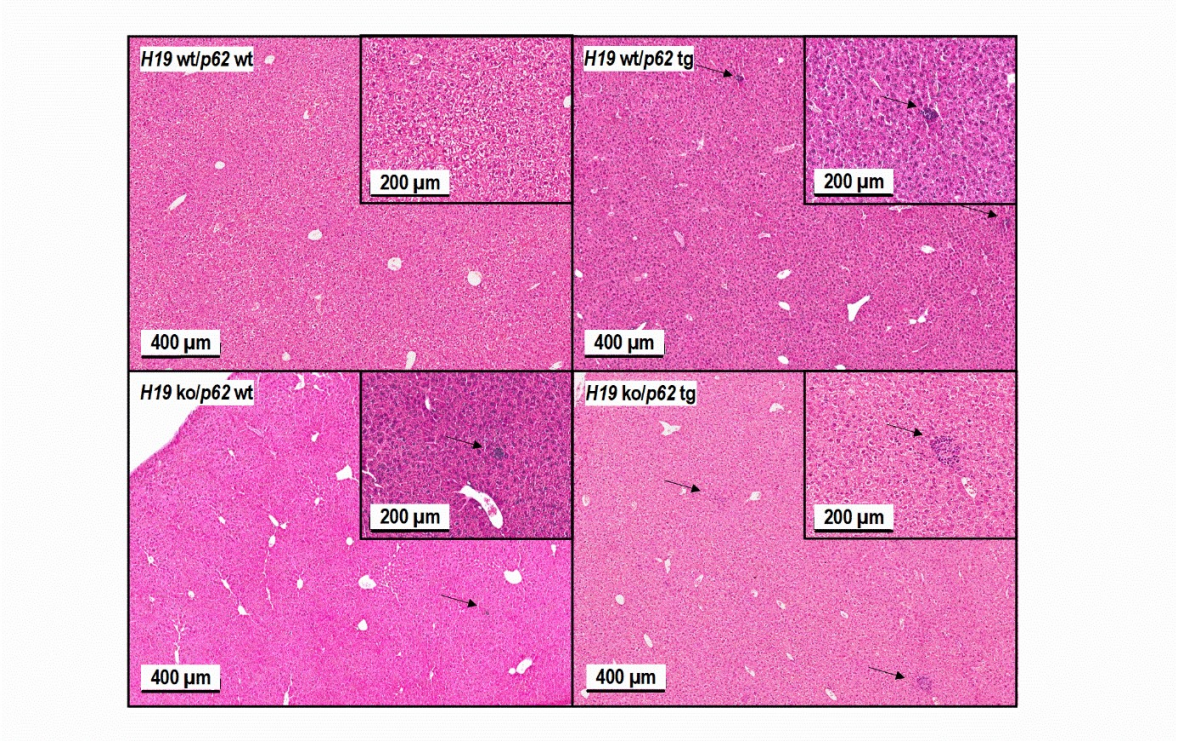

Figure 13: **Inflammation in livers of female mice.** Representative H&E stains of untreated mice are shown (arrows indicate inflammatory infiltrates).

Discussion

Experimental mouse models are widely used in hepatocellular carcinoma research and accounted for the current state of knowledge on hepatocarcinogenesis and tumor progression (Heindryckx et al., 2009). The *p62* transgenic mouse model on a DBA2J/C57BL/6J background has been well described with respect to steatosis, steatohepatitis, and fibrosis (Kessler et al., 2013, Laggai et al., 2014, Simon et al., 2014a, Simon et al., 2014b, Tybl et al., 2011). Steatohepatitis and fibrosis are amplified under transgenic *p62* expression in respective models, but tumor development was only detected after induction by the carcinogen DEN (Kessler et al., 2015). Since the mouse strain has an impact on hepatocarcinogenesis (Heindryckx et al., 2009), tumor development in our *p62* transgenic mice with a different genetic background (129sv/DBA2J/C57BL/6J) was analyzed. The tumor-promoting effect of p62 in mice treated with DEN as well as the lack of tumor development in *p62* transgenic mice without tumor induction by DEN were confirmed on a 129sv/DBA2J/C57BL/6J background.

Regarding the tumor phenotype, our results fit to the described characteristics (Kessler et al., 2015): the tumor marker Gp73 was detected as positive in all tumors, whereas GS was mostly negative with only two tumors of male *p62* transgenic mice positively tested for both HCC markers.

The influence of p62 on inflammation by increasing ROS generation has recently been described in hepatoma cells (Kessler et al., 2015). The significantly elevated amount of inflammatory infiltrates in female *p62* transgenic mice confirmed the inflammation-promoting action of p62.

The crossing of *p62* transgenic with *H19* knockout mice was performed in order to elucidate the role of *H19* in the validated tumor-promoting action of p62. The first distinctive feature of our *H19* knockout mice was an elevated body weight (11.5% higher compared to wild-type mice). These results fit to the previously reported weight increase of *H19* knockout mice (Ripoche et al., 1997). The weight gaining effect was suggested to be caused by the regulatory function of *H19* in an imprinted gene network consisting of growth control genes (Gabory et al., 2009, Varrault et al., 2006).

The role of *H19* in carcinogenesis is controversely discussed. Although some researchers reported oncogenic properties of *H19* (Barsyte-Lovejoy et al., 2006, Berteaux et al., 2005,

Matouk et al., 2007), a tumor-suppressive effect of *H19* has been described in murine models of colorectal cancer, teratocarcinoma, and SV40-induced hepatocarcinoma (Yoshimizu et al., 2008). Our data support the tumor-suppressive function of *H19*: the *H19* knockout promoted DEN-triggered tumor development, tumor cell dysplasia, and tumor cell proliferation. In contrast to our hypothesis, *H19* ko/*p62* tg mice did not show the strongest tumor induction. This could be possibly explained by the following circumstances: Expression data from Laggai 2014 revealed a significantly downregulated *H19* expression in *p62* transgenic mice after DEN-treatment comparable to the conditions of our study (Laggai, 2014). In contrast, *H19* expression is significantly elevated after DEN-treatment in *p62* wild-type mice. Thus, the *H19* knockout has a stronger impact in *p62* wild-type than in *p62* transgenic mice and this could be responsible for the missing additive effect of transgenic *p62* and lack of *H19* expression on tumor development.

The *H19* knockout stimulated p62-independent inflammation in mouse livers. Li et al. also reported an anti-inflammatory effect of *H19* (Li et al., 2016), employing an *H19* overexpressing rat model. Since inflammation is an important carcinogenesis-inducing factor (Hanahan & Weinberg, 2011), the anti-inflammatory action of *H19* further underlines its tumor-preventing potential.

Taken together, the hypothesized tumor-protective function of *H19* in *p62* transgenic mice was not significant. However, some tumor characteristics of *H19* ko/*p62* tg mice - e.g. tumor cell dysplasia - were shifted towards the direction of a more advanced tumor state suggesting an inhibitory effect of *H19* on tumor progression.

The impact of *H19* was mostly independent of transgenic *p62* expression. Our data indicate a tumor-suppressive, anti-proliferative, and anti-inflammatory action of *H19* and thereby underline its important role in initiation and progression of HCC.

Part of the data concerning *p62* wild-type mice were published in: **Schultheiss C.S.**, Laggai S., Czepukojc B., Hussein U.K., List M., Barghash A., Tierling S., Hosseini K., Golob-Schwarzl N., Pokorny J., Hachenthal N., Schulz M., Helms V., Walter J., Zimmer V., Lammert F., Bohle R.M., Dandolo L., Haybaeck J., Kiemer A.K., and Kessler S.M. (2017) The long non-coding RNA *H19* suppresses carcinogenesis and chemoresistance in hepatocellular carcinoma. *Cell Stress*. 1(1), 37-54.

Chapter 3

The long non-coding RNA *H19* suppresses carcinogenesis and chemoresistance in hepatocellular carcinoma

Introduction

Non-coding sequences constitute the considerably larger part of the transcribed human genome compared to coding sequences since only 2% of the genome encode for proteins (International Human Genome Sequencing Consortium 2004).

Recently, RNA-seq datasets were used to identify lncRNAs aberrantly expressed under inflammatory conditions. The well-described lncRNA *H19* (long intergenic non-protein coding RNA 8), a maternally expressed imprinted gene product, was the lncRNA with the most consistent overexpression among all conditions investigated (Wang et al., 2016c). Since cholangiocarcinoma represents a tumor type that develops under inflammatory conditions and in settings of oxidative stress, the authors investigated the role of *H19* in cholangiocarcinoma cell lines and observed tumor-promoting and pro-inflammatory actions of *H19* (Wang et al., 2016c). In contrast, *H19* was found to have tumor-suppressing abilities in colorectal cancer, another inflammation-associated tumor entity (Ohtsuka et al., 2016), and the role of *H19* in inflammation is conflicting (Chen et al., 2016, Li et al., 2016).

Embedded in *H19*'s first exon is the microRNA *miR-675* (Cai & Cullen, 2007), the processing of which is negatively regulated by the RBP ELAV like RNA-binding protein 1 (ELAVL1 / HuR) (Keniry et al., 2012), and has also been reported to affect cancer (Raveh et al., 2015) and inflammation (Chen et al., 2016, Kohno et al., 2014, Li et al., 2016, Lu et al., 2012).

Also HCC evolves in an environment governed by metabolic and inflammatory stress as found in chronic viral hepatitis, as well as in alcoholic and non-alcoholic steatohepatitis (El-Serag & Rudolph, 2007). HCC represents the second most common cause of cancer-related death worldwide (Stewart & Wild, 2014), which is not least due to its high chemoresistance. However, the role of *H19* in HCC development, progression, and chemoresistance is still unclear. While Yoshimizu et al. reported accelerated tumor development in *H19* knockout mice in SV40-induced HCC (Yoshimizu et al., 2008), Matouk et al. observed an enhanced tumorigenic potential of carcinoma cells *in vivo* upon ectopic *H19* expression (Matouk et al., 2007). Allelic expression of *H19* is controlled by an imprinting control region and by a promoter, which can be differentially methylated (Gabory et al., 2006). Loss of imprinting (LOI), i.e. biallelic *H19* expression, was reported

for HCC using small sample size cohorts (Kim & Lee, 1997, Wu et al., 2008). In general, human data on *H19* expression in HCC should be interpreted with caution because the number of samples available for the studies dealing with this topic was mostly rather small (Kim & Lee, 1997, Wu et al., 2008).

We therefore conducted comprehensive studies using four independent patient cohorts, *H19* knockout mice, and three different human hepatoma cell lines to decipher the role of *H19* in HCC development, hepatoma cell growth, and chemoresistance.

Results

Based on recent reports suggesting *H19* as an inflammation-inducible lncRNA and HCC representing a disease developing in an inflammatory environment, we sought to determine *H19* expression in human HCC. The comparison of n=364 HCC tissues with n=49 normal liver tissues from TCGA sequencing data revealed highest *H19* expression in a subgroup of HCC samples. Still, statistical analysis of all samples showed an allover decreased expression of *H19* in HCC tissues (**Figure 1A**). Comparing *H19* expression of HCC tissues only to their respective adjacent tissues, *H19* expression was still decreased with high statistical significance (data not shown, p=5.28E-7). Also analysis of two microarray GEO datasets with n=39/39 (GSE57957) and n=74/74 (GSE54236) HCC tissues *vs*. non-tumor tissues revealed a distinct downregulation of *H19* (**Figure 1B and C**) as did qPCR quantification of *H19* in a previously described patient cohort (**Figure 1D**) (Kessler et al., 2013, Kessler et al., 2014). *In situ* hybridization against *H19* revealed low expression of *H19* in tumor tissues, but higher expression in the non-tumorous tissues adjacent to the tumor site in an additional patient cohort (**Figure 1E**). All cohorts comprised patients with HCC from different etiologies. Q-PCR of hepatocytes, microdissected from the small subgroup of HCC samples showing high *H19* expression (**Figure 1D**) suggested that *H19* was in fact overexpressed in hepatocytes (**Figure S2**).

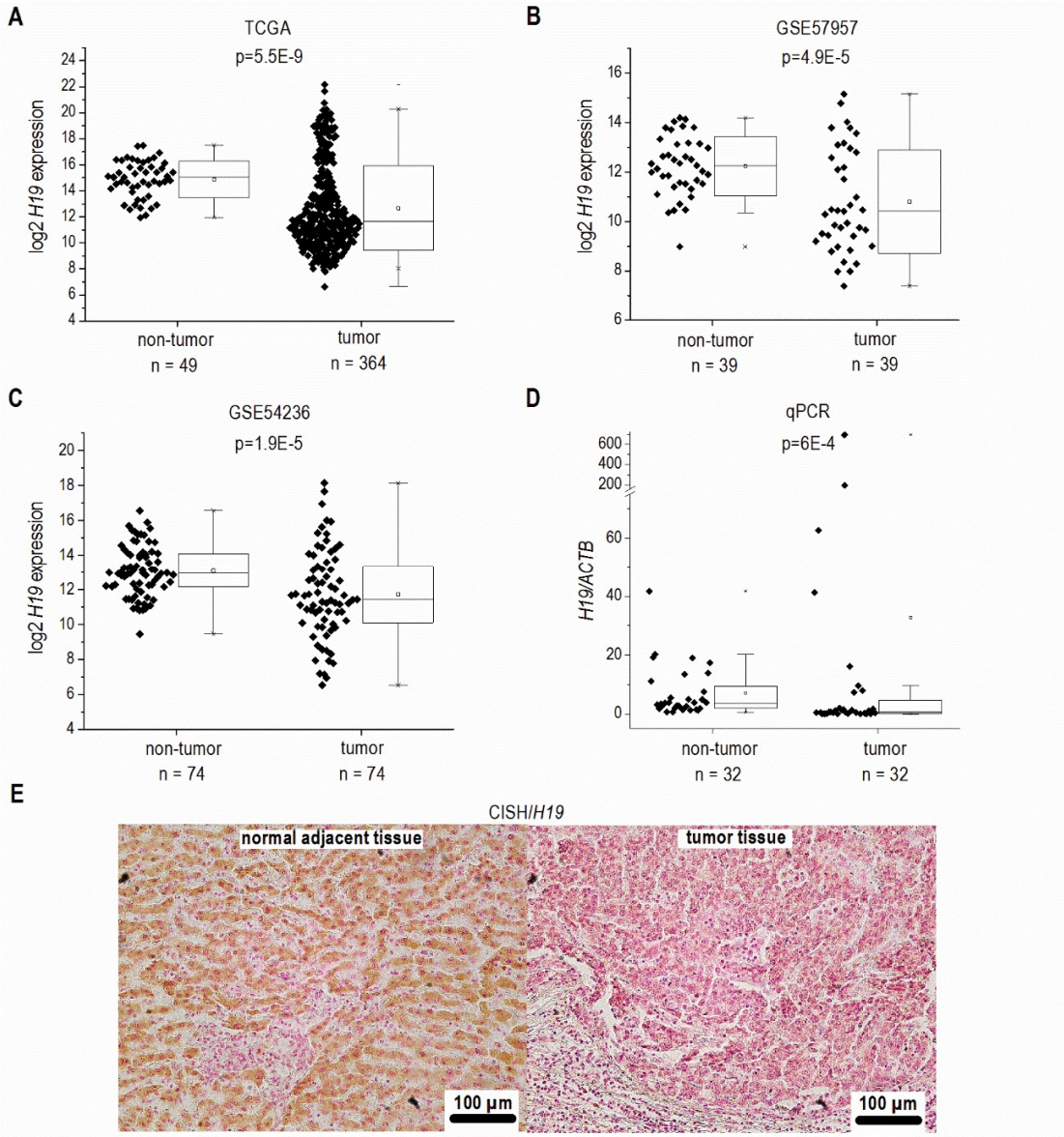

Figure 1: ***H19* expression in human** HCC tissues (tumor) compared to non-tumorous tissues (non-tumor). (**A**) Log2 *H19* expression in HCC tissues from TCGA dataset (non-tumor: n=49, tumor: n=364, Mann-Whitney *U* test). (**B**) Log2 *H19* expression in HCC tissues from GEO dataset GSE57957 (each, n=39, Kolmogorov-Smirnov test). (**C**) Log2 *H19* expression in HCC tissues from GEO dataset GSE54236 (each, n=74, Kolmogorov-Smirnov test). (**D**) *H19* expression in HCC tissues from Saarland University Medical Center determined by qPCR (each, n=32, Mann-Whitney *U* test). (**E**) Representative chromogenic *in situ* hybridization (CISH) of *H19* (*H19* positive cells: brown; *H19* negative cells: red) (each, n=8).

In accordance with the results from *H19* expression, which encodes *miR-675*, the more abundant *miR-675-3p* was downregulated in HCC (**Figure 2A**) and strongly correlated with *H19* (R^2=0.91, p<1.0E-15). The less abundant *miR-675-5p* was not detectable in most

samples. The RBP HuR/ELAVL1 has been shown to represent a negative regulator of *miR-675* processing in the mouse system by binding to *H19* (Keniry et al., 2012). Interestingly, expression of *ELAVL1* was significantly upregulated in HCC (**Figure 2B**) suggesting an inhibited processing of *H19* into *miR-675*. RNA immunoprecipitation (RIP) experiments in Huh7 cells confirmed that HuR/ELAVL1 also binds to human *H19*: *H19* was significantly enriched in HuR immunoprecipitates over the negative control *GAPDH* (**Figure 2C**). Also the positive control *CCNB1* showed a significantly enriched binding compared to the negative control.

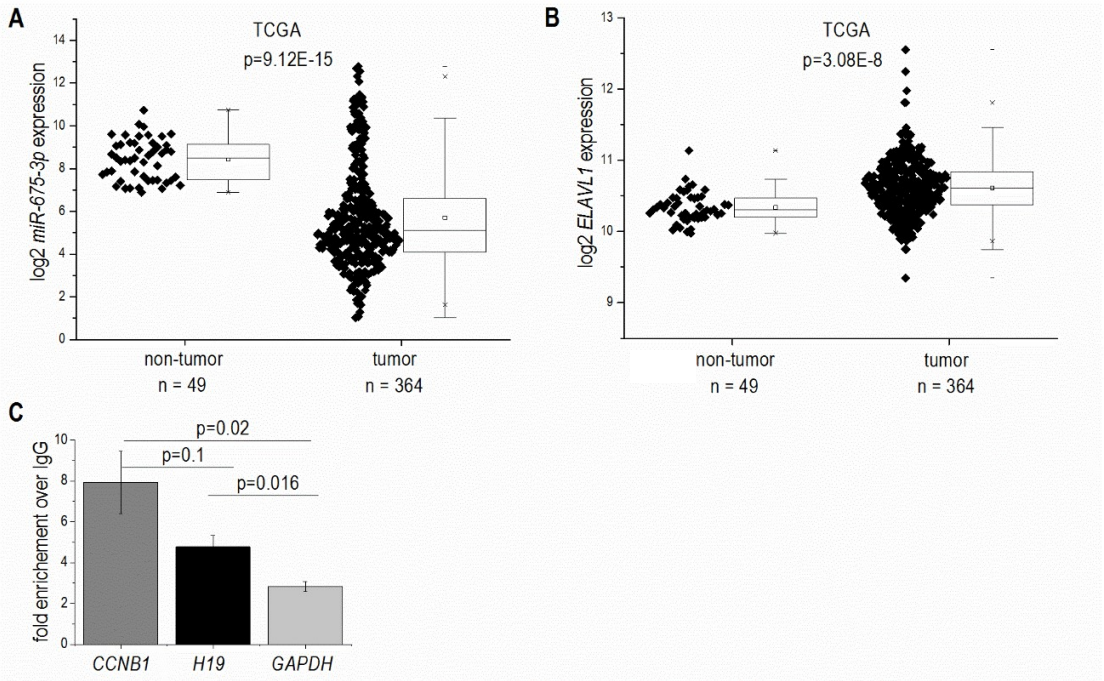

Figure 2: ***miR-675* and *ELAVL1/HuR* expression in human HCC** tissues (tumor) compared to non-tumorous tissues (non-tumor). (**A**) Log2 *miR-675-3p* expression and (**B**) Log2 *ELAVL1* expression in HCC tissues from the TCGA dataset (non-tumor: n=49, tumor: n=364, Mann-Whitney *U* test). (**C**) RIP was performed using either IgG or an HuR antibody. Co-precipitated mRNAs *H19*; *CCNB1*, as a positive control; *GAPDH*, as a negative control; were determined by qPCR (n=3, duplicates). Data show x-fold enrichment over the levels found in IgG immunoprecipitates.

The data from independent patient cohorts showed a clear downregulation of *H19* in HCC as a strongly inflammation-associated tumor type. This is why we investigated whether *H19* expression is in fact downregulated due to an inflammatory reaction. In fact, we found

a downregulation of *H19* in mice treated with the inflammation-inducing carcinogen DEN (n=5, 0.11 fold ± 0.04, p=0.0508, two-sample t-test).

Since *H19*`s expression is epigenetically controlled and LOI of *H19* has been found in some tumor types, we determined allelic expression of *H19* in human HCC by RFLP analysis employing the 32 samples from our patient cohort (**Figure 1D**). The experiment showed that nine of the patients were heterozygous and therefore informative for RFLP analysis (**Figure 3A**). LOI was observed in three normal as well as in three tumor tissues while the other tissues showed monoallelic expression (**Figure 3A**). These findings suggest that LOI is not involved in the deregulation of *H19* expression in HCC.

Besides its regulation by imprinting mechanisms *H19* expression is also distinctly regulated by the extent of its promoter methylation (Gao et al., 2002, Hadji et al., 2016). Thus, we analyzed the HCC methylation dataset GSE57956 regarding *H19* promoter methylation. This dataset also comprises the 39 samples for which *H19* expression was already determined (GSE57957, **Figure 1B**). The analysis revealed a distinctly decreased *H19* promoter methylation with high statistical significance in HCC *vs*. normal tissues (**Figure 3B**).

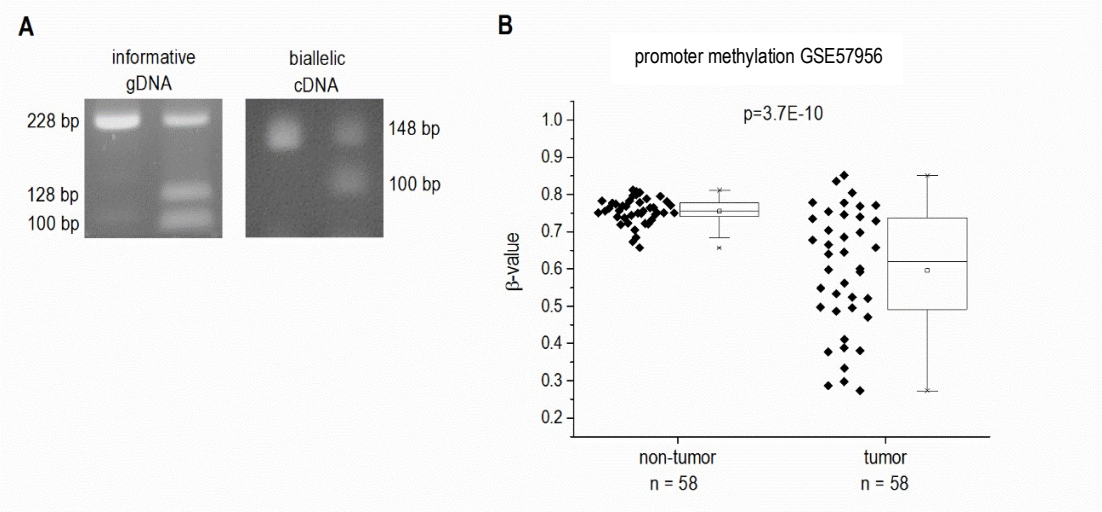

Figure 3: **Epigenetic state of the *H19* locus in human HCC tissues** (tumor) and non-tumorous tissues (non-tumor). (**A**) LOI was analyzed by RFLP analysis of 9 informative gDNA samples. Representative agarose gel with gDNA and cDNA before (left) and after digestion with the restriction enzyme AluI (right). (**B**) *H19* promoter methylation represented as fractional β-values from GEO dataset GSE57956 (each, n=58, Kolmogorov-Smirnov test).

Due to the downregulation of *H19* in HCC we aimed to determine functional aspects of *H19* overexpression in liver cancer cells. Thus, the colony formation assay - a well established method to determine in a cell population every cell's ability to undergo unlimited division (Franken et al., 2006) - was performed in three different stably *H19* overexpressing human hepatoma cell lines. All three cell lines we investigated, i.e. HepG2, Plc/Prf/5, and Huh7, showed that *H19* suppresses tumor cell survival, as indicated by a reduced colony number (**Figure 4A-D**).

To explore the potential role of *H19* in chemosensitivity, the three stably *H19* overexpressing cell lines were treated with either sorafenib or doxorubicin, two therapeutics which have clinically been tested for HCC treatment (Germano & Daniele, 2014, Lencioni et al., 2016). All stably *H19* overexpressing cell lines showed significantly increased sensitivity in the clonogenicity assay, suggesting a chemotherapy-sensitizing action of *H19* (**Figure 4A-D**). In order to distinguish reduced colony formation from chemosensitizing actions of *H19*, we also performed a different data normalization strategy, which can be found as supplemental **Figure S3**. Also this quantification confirmed a chemosensitizing action of *H19*.

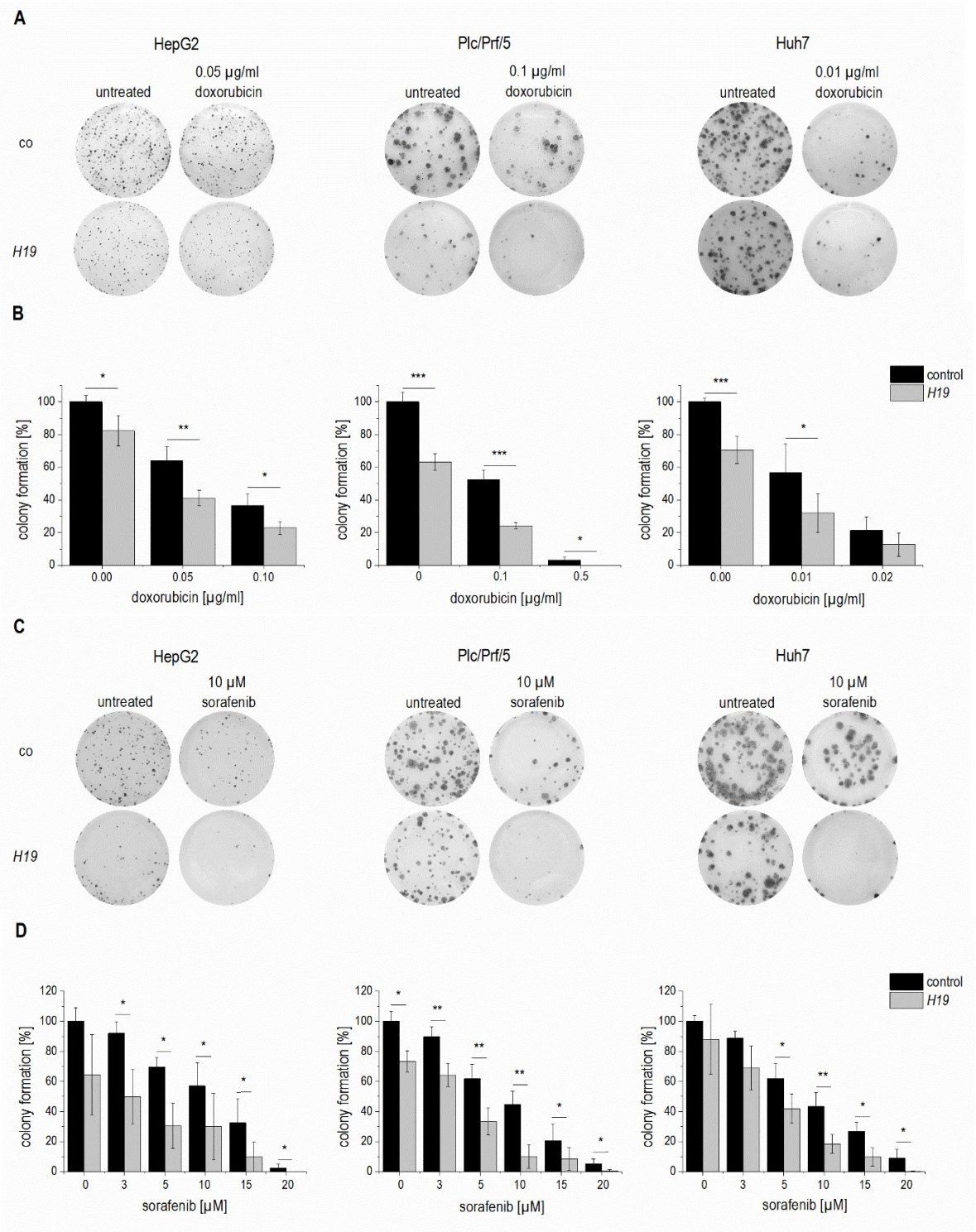

Figure 4: **Effect of *H19* overexpression on colony formation ability** in stably *H19* overexpressing (*H19*) and vector control (control, co) HepG2 (left panels), Plc/Prf/5 (middle panels), and Huh7 (right panels) cells. (**A, C**) Representative results of clonogenicity assays using untreated and (**A**) doxorubicin or (**C**) sorafenib treated hepatoma cells. (**B, D**) Colony formation ability of *H19* overexpressing cells normalized to their respective untreated control cells after (**B**) doxorubicin (n≥3, duplicates) or (**D**) sorafenib (n=3, triplicates) treatment. The p values were calculated by two-sample t-test or Mann-Whitney *U* test depending on the data distribution. * $p < 0.05$, ** $p < 0.01$, *** $p < 0.001$.

miR-675 is unlikely to be responsible for this action: while *H19* expression was significantly upregulated up to 65-fold ± 9.4 in stably transfected cells (n=3, triplicates, p=2.4E-6, two-sample t-test), two of the three cell lines showed no increase in *miR-675* expression (n=3, triplicates, each: HepG2: 9.2-fold ± 7.3, p=0.06, Mann-Whitney *U*; Huh7: 1.7-fold ± 1.0, p=0.36, Mann-Whitney *U*). Only stably *H19* overexpressing Plc/Prf/5 cells revealed slightly upregulated *miR-675* expression (n=3, triplicates, 1.5-fold ± 0.17, p=1.2E-3, two-sample t-test), while *H19* was 6.9-fold higher expressed (n=3, triplicates, 10.3-fold ± 2.3, p=1E-4). Concordantly, *ELAVL1* mRNA levels were not affected in all three cell lines upon *H19* overexpression (data not shown). In HepG2 and Huh7, the action was independent of the anti-apoptotic growth factor *IGF2* (Kessler et al., 2013), frequently regulated in parallel with *H19* due to the genomic vicinity and shared imprinting control region (Rachmilewitz et al., 1992): *IGF2* expression was unchanged in both stably *H19* overexpressing cell lines compared to empty vector-transfected controls (n=3, triplicates, each: HepG2: 1.4-fold ± 0.6, p=0.16, Mann-Whitney *U* test; Huh7: 1.1-fold ± 0.1, p=0.17, two-sample t-test). Still, in Plc/Prf/5 the expression of *IGF2* was significantly downregulated (n=3, triplicates, 0.3-fold ± 0.1, p=3.9E-6, two-sample t-test). Interestingly, Plc/Prf/5 exhibited a highly increased intrinsic chemoresistance compared to the other two cell lines.

In order to determine whether *H19* overexpression or knockdown directly affected cytotoxicity, cell viability was measured by MTT assay either in stably *H19* overexpressing cells or in cells with a gapmer-facilitated *H19* knockdown upon treatment with the cytotoxic agent doxorubicin. Cell viability with overexpressed or knocked down *H19* was largely unchanged in Plc/Prf/5 and Huh7 cells, although a few values reached statistical significance (**Figure 5A, B**). Only in *H19* gapmer-treated HepG2 cell viability was distinctly elevated compared to gapmer control cells (**Figure 5B**). These heterogenous findings suggested that *H19*-facilitated chemosensitization in Plc/Prf/5 and Huh7 is unlikely to depend on altered cell death but might rather depend on reduced proliferative capacity.

Therefore, proliferation measurements in *H19* overexpressing cells by Ki67 staining and subsequent FACS quantification were performed. Interestingly, while proliferation of HepG2 cells was unchanged in *H19* overexpressing cells, *H19* exhibited a significant proliferation-suppressing activity in Plc/Prf/5 and Huh7 cells (**Figure 5C**).

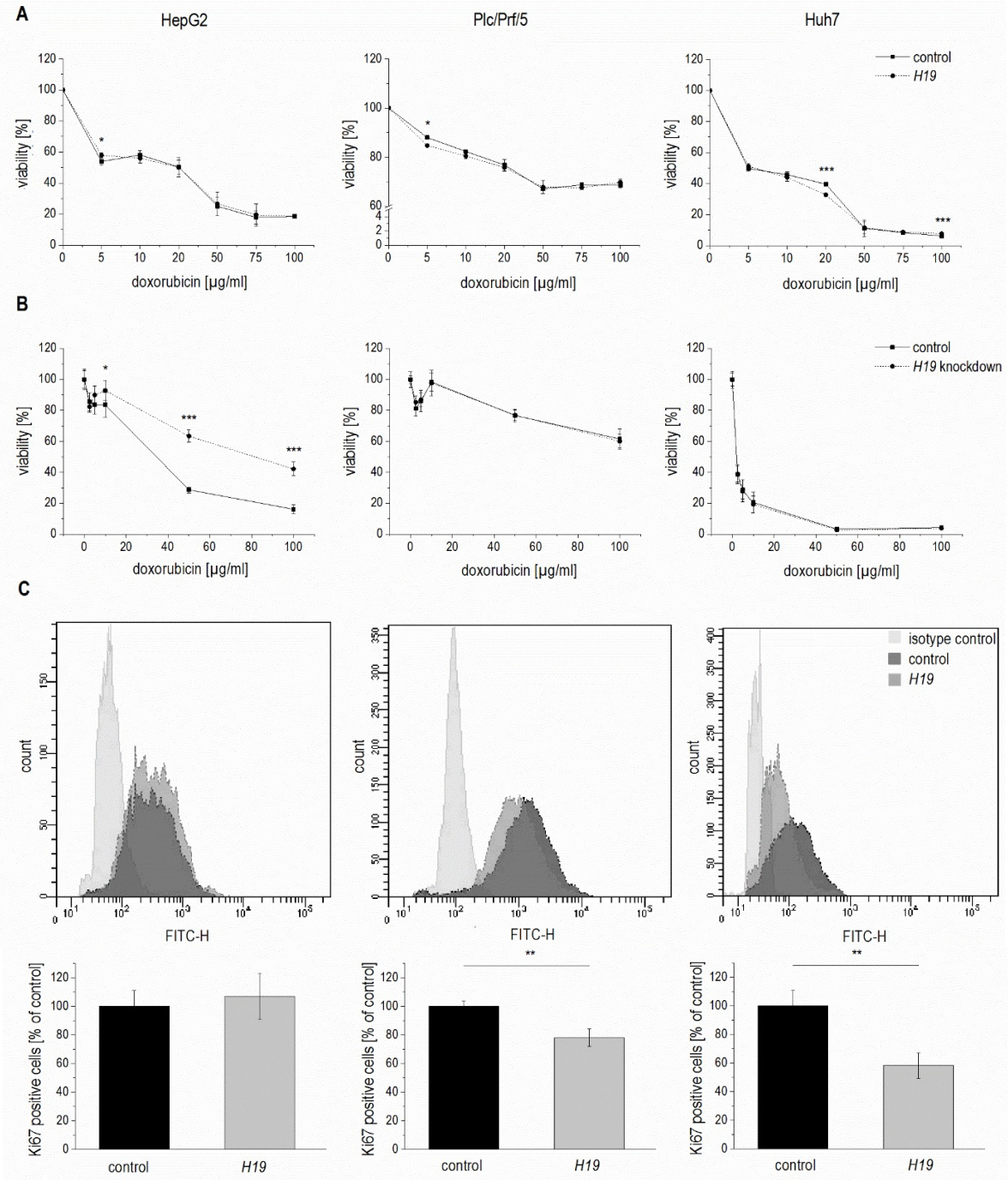

Figure 5: **Effect of *H19* overexpression and knockdown on cell viability and proliferation** in HepG2 (left panels), Plc/Prf/5 (middle panels), and Huh7 (right panels) cells. (**A**) Cytotoxicity assay with doxorubicin in stably *H19* overexpressing (*H19*) or vector control (control) cells normalized to their respective untreated control (n=2, sextuplicates). (**B**) Cytotoxicity assay with doxorubicin after transfection with *H19* gapmer (*H19* knockdown) and control gapmer (control) normalized to their respective untreated control (n=2, sextuplicates). (**C**) FACS analysis of the proliferation marker Ki67 in stably *H19* overexpressing (*H19*) and vector control cells (control). Representative histograms of Ki67 FACS analysis are shown (upper panels). Quantification of Ki67 positive cells expressed as percent of control (n≥2, triplicates). The p values were calculated by two-sample t-test or Mann-Whitney *U* test depending on the data distribution. * $p < 0.05$, ** $p < 0.01$, *** $p < 0.001$.

We hypothesized that a downregulation of *H19* might also contribute to chemoresistance as induced by repeated treatment with chemotherapeutics. To test this hypothesis, we established doxorubicin- and sorafenib-resistant HepG2, Plc/Prf/5, and Huh7 cell lines by repeated treatment with the drugs. Their chemoresistance was confirmed by directly comparing their sensitivity with non-resistant cells towards the drugs in a dose-response analysis (**Figure 6A, B**).

Quantifying *H19* expression by qPCR revealed that chemoresistance was associated with strongly downregulated *H19* expression in doxorubicin resistant cells (**Figure 6C**). However, *miR-675* was not significantly affected in any of the doxorubicin resistant cells (n=2, duplicates, each: HepG2-Dox-R: 0.52-fold ± 0.30, p=0.11, two-sample t-test; Plc/Prf/5-Dox-R: 0.71-fold ± 0.25, p=0.20, two-sample t-test; Huh7-Dox-R: 2.13-fold ± 0.86 p=0.16, two-sample t-test). Also in sorafenib resistant cell lines *H19* expression was significantly suppressed (**Figure 6C**).

Analysis of the *multidrug resistance protein 1* (*MDR1, ABCB1)* showed increased expression in all doxorubicin (n=2, duplicates, each: HepG2-Dox-R: 44.2-fold ± 8.8, p=6.2E-3, two-sample t-test; Plc/Prf/5-Dox-R: 1.8-fold ± 0.2, p=3.1E-2, Mann Whitney *U* test; Huh7-Dox-R: 6.7-fold ± 0.4, p=2.3E-4, two-sample t-test) and sorafenib resistant (n=3, triplicates, each: HepG2-Sora-R: 4.1-fold ± 0.7, p=4.5E-5, two-sample t-test; Huh7-Sora-R: 1.5-fold ± 0.2, p=3.4E-4, two-sample t-test) cell lines except for sorafenib resistant Plc/Prf/5 cells (n=3, triplicates, Plc/Prf/5-Sora-R: 0.6-fold ± 0.1, p=2.8E-6, two-sample t-test).

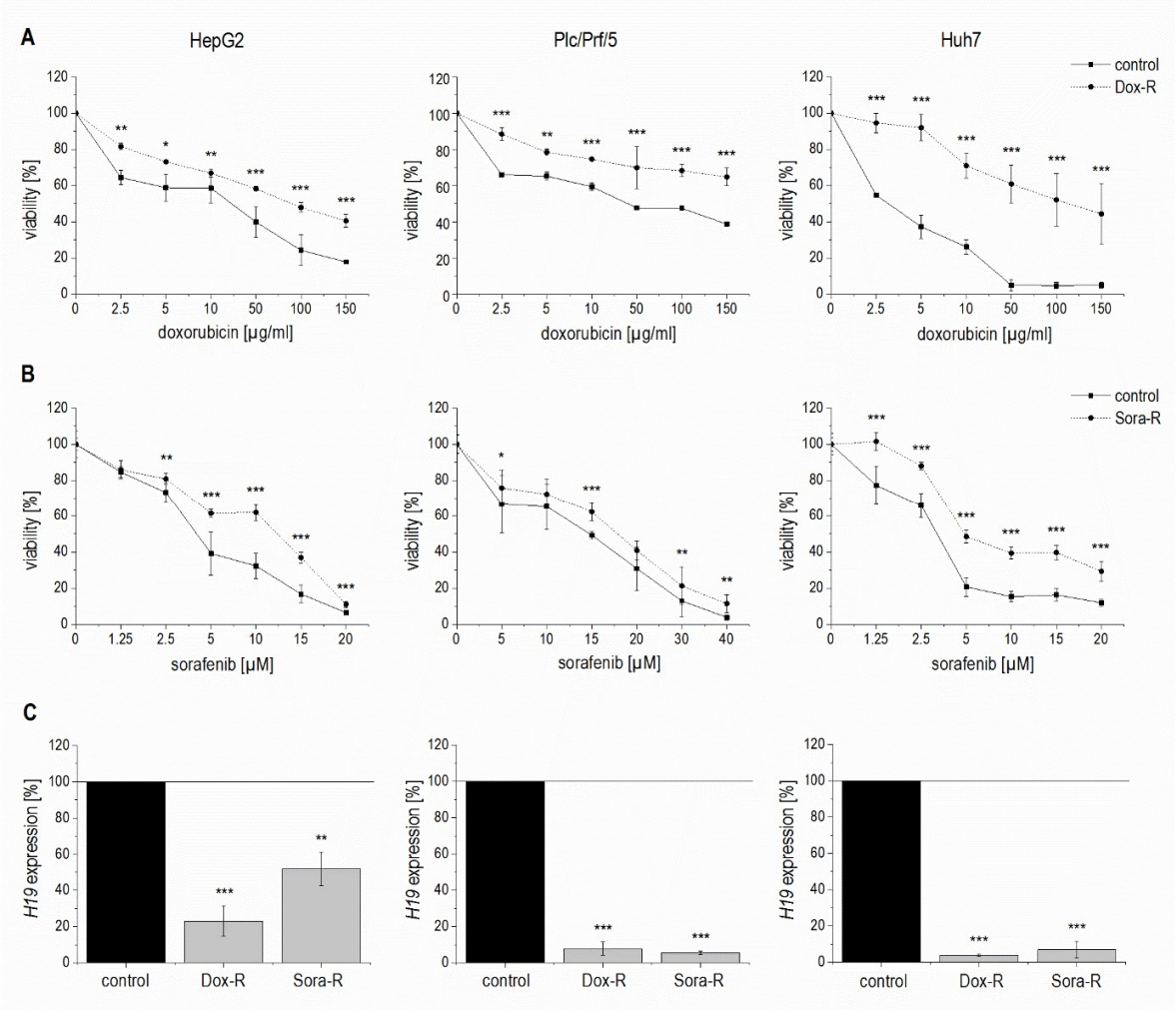

Figure 6: **Validation of chemoresistance and expression of *H19*** in sorafenib resistant (Sora-R), doxorubicin resistant (Dox-R), and chemosensitive (control) HepG2 (left panels), Plc/Prf/5 (middle panels), and Huh7 (right panels) cells. (**A, B**) Cytotoxicity assay normalized to the respective untreated control in (**A**) doxorubicin resistant cells (n=2, quintuplicates) and (**B**) sorafenib resistant cells (n=3, quintuplicates). (**C**) *H19* expression determined by qPCR in doxorubicin (n=3, duplicates) and sorafenib (n=3, triplicates) resistant cells normalized to control cells. The p values were calculated by two-sample t-test or Mann-Whitney *U* test depending on the data distribution. * $p < 0.05$, ** $p < 0.01$, *** $p < 0.001$.

To elucidate if altered promoter methylation is again linked to changed *H19* expression, the *H19* promoter methylation status was analyzed by local deep bisulfite sequencing (Bi-PROF) covering 23 CpG sites (**Figure 7A**) in the six chemoresistant cell lines. All three cell lines resistant for sorafenib showed elevated CpG methylation compared to their sensitive counterparts (**Figure 7C**): in Plc/Prf/5 cells 18 out of 23 investigated CpGs showed an elevated methylation; in HepG2 only five CpGs were hypermethylated (with

two hypomethylated), while most CpGs were hypermethylated in Huh7 cells. Almost all investigated CpGs in Huh7 also showed an elevated methylation in doxorubicin resistance. Interestingly, though, almost half of the CpGs were hypomethylated in doxorubicin resistant Plc/Prf/5 cells and an almost equal number of CpGs was hyper- or hypomethylated in doxorubicin resistant HepG2 (three up, four down) (**Figure 7B**). Taken together, although only Huh7 cells showed a consistent distinct hypermethylation, all three cell lines altered the methylation state of the *H19* promoter during chemoresistance. Most differences were found at CpG sites close to the transcription start site of *H19* (**Figure 7A-C**). Since these findings were highly reproducible in three independent biological replicates and similar to deregulated promoter methylation in HCC samples, we suggested an involvement of a deregulated promoter methylation in suppressed *H19* expression during chemoresistance.

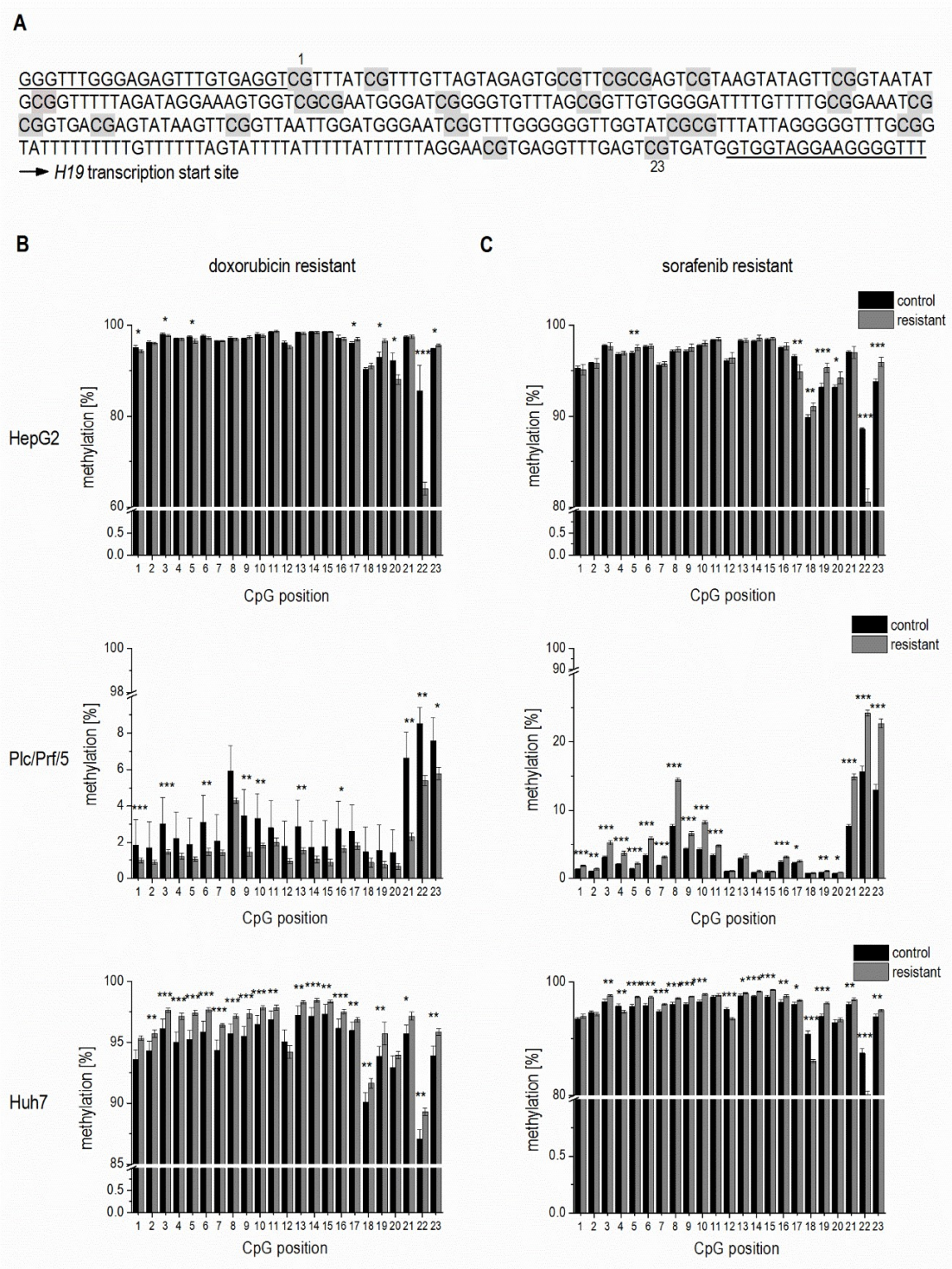

Figure 7: **Methylation state of the *H19* promoter in chemoresistant cells.** (**A**) Analyzed *H19* promoter region. The bisulphite-converted DNA sequence is shown; CpG sites 1-23 (Chr.11: 2,019,761 - 2,019,488) are labelled in grey; amplification primers are underlined. (**B, C**) Absolute methylation of 23 CpG sites located in the *H19* promoter in chemoresistent (resistant) and chemosensitive (control) HepG2 (upper panels), Plc/Prf/5 (middle panels), and Huh7 (bottom panels) cells analyzed by Bi-PROF (n=3, triplicates). (**B**) Doxorubicin resistant and (**C**) sorafenib resistant hepatoma cells. The p values were calculated by two-sample t-test or Mann-Whitney *U* test depending on the data distribution. * $p < 0.05$, ** $p < 0.01$, *** $p < 0.001$.

Therefore, we tested whether 5-azacytidine, a DNA demethylating agent, had an effect on chemosensitivity. As expected, the compound altered the CpG methylation of the *H19* promoter in two of the three cell lines as measured by SNuPE (**Figure 8A**) and significantly increased *H19* expression in the same two cell lines (**Figure 8B**) with the strongest effect being seen in HepG2 cells, which were also distinctly sensitized towards doxorubicin in the presence of 5-azacytidine (**Figure 8C**). This is why HepG2 cells were also employed for an approach to test whether *H19* overexpression can reverse chemoresistance. We in fact observed an increased induction of cell death by doxorubicin after transfecting chemoresistant cells with *H19* (**Figure 8D**). Since *H19* rather seemed to act on proliferative actions in Huh7, we overexpressed *H19* in chemoresistant Huh7 cells and in fact also observed chemosensitization (**Figure 8E**).

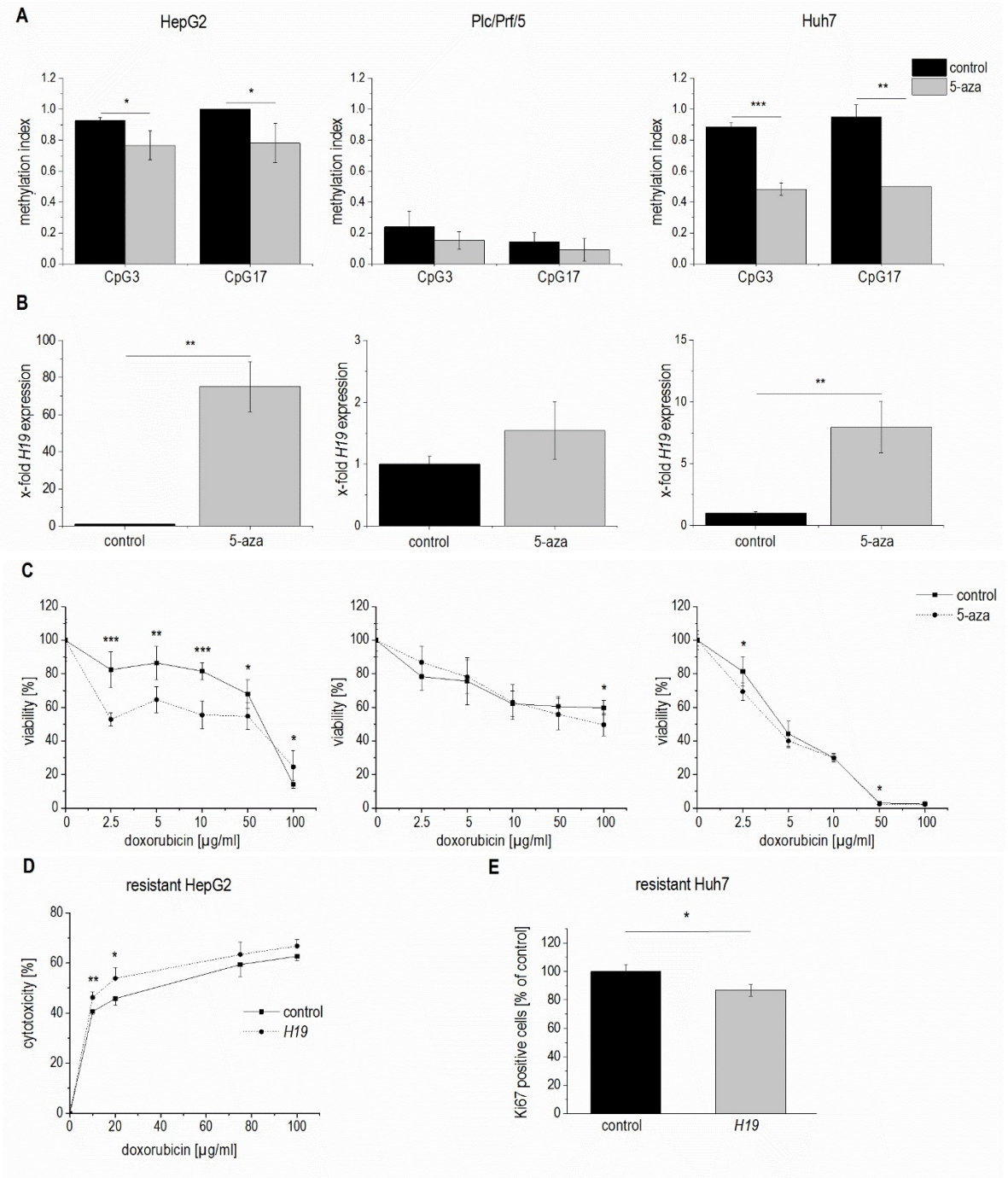

Figure 8: **Methylation dependent *H19* expression and its effect on cell viability and proliferation.** (**A-C**) HepG2 (left panels), Plc/Prf/5 (middle panels), and Huh7 cells (right panels) treated with 5-azacytidine (5-aza) and untreated control cells (control) were analyzed for (**A**) methylation index of two CpG sites of the *H19* promoter by SNuPE (n=2, duplicates), (**B**) *H19* expression determined by qPCR (n=2, duplicates), and (**C**) viability after treatment with doxorubicin by cytotoxicity assay (n=2, quintuplicates). (**D**) Cytotoxicity estimated by MTT assay after treatment with doxorubicin in doxorubicin resistant HepG2 either transiently overexpressing *H19* (*H19)* or vector control transfected (control) for 48 h normalized to the respective untreated control (n=2, triplicates). (**E**) Quantification of Ki67 positive cells by FACS in sorafenib resistant Huh7 either transiently overexpressing *H19* (*H19)* or vector control transfected (control) for 48 h and expressed as percent of control (each, n≥2, duplicates). The p values were calculated by two-sample t-test or Mann-Whitney *U* test depending on the data distribution. * $p < 0.05$, ** $p < 0.01$, *** $p < 0.001$.

The data on reduced expression of *H19* in human HCC and its chemosensitizing actions suggested tumor-suppressive actions of *H19* in HCC. To determine whether the presence of *H19* has an impact on tumorigenesis, wild-type and *H19* knockout animals were treated with the carcinogen DEN for 24 weeks. As expected (Nakatani et al., 2001), male mice developed more tumors than female mice (**Figure 9A**). In both sexes, *H19* knockout significantly increased the number of solid tumors. Trabecular tumors were only detectable in male *H19* knockout mice. The histological analysis also indicated that tumors of DEN-treated *H19* deficient mice were characterized by small cell changes representing dysplastic lesions found in the process of liver carcinogenesis (**Figure 9B**).

The proliferation-suppressive actions of *H19*, as shown in the two human hepatoma cell lines Huh7 and Plc/Prf/5, could also be verified *in vivo*: *H19* deficient long-term DEN-treated animals exhibited elevated Ki67 staining (**Figure 9C**). The expression of the oncogenic growth factor *Igf2* was not different between wild-type and *H19* knockout mice (**Figure 9D**), although *Igf2* expression was significantly induced upon DEN treatment in *H19* knockouts (**Figure 9D**).

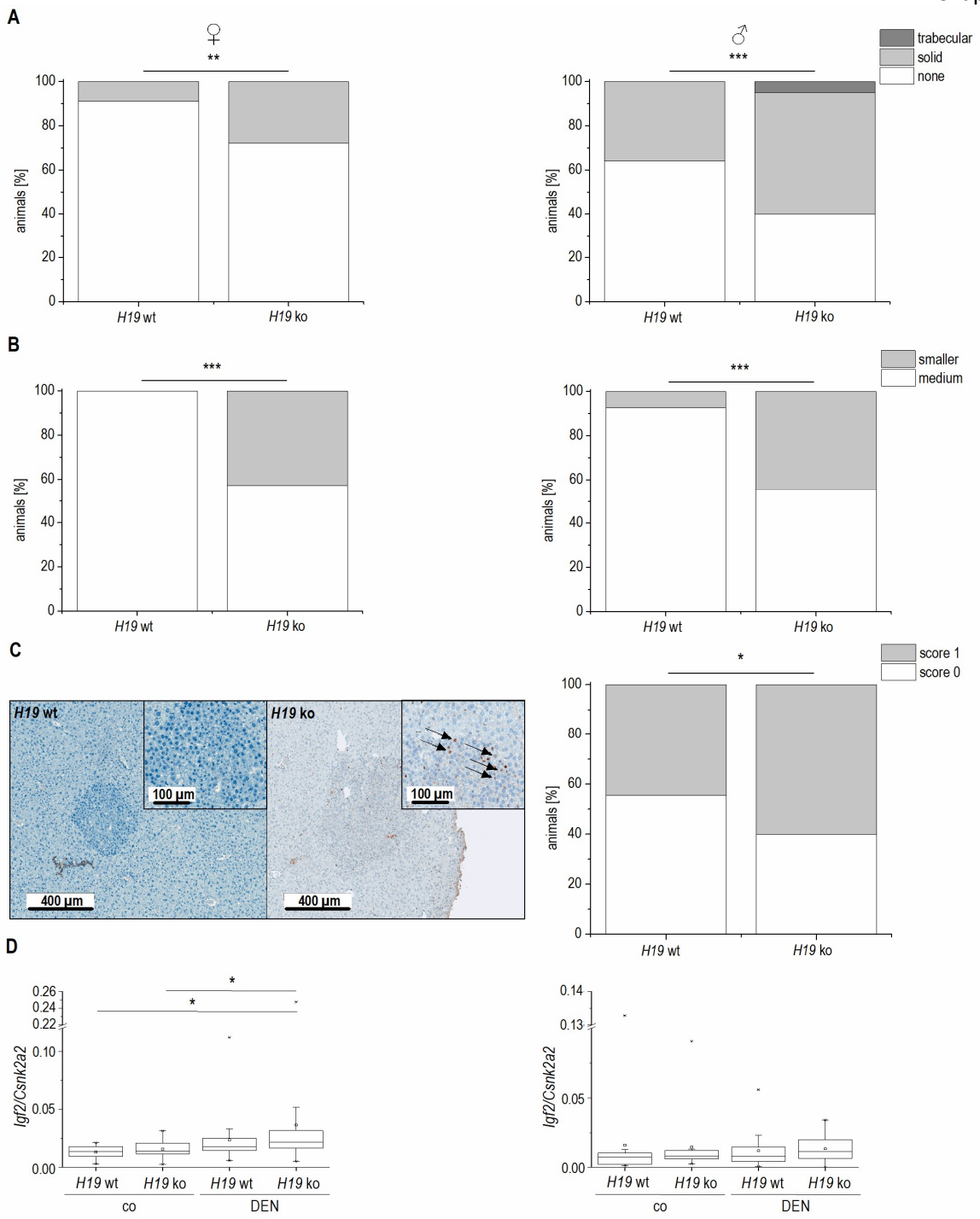

Figure 9: **Tumor development and characterization in long-term DEN-treated *H19* knockout (*H19* ko) compared to *H19* wild-type (*H19* wt) mice.** (**A**) Tumor development in female (left) and male (right) DEN-treated mice (female: *H19* wt n=22, *H19* ko n=25; male: *H19* wt n=25, *H19* ko n=20). (**B**) Predominant cell size in tumors of DEN-treated female (left) and male (right) mice. (**C**) Representative immunohistological staining of proliferation marker Ki67 (left, score 0: no proliferating cells detectable; score 1: less than 1% proliferating cells with brown stained nuclei (arrow)) and expression of Ki67 in tumors of male DEN-treated mice (right, *H19* wt n=9, *H19* ko n=10). (**A-C**) The p values were calculated by Chi-square test. * $p < 0.05$, ** $p < 0.01$, *** $p < 0.001$. (**D**) *Igf2* expression in female (left) and male (right) control (co) and DEN-treated (DEN) mice determined by qPCR (co n=10-23, DEN n=20-25). The p values were calculated by Mann-Whitney *U* test. * $p < 0.0125$.

Discussion

H19 was first described more than thirty years ago, at a time when the biological role of non-coding RNAs was still undefined (Pachnis et al., 1984). Since *H19* together with *Igf2* and *Igf2r* belongs to the first imprinted genes described (Bartolomei et al., 1991, Tilghman et al., 1993), most of the first two decades of *H19* research focused on its epigenetic regulation.

While mouse data show a distinct downregulation of *H19* expression in all tissues except for skeletal muscle after birth (Bartolomei et al., 1991), analysis of human samples shows well detectable *H19* levels in a wide array of tissue types (see e.g. http://medicalgenome.kribb.re.kr/GENT/). In fact, our analyses of four different patient cohorts comprising several hundreds of samples showed significantly higher *H19* expression in normal liver tissue compared to HCC tissue. These findings support the findings of a previous study that analyzed *H19* expression in 33 HCC tissues by qPCR compared to either adjacent non-tumor tissue or remote relative normal tissue (Zhang et al., 2013). As in our results, some HCC tissues of that study showed a dramatic increase in *H19* expression, but altogether *H19* was downregulated in HCC with high statistical significance. In fact, *H19* expression was significantly lower in invasive HCC samples (n=31) compared to non-invasive HCC tumors (n=41) (Zhang et al., 2013).

Interestingly, other studies reported elevated *H19* expression in HCC, e.g. Ariel et al., 1998, Fellig et al., 2005, Sohda et al., 1998, Wu et al., 2008. It has to be noted, however, that these studies investigated a considerably lower number of samples and/or used methods, such as *in situ* hybridization with limited quantitative reliability. Taking into account that all of our four patient cohorts, as well those investigated by Zhang et al. (2013), contained a small HCC patient subcohort with very high *H19* levels, it becomes clear that investigations of small patient cohorts can lead to contradictory findings.

Also reports on a potential LOI, i.e. biallelic *H19* expression, are of limited significance. In fact, some studies have reported LOI in a subset of HCC tissues ranging between 21% and 66%. The sample numbers of these studies, again, were very low (n=3 or n=23) (Kim & Lee, 1997, Wu et al., 2008). Our data revealed no difference in the imprinting status between normal and HCC tissue, with an equal proportion of samples exhibiting biallelic expression.

With the knowledge on a distinct regulation of *H19* expression by epigenetic modifications, we focused on potential alterations in the methylation state of the *H19* promoter. Indeed, we observed strongly altered *H19* promoter methylation in human HCC *vs*. normal liver tissue. While decreased promoter methylation is typically thought to be linked to elevated gene expression (Kong et al., 2011, Okada et al., 2005, Yang et al., 2017), a hypermethylated promoter region has also been associated with increased expression of some genes (Ding et al., 2009, Wagner et al., 2014). In fact, our data from a large HCC patient cohort suggested reduced promoter methylation correlating with reduced gene expression. Since HCC and other cancer types are associated with global DNA hypomethylation (Kim et al., 1994, Lin et al., 2001, Shen et al., 1998), the link between *H19* expression and promoter methylation remains unclear and should be clarified in further studies. We observed the same in the investigated doxorubicin resistant Plc/Prf/5 cell line, which showed both reduced *H19* expression and reduced promoter methylation compared to its chemosensitive counterpart. Interestingly, Plc/Prf/5 showed a much lower baseline promoter methylation compared to both HepG2 and Huh7 suggesting a differential epigenetic profile. Along this line, treatment of Plc/Prf/5 cells with the DNA demethylating agent 5-azacytidine neither affected *H19* promoter methylation nor *H19* expression.

All three sorafenib resistant cell lines as well as doxorubicin resistant Huh7 cells exhibited significantly elevated *H19* promoter methylation and at the same time significantly reduced *H19* expression compared to their respective chemosensitive counterparts. These findings are in line with anti-correlated methylation of the *H19* promoter and expression of *H19* as found by others (Gao et al., 2002, Hadji et al., 2016). Accordingly, treatment with the methyltransferase inhibitor 5-azacytidine reduced *H19* promoter methylation in both HepG2 and Huh7 cells and significantly increased *H19* expression, as previously observed in other cell types (Diesel et al., 2012). Interestingly, *H19* itself has been reported to increase DNMT3B-mediated cytosine methylation (Zhou et al., 2015a), suggesting diverse feedback processes.

Induction of *H19* by 5-azacytidine in HepG2 and Huh7 cells increased their chemosensitivity. This confirms findings in the literature on chemosensitizing actions of the compound (Festuccia et al., 2009). Chemoresistant versions of all three investigated cell lines showed downregulated *H19* expression. This suggested chemosensitizing

actions of *H19*. In fact, *H19* overexpression sensitized all three tested cell lines against both sorafenib and doxorubicin in clonogenicity assays. This effect seems to result from a synergistic effect of *H19*'s anti-proliferative and chemosensitizing actions. These findings on chemosensitizing action of *H19* are in contrast to a paper reporting chemoresistance induction by *H19* and linking it to induction of the multidrug resistance protein (*MDR1, ABCB1)* (Tsang & Kwok, 2007). Our investigations employing three different hepatoma cell lines could not verify these effects.

Chemosensitizing actions of *H19* in our hands seemed to differ between the different cell lines: in HepG2 cells, modulation of *H19* expression rather affected cell death, whereas in Huh7 cells, *H19* suppressed proliferation.

Our clonogenicity data suggest growth-suppressive actions of *H19* in the absence of any drug treatment. These data corroborate a hypothesis on the role of maternally expressed genes in embryonic development, already formulated in the early 1990s (Moore & Haig, 1991). It provided a model of parental conflict, in which the females, through maternally expressed genes, balance resources allocated to current and future offspring. This notion led to the anticipation that maternally expressed genes limit growth.

Our *in vivo* data employing *H19* knockout mice showed accelerated tumor development and more aggressive tumors. The literature contains two different *H19* knockout mouse models. One of them, the *H19Δ13* mouse, shows a distinct overgrowth phenotype (Leighton et al., 1995). This overgrowth is facilitated by a full re-expression of the adjacent *Igf2* gene from the normally silent maternal allele due to the combined 13 kb deletion of the *H19* gene and of the imprinting control region (Leighton et al., 1995). In the *H19Δ3* knockout model, which we used and which only carries a 3 kb deletion of the *H19* gene, only a slight re-expression of the maternal *Igf2* was detected in mesodermal tissue (Ripoche et al., 1997). With liver representing an endodermal tissue, *Igf2* expression is not increased in *H19Δ3* mice as previously reported (Ripoche et al., 1997) and confirmed by ourselves.

In contrast to our findings Matouk et al. (2007) suggested tumor-promoting actions of *H19* in a xenograft model employing Hep3B cells. Different aspects might be responsible for this discrepancy. While our model involves *in vivo* tumor induction, a xenograft model employs established tumor cells. So tumor-inducing actions can not be investigated with a xenograft model. Another aspect relates to the role of the immune defense since tumor

growth and development are strongly controlled by the immune system and xenograft models employ immune deficient mice. In 2008, Yoshimizu and colleagues investigated the role of *H19* and reported in fact that *in vivo* HCC development was accelerated in *H19* knockout mice (Yoshimizu et al., 2008).

There are several papers that regard *H19* as a promoter of cancer initiation and progression in a set of tumor types (Raveh et al., 2015). Interestingly, most of the *H19* actions in this context have been explained by *miR-675*, a microRNA embedded within *H19*. This microRNA targets a whole array of transcripts, such as *Igf1r*, *Smad1*, *Smad5*, *Cdc6*, *CDH-11* and *-13* , *RB1*, *RUNX1*, *NOMO 1* , *TGFBI*, *CALN1*, and *MITF* (reviewed in Raveh et al., 2015) and promotes cell proliferation (Yu et al., 2016). In contrast, a recently published paper clearly showed that *H19* reduces proliferation (Martinet et al., 2016).

Taken together, the discrepancy of effects of *H19* in the three different cell lines and the controversial literature data suggest a strong context dependency, and needs to be addressed in further studies.

While the expression of *H19* was always strongly affected in our chemoresistance and proliferation studies, *miR-675* showed minimal expression alterations. This is why we assume that in HCC it is rather *H19* than *miR-675*, which exerts biological actions. Interestingly, the RBP HuR/ELAVL1, which has immunoregulatory potential (e.g. Hoppstädter et al., 2016) and suppresses the processing of *H19* into *miR-675* (Keniry et al., 2012), is overexpressed in human HCC (Vazquez-Chantada et al., 2010, Zhu et al., 2015), but not differentially expressed in our chemoresistant cell lines. In fact, tumor-promoting actions by HuR/ELAVL1 *via* the inhibition of microRNA processing in HCC have recently been reported (Zhang et al., 2015).

Taken together, despite a small patient subcohort showing overexpressed *H19*, the majority of HCC tissues contained significantly reduced levels of this epigenetically regulated lncRNA. With its effect on HCC cancer cell growth, chemosensitivity, and carcinogenesis, *H19* shows tumor-suppressive actions. Restoring *H19* actions might therefore represent an interesting approach for future HCC therapy.

These data were published in: **Schultheiss C.S.**, Laggai S., Czepukojc B., Hussein U.K., List M., Barghash A., Tierling S., Hosseini K., Golob-Schwarzl N., Pokorny J., Hachenthal N., Schulz M., Helms V., Walter J., Zimmer V., Lammert F., Bohle R.M., Dandolo L., Haybaeck J., Kiemer A.K., and Kessler S.M. (2017) The long non-coding RNA *H19* suppresses carcinogenesis and chemoresistance in hepatocellular carcinoma. *Cell Stress*. 1(1), 37-54.

Chapter 4

H19 as a molecular sponge

Introduction

Micro RNAs (miRNAs) are single-stranded, 18-24 nucleotides long molecules that typically facilitate the translational repression or degradation of mRNA transcripts achieved by base pairing (Ambros, 2004). A dysregulation of miRNAs is associated with numerous diseases including HCC (Vrijens et al., 2015).

LncRNAs can act as molecular sponges or competing endogenous RNAs (ceRNA) to affect miRNA activity and thereby their target mRNA levels (Poliseno et al., 2010). In this way, ceRNAs exert strong regulatory control in so-called sponge or ceRNA networks. For *H19*, many interactions with miRNAs are already known, e.g. with the tumor-suppressive miRNAs *let-7*, *miR-200b*, and *miR-200c* (Kallen et al., 2013, Zhou et al., 2017), the proliferation associated *miR-194* (Wang et al., 2016b), and *miR-200a*, *miR-138*, and *miR-141*, which are involved in epithelial to mesenchymal transition (Liang et al., 2015, Zhou et al., 2015b). However, these previous studies about a sponge function of *H19* did not represent its capacity in the biological regulatory network system, where most mRNAs contain binding sites for different miRNAs and the miRNAs target more than one mRNA. In this study we analyzed whether *H19* acts as a ceRNA within a whole miRNA sponge network in HCC.

Results

A novel method called sparse partial correlation on gene expression (SPONGE) was developed by the group of Dr. Marcel Schulz (Department for Computational Biology and Applied Algorithmics, Max Planck Institut for Informatics (MPI-I), Saarland University) to predict the potential targets of *H19* in HCC progression (List et al., 2017). **Figure 1A** shows the generated *H19* network: the top 27 mRNAs are predicted targets for 28 miRNAs with more than three interactions among the target genes (prediction was performed by Dr. Marcel Schulz and Dr. Markus List from the MPI-I). 14 out of the 267 *H19* sponge targets were investigated by qPCR in stably *H19* overexpressing HepG2 cells to confirm the prediction. While most predicted targets showed a tendency of higher expression, only *H2AFY2*, *IKBKAP*, *NINL*, and *SMYD3* were significantly upregulated in *H19* overexpressing HepG2 compared to vector control cells. A significant downregulation was detected only for *AFP*, which was predicted to be a strong molecular sponge itself (**Figure 1B**).

The results of these experiments were essential for the assessment of the prediction quality of sensitivity correlation-based ceRNA interaction inference und fueled the development of a new version of SPONGE that takes several confounding factors into account, such as gene-gene correlation, which were neglected before.

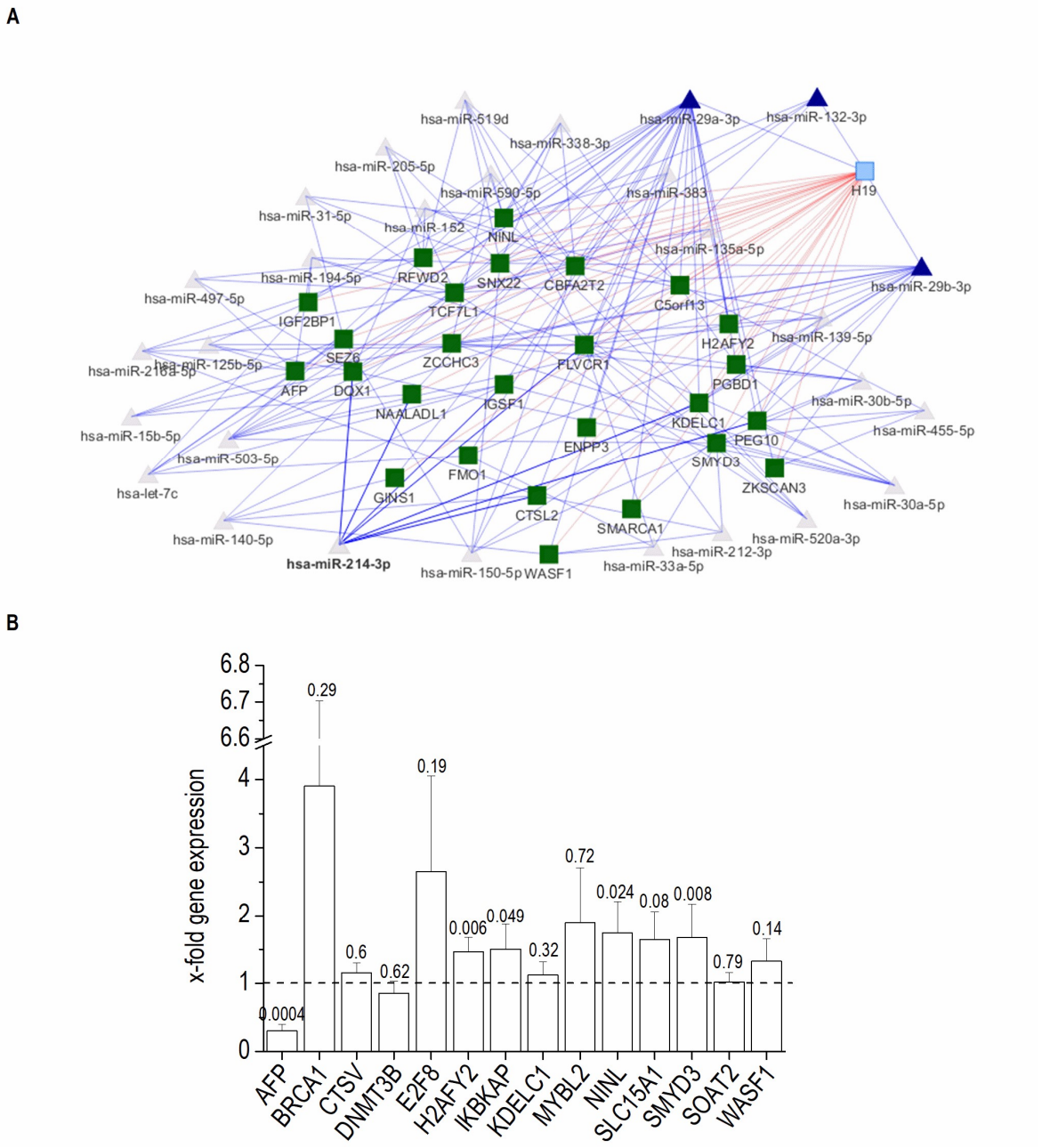

Figure 1: **Predicted *H19* sponge genes.** (**A**) Bioinformatically generated *H19* network including 27 mRNAs and 28 miRNAs. (**B**) Gene expression analysis of predicted *H19* sponge genes in *H19* overexpressing cells normalized to vector control cells (n=3) determined by qPCR. The p values were calculated by two-sample t-test for *DNMT3B, H2AFY2, IKBKAP, KDELC1, NINL, SLC15A1, SOAT2*, and *WASF1;* and Mann-Whitney *U* test for *AFP, BRCA1, CTSV, E2F8, MYBL2,* and *SMYD3.*

Discussion

The mRNA expression analyses of the predicted target genes in stably *H19* overexpressing cells validated the bioinformatical prediction: most of the analyzed *H19* targets were upregulated in stably *H19* overexpressing cells, with four of them reaching statistical significance. The majority of predicted miRNAs and target mRNAs in the generated network has not been associated with *H19* before. They include, for example, *SMYD3* encoding a histone methyltransferase that activates cell-cycle associated genes (Hamamoto et al., 2004). The influence of *H19* on genes facilitating epigenetic regulations is already known from the literature: in a complex together with methyl-CpG-binding protein domain 1 (MBD1) it interacts with histone lysine methyltransferases (Monnier et al., 2014). Further, Zhou et al. pointed out an interaction of *H19* with the DNA methyltransferase DNMT3B through an S-adenosylhomocysteine hydrolase resulting in a genome-wide alteration of DNA methylation in embryonic cells (HEK-293) (Zhou et al., 2015a). Our prediction also included *DNMT3B* as a target gene of *H19*, but the *DNMT3B* mRNA level was not significantly altered in stably *H19* overexpressing cells. Still, our results fit to the hypothesis that *H19* partly exerts its function by affecting genes involved in epigenetic processes.

The predicted targets further include *H2AFY2* and *BRCA1*, two genes encoding tumor suppressors (Bochar et al., 2000, Cantarino et al., 2013, Miki et al., 1994). They are associated with breast cancer development, but not linked to HCC so far. Both genes are upregulated in stably *H19* overexpressing hepatoma cells, with *H2AFY2* reaching statistical significance. These findings indicate that *H19* acts, in part, as an inducer of tumor suppressors.

Another interesting predicted *H19* target is *SLC15A1*. It belongs to the solute carrier (SLC) membrane transporters, which are often involved in drug resistance (Hediger et al., 2004). The upregulation of *SLC15A1* expression under stable *H19* overexpression – which caused chemosensitization in hepatoma cells – suggests a role of SLC15A1 in chemoresistance of HCC.

In summary, the experimentally verified bioinformatic predictions endorse the molecular sponge function as an important biological action of *H19* modulating the expression of

different gene classes including epigenetic regulators, tumor suppressors, and drug transporters.

Chapter 5

H19 proteins

Introduction

Although *H19* was described as a non-coding RNA because of the absence of a protein in mice (Brannan et al., 1990), Onyango and Feinberg identified in 2011 the *H19* opposite tumor suppressor (HOTS) protein (17 kDa) encoded by the *H19* antisense transcript. Furthermore, Gascoigne et al. composed in 2012 a suite of programs for the identification of novel proteins resulting, among others, in the detection of H19 sense protein (26 kDa). The HOTS protein is maternally expressed in primates, while no open reading frame (ORF) for this protein was found in mice (Onyango & Feinberg, 2011). Onyango and Feinberg reported a tumor growth inhibitiory function of HOTS, which was not confirmed by others so far.

The expression of H19 sense protein was identified only in fetal liver, a myelogenous leukemia cell line (K562), and in testes (Gascoigne et al., 2012), while functional analyses of this protein have not been performed to date.

In this chapter, the existence of HOTS and H19 sense protein is reported in three different hepatoma cell lines. Investigations of their expression in long-term doxorubicin- and sorafenib-treated cells, as well as in chemosensitized hepatoma cells were undertaken to clarify the function of these proteins during chemoresistance.

Results

Investigations of HOTS and H19 sense proteins in HepG2, Plc/Prf/5, and Huh7 cells showed detectable baseline expression (**Figure 1A**). While the basal *H19* mRNA expression showed highly significant differences between the hepatoma cell lines (4,539-fold higher *H19* mRNA expression in Plc/Prf/5 than in HepG2) (**Figure 1B**), the H19 proteins were rather equally expressed.

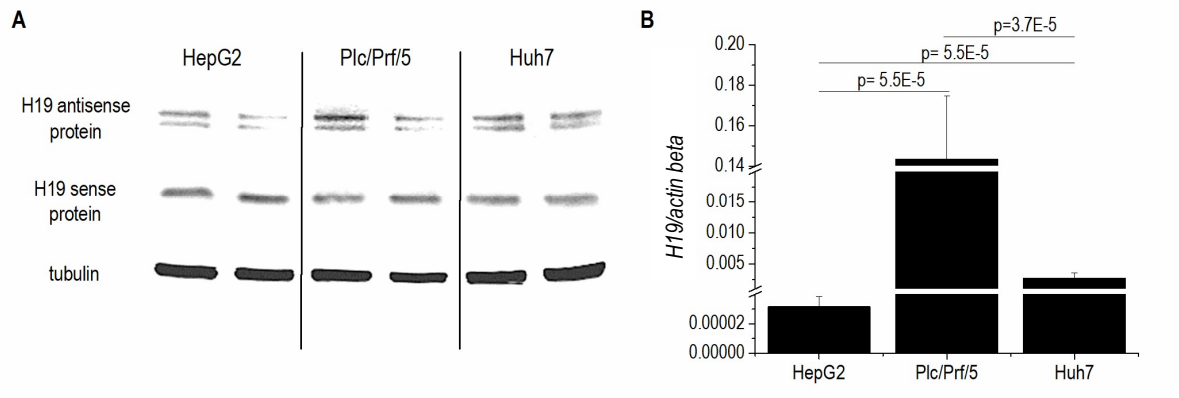

Figure 1: **H19 protein and *H19* mRNA baseline expression.** (**A**) Basal levels of H19 sense and H19 antisense protein in HepG2, Plc/Prf/5, and Huh7 cells. A representative Western blot is shown (n=3, duplicates). (**B**) Baseline *H19* mRNA expression determined by qPCR in HepG2, Plc/Prf/5, and Huh7 cells (n=5, duplicates). The p values were calculated by Mann-Whitney *U* test.

H19 proteins in stably *H19* overexpressing cells

In order to clarify whether *H19* mRNA or the proteins derived from the *H19* locus were responsible for the chemosensitizing action in the stably *H19* overexpressing cell lines, potential changes in protein expression were determined. The expression of H19 sense protein was not altered in any of the stably *H19* overexpressing cells (**Figure 2A**). The HOTS (H19 antisense) protein level was only increased in stably *H19* overexpressing HepG2 cells and not elevated in the stably *H19* overexpressing Plc/Prf/5 and Huh7 cells (**Figure 2B**). Hence, due to minor or no alterations of the protein levels, it seems rather unlikely that the increased chemosensitivity of stably *H19* overexpressing cells was facilitated by H19 sense or HOTS protein.

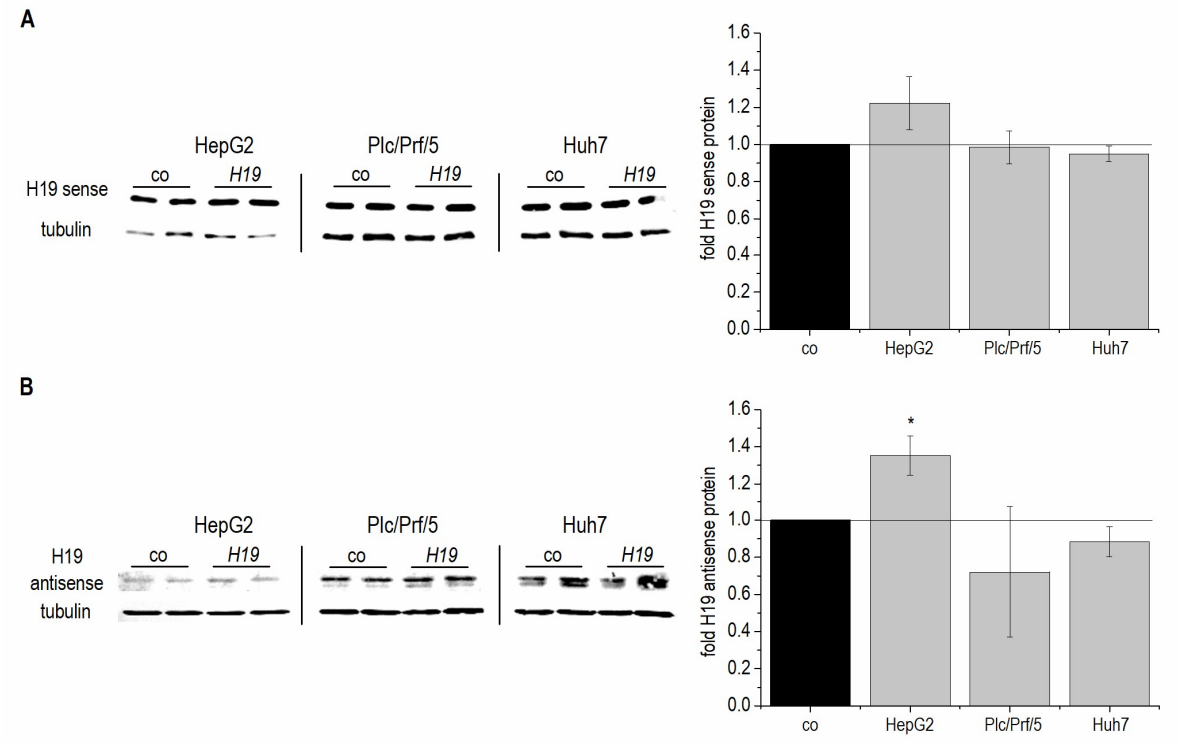

Figure 2: **Effect of stable *H19* overexpression on** (**A**) **H19 sense and** (**B**) **H19 antisense protein levels.** Representative Western blots are shown (left panels). H19 sense and H19 antisense protein levels in *H19* overexpressing (*H19*) HepG2, Plc/Prf/5, and Huh7 cells compared to respective control cells (co) are normalized to tubulin (right panels, n=2, duplicates).

H19 proteins in chemoresistance

To elucidate the role of H19 proteins in chemoresistance, their levels were examined in doxorubicin and sorafenib resistant cells. All doxorubicin resistant cell lines exhibited a downregulation of the H19 sense protein compared to the respective chemosensitive cell lines. The H19 antisense protein was significantly downregulated in HepG2 and Plc/Prf/5 cells, while the data did not reach statistical significance in Huh7 cells (**Figure 3**).

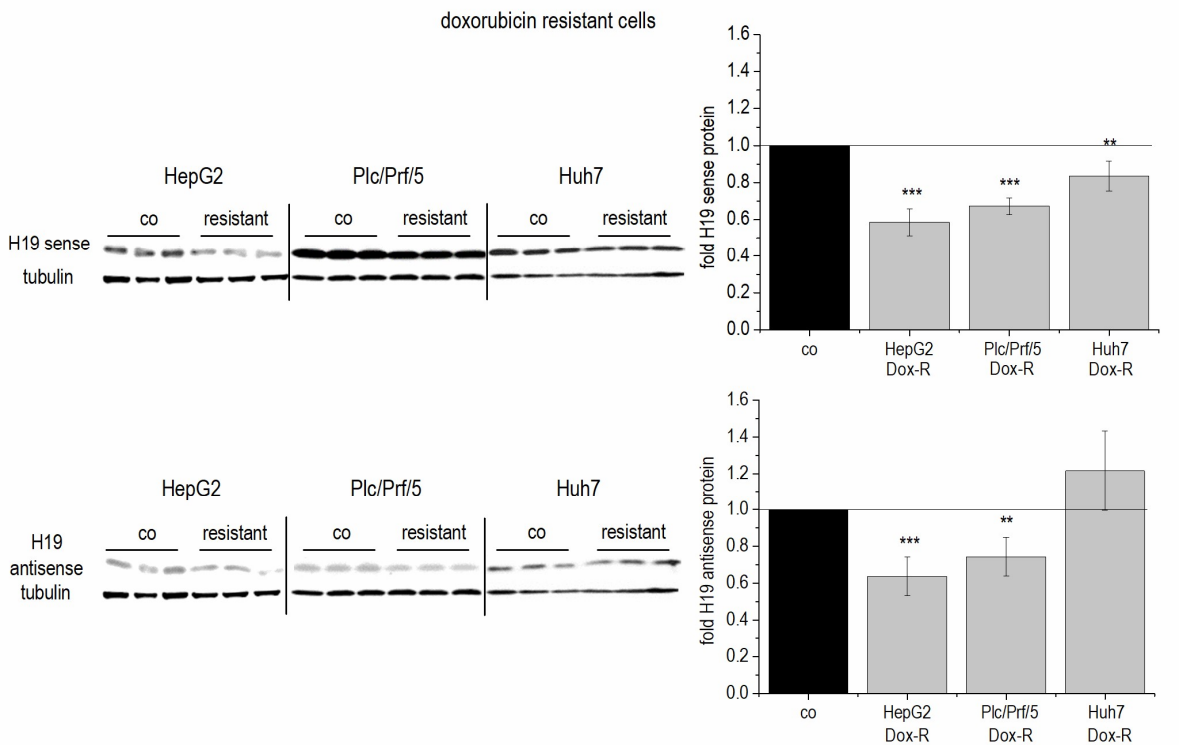

Figure 3: **Influence of doxorubicin resistance on H19 sense and H19 antisense protein expression**. Representative Western blots are shown (left panels). H19 sense (upper panels) and H19 antisense (lower panels) protein levels in doxorubicin resistant (resistant, Dox-R) HepG2, Plc/Prf/5, and Huh7 cells compared to respective control cells (co) were normalized to tubulin (right panels, n=3, triplicates).

Regarding sorafenib resistance, neither alteration of H19 sense nor antisense protein expression could be detected (**Figure 4**). These findings suggest a potential role of H19 proteins in doxorubicin resistance but not in sorafenib resistance.

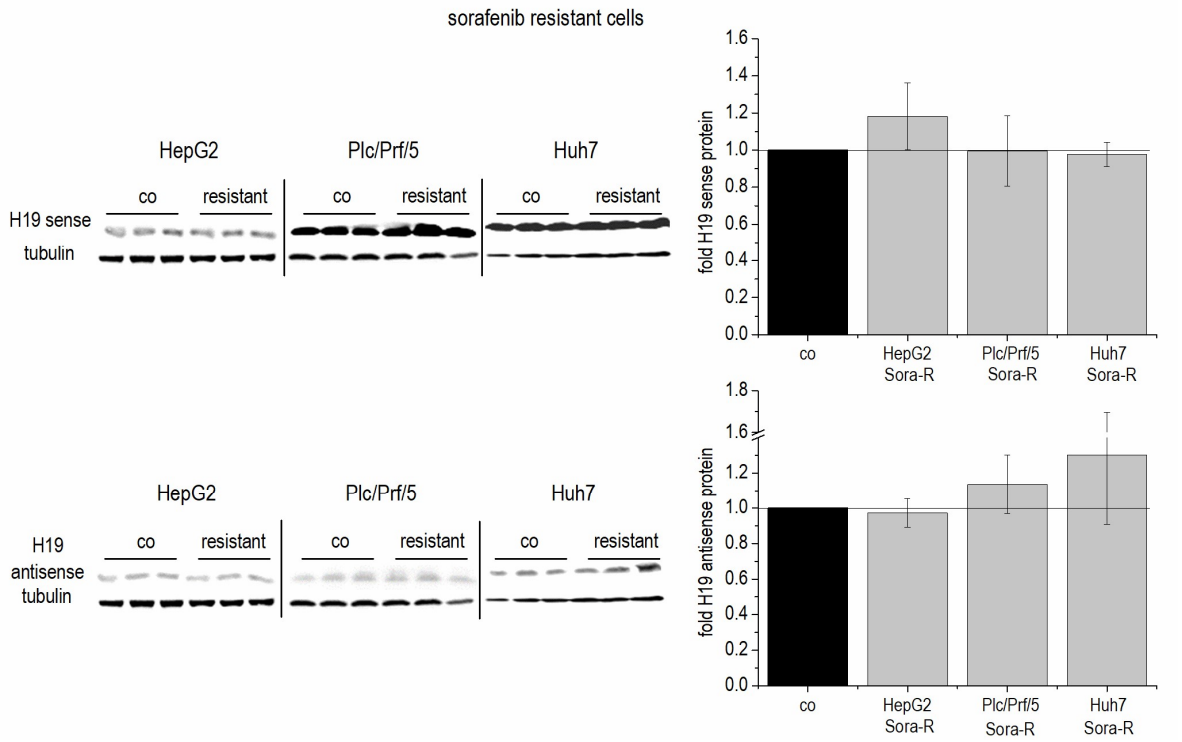

Figure 4: **Influence of sorafenib resistance on H19 sense and H19 antisense protein expression**. Representative Western blots are shown (left panels). H19 sense (upper panels) and H19 antisense (lower panels) protein levels in sorafenib resistant (resistant, Sora-R) HepG2, Plc/Prf/5, and Huh7 cells compared to respective control cells (co) were normalized to tubulin (right panels, n=3, triplicates).

Discussion

The imprinted *H19* locus contains one of the first identified long non-coding RNA genes (Brannan et al., 1990). However, our results confirmed the presence of the H19 sense and HOTS proteins in the human system as reported by Gascoigne et al. and Onyango and Feinberg (Gascoigne et al., 2012, Onyango & Feinberg, 2011): to our knowledge the expression of H19 proteins in the hepatoma cell lines HepG2, Plc/Prf/5, and Huh7 was shown for the first time.

A correlation between *H19* mRNA and H19 sense protein expression could not be identified: while *H19* mRNA was overexpressed up to 65-fold in the stably transfected cells and downregulated in sorafenib-resistant cells, no significant alteration in the expression of the H19 sense protein was detectable. Further, the hepatoma cell lines showed highly different baseline levels of *H19* mRNA, but the H19 sense protein was almost equally expressed. These findings gave a hint towards a potential post-transcriptional inhibition of translation into H19 sense protein.

The HOTS protein was significantly downregulated during doxorubicin resistance in two of three cell lines. This finding is in line with the tumor-suppressive function of HOTS described by Onyango and Feinberg (Onyango & Feinberg, 2011).

Interestingly, HepG2 cells overexpressing *H19* mRNA revealed a significantly upregulated HOTS expression, whereas doxorubicin resistant HepG2 cells, in which the *H19* mRNA expression was significantly downregulated, showed lower HOTS levels. This positive correlation between the expression of a mRNA and a protein derived from the antisense transcript of this mRNA has not been described so far and has to be further investigated.

The expression of H19 proteins was not altered in stably *H19* overexpressing cells, which showed increased sensitivity towards doxorubicin and sorafenib treatment (as shown in chapter 3). Thus, the H19 proteins are unlikely to be responsible for the chemosensitizing actions of *H19* overexpression. These findings underline our hypothesis that *H19* mRNA itself - and not the proteins derived from the *H19* locus - caused the sensitization of hepatoma cells.

Materials and Methods

1. Materials

Materials are listed in **Table 1**. All other chemicals were obtained from Roth (Karlsruhe, Germany) or Sigma-Aldrich (Taufkirchen, Germany).

Table 1: **Materials and respective order information**.

Material	Company	City	Country
10x buffer C	Solis BioDyne	Tartu	Estonia
10x Hot Star *Taq*-buffer	Qiagen	Hilden	Germany
10x *Taq*-buffer	GenScript	Piscataway	USA
7x Complete protease inhibitor	Roche	Mannheim	Germany
5x HOT FIREPol Evagreen qPCR Mix Plus	Solis BioDyne	Tartu	Estonia
AluI	Fermentas	St. Leon-Rot	Germany
Ambion linear acrylamide	Invitrogen	Darmstadt	Germany
Anti-human RAC1, mouse IgG clone 23A8	Merck Millipore	Darmstadt	Germany
Biotin- and digoxin labeled probes	Exiqon	Vedbaek	Denmark
ddCTP	Larova	Jena	Germany
ddTTP	Larova	Jena	Germany
DNA free Kit	Invitrogen	Darmstadt	Germany
dNTPs mix	GenScript	Piscataway	USA
Exonuclease I/SAP shrimp alkaline phosphatase	USB Corporation	Cleveland	USA
EZ DNA Methylation-Gold Kit	Zymo Research	Freiburg	Germany
Flow cytometry buffer (FCB)	BD Biosciences	Heidelberg	Germany
Geneticin	Invitrogen	Darmstadt	Germany
Glass membrane slides	Leica Microsystems CMS	Wetzlar	Germany
Glutathione sepharose beads	GE Healthcare Life Sciences	Freiburg	Germany
High-Capacity cDNA Reverse Transcription Kit	Invitrogen	Darmstadt	Germany
HiSpec Buffer	Qiagen	Hilden	Germany
Hot Star *Taq*-polymerase	Qiagen	Hilden	Germany
Immobilon FL-PVDF membrane	Rockland Immunochemicals Inc.	Limerick	USA
INTERFERin	Polyplus-Transfection	Illkirch	France
IRDye 800CW conjugated goat, anti-mouse IgG	Li-COR Biosciences	Bad Homburg	Germany
IRDye 800CW conjugated goat, anti-rabbit IgG	Li-COR Biosciences	Bad Homburg	Germany
jetPEI Hepatocyte reagent	VWR International GmbH	Darmstadt	Germany
LNA gapmers	Exiqon	Vedbaek	Denmark
$MgCl_2$ solution	Qiagen	Hilden	Germany

miCURY LNA microRNA ISH Optimization Kit (FFPE)	Exiqon	Vedbaek	Denmark
Nuclear Fast Red Counterstain	Vector Laboratories	Burlingame	USA
PKD buffer	Qiagen	Hilden	Germany
Primers	Eurofins Genomics	Ebersberg	Germany
Proteinase K	Roche	Mannheim	Germany
QIAamp DNA FFPE Tissue Kit	Qiagen	Hilden	Germany
QIAzol lysis reagent	Qiagen	Hilden	Germany
RAC1 inhibitor NSC23766	R&D Systems	Wiesbaden	Germany
Recombinant DLK1	R&D Systems	Wiesbaden	Germany
RNaseOUT	Invitrogen	Darmstadt	Germany
RNeasy FFPE Kit	Qiagen	Hilden	Germany
Rockland Blocking Buffer	Rockland Immuno-chemicals Inc.	Limerick	USA
Sorafenib	Biomol GmbH	Hamburg	Germany
Taq-polymerase	GenScript	Piscataway	USA
TermiPol	Solis BioDyne	Tartu	Estonia
Tsp509I	New England Biolabs	Ipswich	USA

2. Mice

2.1 Animal welfare

All animal procedures were performed in accordance with the local animal welfare committee (approval number 36/2013). Mice were kept under controlled conditions regarding temperature, humidity, 12 h day/night rhythm, and food access.

2.2 Generation of *p62* transgenic *H19* knockout mice

Female C57BL/6J mice carrying a liver enriched activator protein under control of a tetracycline transactivator (tTA) (Tybl et al., 2011) (*LT2* positive mice) were crossed with male 129sv *H19* knockout (*H19* ko) mice, in which a 3 kb region of the *H19* gene was replaced by a neomycin resistance gene (neo) cassette (Gabory et al., 2010, Ripoche et al., 1997). The littermates carried the *H19* ko on the maternal allele, whereas the paternal allele remained wild-type (wt). Female *LT2* positive *H19* ko mice were bred with male DBA2J *p62* transgenic mice, in which *p62* expression was repressed by the TRE-CMV_{min}

promoter. In the obtained *p62* positive *LT2* positive mice, the tetracycline transactivator derepressed the TRE-CMV_{min} promoter and thereby allowed human p62 expression in mouse livers (*p62* tg). The following four genotype groups were generated: *H19* wt/*p62* wt, *H19* ko/*p62* wt, *H19* wt/*p62* tg, and *H19* ko/*p62* tg mice.

2.3 Genotyping

For genotyping of mice, an ear biopsy was taken and digested with proteinase K (0.2 mg/ml) in *Taq*-buffer at 55°C. After total lysis of the tissue, PCRs were performed using the following conditions and primer sequences (**Table 2**):

H19 wild-type

Reaction mixture		PCR program		
Evagreen	4 µl	94°C	5 min	
Primer (10 µM)	0.4 µl	94°C	45 sec	
H_2O	11.2 µl	58°C	45 sec	30x
Template DNA	4 µl	72°C	1 min	
		72°C	7 min	

Neo

Reaction mixture		PCR program		
10x*Taq*-buffer	5 µl	95°C	5 min	
$MgCl_2$ (50 mM)	1.5 µl	66°C	1 min	
dNTPs (10 mM)	1 µl	72°C	1 min	
Primer (10 µM)	1 µl	95°C	20 sec	
Taq-Polymerase	0.25 µl	66°C	30 sec	35x
H_2O	39.25 µl	72°C	1 min	
Template DNA	2 µl	72°C	10 min	

p62/tTA

Reaction mixture		PCR program		
10x*Taq*-buffer	2 µl	94°C	5 min	
dNTPs (10 mM)	0.25 µl	94°C	30 sec	35x
Primer (10 µM)	1 µl	57°C	30 sec	
Taq-Polymerase	1 µl	72°C	30 sec	
H_2O	11.75 µl	72°C	5 min	
Template DNA	1 µl			

Table 2: **Primer information for genotyping PCRs.**

Target	**Forward primer sequence 5' → 3'**	**Reverse primer sequence 5' → 3'**	**Product size**
Neo	GTGTTCCGGCTGTCAGCGCA	GTCCTGATAGCGGTCCGCCA	500 bp
H19 wt	CCATCTTCATGGCCAACTCT	AATGGGGAAACAGAGTCACG	150 bp
tTA	GTGCAGAGCCAGCCTTCTTA	CCTCGATGGTAGACCCGTAA	150 bp
p62	CATCAAACAGCTGGCGAGAT	GTGCCCGATAATTCTGACGA	450 bp

2.4 Treatment

Short-term DEN experiment

For the short-term experiment nine week old wild-type male C57BL/6J mice were intraperitoneally injected with either 100 mg/kg body weight DEN or NaCl as sham-control (each, n=5). Mice were sacrified 48 h after the injection (Kessler et al., 2015, Naugler et al., 2007, Park et al., 2010).

H19 ko/*p62* tg mice (long-term DEN experiment)

Mice were intraperitoneally injected with 5 mg/kg body weight DEN diluted in saline at the age of two weeks and sacrificed 24 weeks after injection. Untreated mice served as control (**Figure 1**). Analyses were performed with the whole number of experimental mice unless stated otherwise.

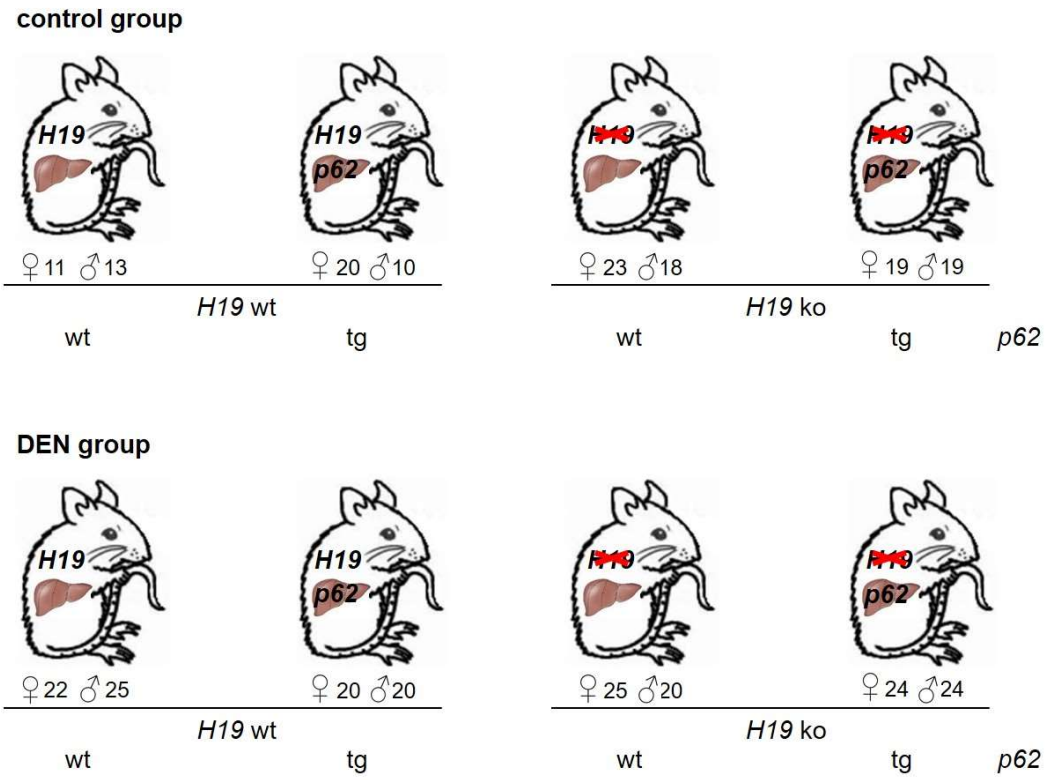

Figure 1: **Genotype and treatment groups of experimental mice.**

2.5 Preparation of liver tissue

Livers were excised and weighed. Each lobe of the liver was divided into two pieces. One piece was flash-frozen in liquid nitrogen and stored at -80°C, the other one was fixed in PBS-buffered formalin and embedded in paraffin for histological analyses. One piece of the left lateral lobe was used for RNA extraction.

2.6 Histological and immunohistological analyses of mouse livers

5 µm and 0.5 µm slices from paraffin-embedded mouse livers were cut with a microtome (Slee, Mainz, Germany). 5 µm slices were stained either with hematoxylin-eosin (H&E) for the detection of tumors, inflammation, and apoptosis, or with Sirius Red to analyze fibrosis. 0.5 µm slices were used for the immunohistological staining of the HCC marker glutamine synthetase (GS), tumor specific surface antigen Golgi membrane protein 73 (Gp73), and proliferation marker Ki67. Antibodies and immunostaining conditions are listed in **Table 3**. The scoring was performed in collaboration with Prof. Dr. Dr. Johannes Haybäck from the Institute of Pathology (Medical University of Graz) and the Department of Pathology (Medical Faculty, Otto-von-Guericke University Magdeburg) blinded to experimental conditions.

Table 3: **Antibodies and conditions for immunostaining.**

Antibody	Product no.	Company	Demasking	Dilution	Detection
anti-Gp73	sc-48011	Santa Cruz, Heidelberg, Germany	citrate buffer pH 6.0, microwave	1:200	rabbit-anti-goat (#A50-204A, Bethyl), Dako Envision, DAB
anti-GS	AB1783	Millipore, Temecula, CA, USA	CC1 mild (Ventana), 30 min	1:5,000	Ultra View (Vantana), DAB
anti-Ki67	PA0230	Novocastra, Newcastle, UK	citrate buffer pH 6.0, microwave	1:1,000	Dako Endvision, AEC

3. Cell culture

3.1 Cell lines

HepG2, Huh7, and Plc/Prf/5 cells were cultured in RPMI-1640 medium with 10% fetal calf serum, 1% penicillin/streptomycin, and 1% glutamine at 37°C and 5% CO_2. All cell lines were authenticated by the DSMZ (Braunschweig, Germany).

3.2 *H19* knockdown

H19 knockdown was performed in 96-well plates with 21,000 HepG2, 17,500 Plc/Prf/5, or 14,000 Huh7 cells in 140 µl medium per well and antisense LNA gapmer for *H19* (5'-GACTTAGTGCAAATTA-3') or negative control A (5'-AACACGTCTATACGC-3') (gapmer concentration per well: HepG2: 0.04 µM, Plc/Prf/5: 0.02 µM, and Huh7: 0.03 µM) using INTERFERin transfection reagent (35 µl mastermix per well) as recommended by the manufacturer. The negative control shows no homology to any known microRNA, lncRNA, or mRNA. *H19* knockdown was confirmed by qPCR.

3.3 Stable *H19* overexpression

Stable *H19* overexpression in hepatoma cells was established by transfection with a vector (pcDNA3.1(+)_A009) containing the synthetic *H19*-sequence or the empty vector as control (**Suppl. Figure S1**) (Ref. No.: 1381790, Life Technologies, California, USA). Vector synthesis and sequencing were performed by Life Technologies.
50.000 hepatoma cells in 1 ml medium per well were seeded into 24-well plates and transfected 24 h after seeding using jetPEI Hepatocyte reagent as recommended by the manufacturer. Resistance to geneticin was conferred by the neomycin resistance gene (Neo (R)). The geneticin concentrations used for selection were determined by MTT assay (HepG2 and Plc/Prf/5 cells: 500 µg/ml, Huh7 cells: 125 µg/ml).
Transient *H19* overexpression in chemoresistant cells was performed accordingly, but cells were treated with doxorubicin or sorafenib (HepG2-Dox-R: 2 µg/ml; Huh7-Sora-R: 2.5 µM) simultaneously with the plasmid transfection for 48 h or 72 h. *H19* overexpression was confirmed by qPCR.

3.4 Establishment of chemoresistant cells

Doxorubicin resistant (HepG2-Dox-R, Huh7-Dox-R, and Plc/Prf/5-Dox-R) and sorafenib resistant (HepG2-Sora-R, Huh7-Sora-R, and Plc/Prf/5-Sora-R) cells were established by treatment with increasing concentrations of the cytostatic drugs over several months. Chemoresistance was confirmed by MTT assay and *MDR1* expression.

In order to maintain the resistance, cells confluent grown in a 175 cm^2 cell culture flask were treated biweekly with doxorubicin (HepG2-Dox-R: 5 µg/ml, Huh7-Dox-R: 1 µg/ml, and Plc/Prf/5-Dox-R: 10 µg/ml) or sorafenib (HepG2-Sora-R, Huh7-Sora-R, and Plc/Prf/5-Sora-R: 5 µM) in 10 ml medium. 24 h after the treatment, the medium was removed and the living cells were transferred into a 75 cm^2 cell culture flask. The medium was exchanged everyday until no dead cells were left.
For mRNA and protein analysis, 400,000 cells per well were seeded into 6-well plates and allowed to attach overnight. They were treated with doxorubicin (HepG2-Dox-R: 2 µg/ml, Huh7-Dox-R: 0.5 µg/ml, and Plc/Prf/5-Dox-R: 5 µg/ml) or sorafenib (HepG2-Sora-R, Huh7-Sora-R, and Plc/Prf/5-Sora-R: 2.5 µM) in 1 ml medium for 72 h before washing with 1 ml PBS per well, and lysis with QIAzol or SB lysis buffer with freshly added 7x Complete protease inhibitor.

Doxorubicin and sorafenib were dissolved in dimethyl sulfoxide (DMSO) and stock solutions (doxorubicin: 50 mg/ml, sorafenib: 40 mg/ml) were prepared. MTT tests were performed to detect the influence of DMSO on cell viability (Suppl. Figure S4-6).

3.5 Cytotoxicity assay (MTT assay)

Hepatoma cells (10,000 HepG2, 5,000 Plc/Prf/5, or 5,000 Huh7) were seeded into 96-well plates and treated with different concentrations of doxorubicin, sorafenib, or the respective solvent control the next day. 24 h after treatment, medium was removed and 100 µl of 0.5 mg/ml MTT (3-[4,5-dimethylthiazol-2-yl]-2,5-diphenyltetrazolium bromide; thiazolyl blue) diluted in medium was added. After 2 h incubation, the medium was removed, formazan crystals were dissolved in 80 µl DMSO, and the absorbance was measured at 550 nm with 630 nm as reference wavelength in a microplate reader (Tecan Sunrise, Tecan Group Ltd., Männedorf, Switzerland).
For MTT assay after the 5-azacytidine treatment, cells were treated over four days with 2 µM of the methyltransferase inhibitor 5-azacytidine, which was freshly added each day.

3.6 Clonogenicity assay

Hepatoma cells were seeded into 6-well plates (Plc/Prf/5 and Huh7: 500 cells per well; HepG2: 5,000 cells per well), allowed to attach overnight, and treated with the indicated concentrations of sorafenib, doxorubicin, or the respective solvent control in 1 ml medium for 24 h. Following the treatment, cells were washed with PBS and allowed to form colonies in 2 ml complete growth medium. After 10 to 15 days, the colonies were fixed in methanol, stained with crystal violet, and counted. For the sorafenib experiments colonies were counted with a clono counter software as previously described (Niyazi et al., 2007, Tripathi et al., 2015) and for the doxorubicin experiments colonies were counted manually.

4. RNA isolation and quantitative real-time RT-PCR (qPCR)

Total RNA was extracted with QIAzol lysis reagent according to the manufacturer`s instructions. Potential contamination with DNA was removed by DNase digestion using the DNA free Kit. Reverse transcription of 0.5 µg RNA was performed with the High-Capacity cDNA Reverse Transcription Kit using random primers. For microRNA analysis, the procedure was performed accordingly with minor modifications: (I) the RNA after isopropanol precipitation was not washed with ethanol and (II) reverse transcription with 2 µg RNA was performed using the miScript II RT Kit and HiSpec Buffer as recommended by the manufacturer. Samples along with plasmid standard dilution series from 80 to 0.00008 attomol were run in triplicates using 5x HOT FIREPol Evagreen qPCR Mix Plus in a CFX96 cycler (Bio-Rad, Munich, Germany) with specific primers (**Table 4**). The reaction conditions for the detection of mRNAs were 95°C for 15 min followed by 40 cycles of 30 sec at 94°C, 30 sec at primer-specific annealing temperature (AT listed in **Table 4**), and 30 sec at 72°C. A melting curve from 55°C to 95°C was recorded to detect potential unintended products. For the detection of microRNAs the reaction conditions were 95°C for 15 min, followed by 40 cycles of 15 sec at 94°C, 30 sec at primer-specific annealing temperature (AT listed in **Table 4**), and 30 sec at 70°C. The human gene expression samples were normalized to *actin beta (ACTB)*, murine samples to *casein kinase 2 alpha 2 (Csnk2a2),* and microRNAs were normalized to *RNU6B*.

For the detection of *H19* sponge targets, the mRNA value stability of three housekeeping genes *(actin beta (ACTB)*, *18S ribosomal 5 (RNA18S5),* and *glyceraldehyde-3-phosphate dehydrogenase (GAPDH))* was compared with the geNorm test (Vandesompele et al., 2002). Since all M-values were less than 1.5 *(ACTB* M=0.605, *RNA18S5* M=0.683, and *GAPDH* M=0.552*)*, the gene expression was normalized to their geometric mean (Vandesompele et al., 2002).

Q-PCR experiments shown in chapter 2 were performed by Beate Czepukojc from the Department of Pharmacy (Pharmaceutical Biology, Saarland University).

Table 4: **Target gene-specific primer information.**

mRNA	Forward primer sequence 5' → 3'	Reverse primer sequence 5' → 3'	Gene bank accession no.	AT [°C]	Product size [bp]	Primer conc. [µM]
hu ABCB1/ hu MDR1	GCTATAATGC GACAGGAGAT AGGCT	CATTCCAATTT TGTCACCAAT AACTT	NM_001348946.1; NM_001348945.1; NM_001348944.1	56	116	0.2
hu ACTB	TGCGTGACAT TAAGGAGAAG	GTCAGGCAGC TCGTAGCTCT	NM_001101.3	60	107	0.2
hu AFP	TTCTTTGGGC TGCTCGCTAT	TGCTGCCTTT GTTTGGAAGC	NM_001134.2	60	86	0.2
hu BRCA1	GCTCTTCGCG TTGAAGAAGT A	ATCAACTCCA GACAGATGGG A	NM_007294.3; NM_007299.3; NM_007298.3; NM_007300.3	60	80	0.2
hu CCNB1 IP	ATGGTGAATG GACACCAACT CT	CATTCTTAGC CAGGTGCTGC	NM_031966.3	60	87	0.25
hu CTSV	GAAGGCCGCC TGGAAACTT	AGGCACCCTC AGCAAACAAG	NM_001333.3	62	94	0.15
hu DNMT3B	AGCAGCCCTG GAGACTCATT	CACGACGCAC CTTCGACTTAT	NM_006892.3	60	139	0.2
hu E2F8	TGAACTGGCC ACCCGAACA	CCCAAAGCTC CAAGTATGCA GT	NM_024680.3	60	128	0.2
hu ELAVL1	GGTGACATCG GGAGAACGAA	CCAAGCTGTG TCCTGCTACT	NM_001419.2	60	142	0.2
hu GAPDH	GGGAAGGTGA AGGTCGGAGT	TCCACTTTACC AGAGTTAAAA GCAG	NM_002046.5; NM_001289745.1; NM_001289746.1	60	82	0.2
hu GAPDH IP	TTCGACAGTC AGCCGCATCT	GCCCAATACG ACCAAATCCG TT	NM_002046.5	63	105	0.2
hu H19	TTCAAAGCCT CCACGACTCT	CTGAGACTCA AGGCCGTCTC	NR_131224.1; NR_131223.1; NR_002196.2; NM_001293171.2	60	100	0.2
hu H19 IP	GCTCCCAGAA CCCACAACAT	CCTTCCAGAG CCGATTCCTG	NR_131224.1; NR_131223.1; NR_002196.2; NM_001293171.2	61	149	0.2
hu H2AFY2	CGGATAGCCC CGAGACACAT	TCCACTGGCG ATGGTCACTC	NM_018649.2	60	87	0.2
hu IGF2	GGACTTGAGT CCCTGAACCA	TGAAAATTCC CGTGAGAAGG	NM_000612.5; NM_001007139.5; NM_001127598.2; NM_001291861.2; NM_001291862.2	56	100	0.25
hu IKBKAP	TCCAGGGAAT CCTCAGTGCT T	AGCCTTCTGC CACCAAAGAA A	NM_001330749.1; NM_003640.4	60	134	0.2
hu KDELC1	ACCGTCATAC TTCTCTTGCTC C	CCAAAGGCCA GTCTCCCAAA T	NM_001318732.1	60	144	0.2

hu MYBL2	AGATTCAGAT GTGCCGGAGC	TGTCCAAACT GCCTCACCAG	NM_002466.3	60	99	0.2
hu NINL	TCATCCCTCG TGTCCCTGTG	TCTGCAAGAT CTCCCTGCCA T	NM_001318226.1; NM_025176.5	60	136	0.2
hu RNA18S5	AGGTCTGTGA TGCCCTTAGA	GAATGGGGTT CAACGGGTTA	NR_003286.2	61	109	0.2
hu SLC15A1	GCCATCGTGC AGGTGGAAAT	TGGGCCAAGT GTCACCATCT	NM_005073.3	60	135	0.2
hu SMYD3	GAGCCGCTGA AGGTGGAAAA G	TGTACGCCAA GGGATCCGAG	NM_001167740.1	60	112	0.2
hu SOAT2	CCGCAAGTCC CTGCTTGAT	GCCAGCGATG AACATGTGGT A	NM_003578.3	60	73	0.2
hu WASF1	GCAGTGTTCT CTTCGTCCC	CCCCCTTTCC TGAGGTTCT	NM_001024936.1; NM_001024935.1; NM_001024934.1; NM_003931.2	60	70	0.2
mu H19	CAGAGGTGGA TGTGCCTGCC	CGGACCATGT CATGTCTTTCT GTC	NR_001592.1	60	80	0.25
mu Igf2	GGAAGTCGAT GTTGGTGCTT CTC	CGAACAGACA AACTGAAGCG TGT	NM_010514.3	60	121	0.2
mu Csnk2a2	GTAAAGGACC CTGTGTCAAA GA	GTCAGGATCT GGTAGAGTTG CT	NM_009974.3	60	85	0.4
miRNA	**Forward primer sequence 5' → 3'**	**Reverse primer sequence 5' → 3'**	**Accession no.**	**AT [°C]**		**Primer conc. [µM]**
hsa-miR-675	TGGTGCGGAA AGGGCCCACA GT	GAATCGAGCA CCAGTTACGC AT	MIMAT0004284	64		0.2
RNU6B	ACGCAAATTC GTGAAGCGTT	GAATCGAGCA CCAGTTACG	e.g. NR_125730.1	55		0.5

AT: annealing temperature

5. DNA methylation analysis

5.1 DNA extraction and bisulfite conversion

Genomic DNA from HepG2, Plc/Prf/5, and Huh7 cells was extracted with the GenElute Mammalian Genomic DNA Miniprep Kit and bisulfite treatment of 500 ng genomic DNA was performed with the EZ DNA Methylation-Gold Kit according to the manufacturer's instructions.

5.2 Single nucleotide primer extension (SNuPE)

Amplicons were generated using region-specific primers for the *H19* promoter (forward (5'-3'): GGGTTTGGGAGAGTTTGTGAGGT; reverse (5'-3'): AACACAAAAAACCCC TTCCTACCA) and the following PCR reaction conditions:

Reaction mixture		PCR program		
10x buffer	3 µl	95°C	15 min	
dNTPs (10 mM)	2.4 µl	95°C	1 min	42x
Primer (10 µM)	0.5 µl	57.6°C	1 min	
Hot Star Taq (5 U/µl)	0.3 µl	72°C	1 min	
H_2O	21.3 µl	72°C	5 min	
Bisulfite DNA	2 µl			

A restriction digestion using Tsp509I (cutting site shown in **Figure 2**) was performed in order to enhance the SNuPE signal. Remaining primers were degraded with Exonuclease I/SAP shrimp alkaline phosphatase (1 U/ 9 U).

```
                          GGGTTTGGGAGAGTTTGTGAGGTCGTTTATCGTTTGTTAG 150
151   TAGAGTGCGTTCGCGAGTCGTAAGTATAGTTCGGTAATATGCGGTTTTTAGATAGGAAAG 210
211   TGGTCGCGAATGGGATCGGGGTGTTTAGCGGTTGTGGGGATTTTGTTTTGCGGAAATCGC 270
271   GGTGATTAGTATAAGTTCGGTTAATTGGATGGGAATCGGTTTGGGGGGTTGGTATCGCGT 330
331   TTATTAGGGGGTTTGCGGTATTTTTTTTGTTTTTTAGTATTTTATTTTTATTTTTTAGG 390
391   AACGTGAGGTTTGAGTCGTGATGGTGGTAGGAAGGGGTTTTTTGTGT
```

Figure 2: **Bisulfite DNA sequence of the analyzed *H19* promoter region** (blue: PCR primers, red: SNuPE primers, gray: CpGs, and purple: Tsp509I cutting site 5'- AATT ↓ 3')).

The single nucleotide primer extension for two CpG sites of the *H19* promoter (CpG 3 primer (5'-3'): TGTTAGTAGAGTG and CpG 17 primer (5'-3'): GTGATTAGTATAAGTT) was performed under the following conditions:

Reaction mixture		PCR program		
10x buffer C	2 µl	96°C	2 min	
ddCTP (1 mM)	1 µl	96°C	30 sec	50x
ddTTP (1 mM)	1 µl	50°C	30 sec	
Primer (30 µM)	2.4 µl	60°C	1 min	
TermiPol (5 U/µl)	1 µl			
$MgCl_2$ (25 mM)	1.6 µl			
H_2O	2.6 µl			
ExoSAP product	6 µl			

SNuPE products were seperated using ion pair reversed phase high performance liquid chromatography (IP/RP-HPLC) with an HPLC WAVE 3000 (Transgenomic), a DNASep-Column at 50°C, and a flow rate of 0.9 ml/min.

5.3 Local deep bisulfite sequencing (Bi-PROF)

For the analysis with next generation sequencing, the recommended adaptors were added to the primer sequences for the amplicon generation (forward (5'-3'): TCTTTC CCTACACGACGCTCTTCCGATCTGGGTTTGGGAGAGTTTGTGAGGT and reverse (5'-3'): GTGACTGGAGTTCAGACGTGTGCTCTTCCGATCTAACACAAAAAACCCCTTCCT ACCA, annealing temperature 60°C). Purified PCR products were pooled in an equimolar ratio and sequenced (Gries et al., 2013) on a MiSeq instrument with the sequencing-by-synthesis technology (2 x 300 bp paired-end) aiming at 10,000 reads per amplicon according to the manufacturer's protocol.

DNA methylation analysis was performed in cooperation with Dr. Sascha Tierling and Prof. Dr. Jörn Walter from the Department of Genetics and Epigenetics (Saarland University).

6. Western blot analysis

Total proteins from HepG2, Plc/Prf/5, and Huh7 cells were extracted using the SB lysis buffer (50 mM Tris pH 6.8, 1% [w/v] SDS, 10% [w/v] glycerol, 0.004% [w/v] bromophenol blue, and 5% [w/v] β–mercaptoethanol in distilled water) with freshly added 7x Complete protease inhibitor. Samples were mixed with loading buffer, denatured for 10 min at 95°C, and loaded onto a 12% polyacrylamide gel. Proteins were separated with SDS-PAGE and transferred to an Immobilon FL-PVDF membrane. After blocking for 1 h with Rockland Blocking Buffer (RBB), the membrane was incubated with H19 antisera (1:5,000 dilution for H19 sense protein and 1:2,000 dilution for H19 antisense protein in RBB) obtained from John S. Mattick (Institute for Molecular Bioscience, University of Queensland, St Lucia, Brisbane, Queensland 4072, Australia) for 1 h. Subsequently, the membrane was washed and incubated with the labeled secondary antibody anti-rabbit 800 (1:5,000 dilution in RBB) for 1 h. Signal intensities were determined using the Odyssey infrared image system (LI-COR, Biosciences, Bad Homburg, Germany).

Experiments were carried out in part by Dr. Stephan Laggai from the Department of Pharmacy (Pharmaceutical Biology, Saarland University).

7. RAC1 pull-down assay

For the detection of activated RAC1, the affinity to the p21 binding domain of its target p21-activated kinase 1 was utilized. A fusion protein consisting of glutathione S-transferase and the p21 binding domain (GST-PBD) was expressed in *Escherichia coli*, purified, and bound to glutathione sepharose beads (Diesel et al., 2013, Fürst et al., 2005). For RAC1 pull-down assays, HepG2 seeded in a density of 8×10^5 cells per well in 6-well plates were treated with 1 µg/ml DLK1 for 2 or 5 min. After a washing step with ice-cold PBS, samples were lysed with PBD-buffer (Tris pH 8.0 25 mM, DTT 1 mM, $MgCl_2$ 20 mM, NaCl 100 mM, EDTA 0.5 mM, Triton X-100 1%, Aproptinin 0.1%, Leupeptin 0.1%, and PMSF 0.1%) and the positive control (untreated HepG2 cells) with GTPγS-PBD-buffer (Tris pH 8.0 25 mM, DTT 1 mM, $MgCl_2$ 5 mM, NaCl 100 mM, EDTA 1 mM, Triton X-100

1%, Aproptinin 0.1%, Leupeptin 0.1%, and PMSF 0.1%). The cell lysate was incubated for 15 min at 4°C under vigorous shaking to complete lysis. The positive control was incubated for 10 min with GTPγS (10 mM) to enrich the activated form of RAC1 (RAC-GDP → RAC-GTP). This reaction was stopped by adding $MgCl_2$ (1 M). The cell lysates were centrifuged and the supernatants were incubated with 30 µl GST-PBD-beads for 2 h at 4°C under vigorous shaking. After centrifugation and washing with PBD-buffer or GTPγS-PBD-buffer (for the positive control), the pellet containing a complex of GST-PBD-bound activated RAC1 was frozen at -80°C.
Western blot analysis was performed as described in chapter 6 using the primary antibody for human RAC1 (1:500 dilution in RBB) overnight at 4°C, followed by incubation with IRDye-conjugated secondary antibody for 1.5 h.

8. ROS assay

HepG2 cells seeded in a density of 50,000 cells per well in a 96-well plate were loaded with 20 µmol/l dichlorodihydrofluorescein diacetate (DCDHF) in PBS for 60 min and treated with 0.5 or 1 µg/ml DLK1 for up to 30 min. For the inhibition of RAC1, cells were pretreated with NSC23766 together with DCDHF. 300 µM H_2O_2 served as positive control for the ROS induction. Fluorescence (excitation, 485 nm; emission, 535 nm) was measured in a SpectraMax M5e (Moleculardevices, Biberach, Germany).

9. Bioinformatic analyses

9.1 TCGA data

RNAseq expression data were obtained from The Cancer Genome Atlas (https://cancergenome.nih.gov) *via* the Genomic Data Commons (https://gdc.cancer.gov), using the TCGAbiolinks R package (v.2.2.6) (Colaprico et al., 2016). The dataset comprised 364 primary solid tumor as well as 49 matched healthy liver tissue samples.

For gene expression analysis, RSEM (Li & Dewey, 2011) normalized read counts were downloaded and log2-transformed.

9.2 GEO datasets

For differential gene expression analyses, 39 tumor and 39 adjacent non-tumor samples from the Total RNA Illumina HumanHT-12 V4.0 dataset GSE57957 were included. Similarly, differential gene expression was analyzed in dataset GSE54236 between tumor (n=74) and non-tumor (n=74) samples of an Agilent-014850 Whole Human Genome Microarray 4x44K G4112F (three samples without sufficient information per group were excluded). Additionally, the methylation of the *H19* promoter region 2 kb around the transcription start site was analyzed using the GSE57956 dataset of bisulfite converted DNA from 58 tumors and 58 adjacent non-tumor samples hybridized to an Illumina Infinium 27k Human Methylation Beadchip (two samples without sufficient information per group were excluded). A subset of samples from GSE57956 was equal to the expression dataset GSE57957.

Bioinformatic analysis was performed by Dr. Marcel Schulz and Dr. Markus List from the Department for Computational Biology and Applied Algorithmics (Max Planck Institut for Informatics, Saarland University).

10. Clinical samples

32 human paraffin-embedded liver samples of tumor and matched non-tumorous adjacent tissue from randomly selected pseudonymized HCC patients who underwent liver resection at the Saarland University Medical Center between 2005 and 2010 were obtained (Kessler et al., 2013). The study protocol was approved by the local Ethics Committee (Kenn-Nr. 47/07). Clinical data were described previously (Kessler et al., 2013, Kessler et al., 2014).

Clinical samples were prepared and collected by Dr. Juliane Pokorny and Prof. Dr. Rainer M. Bohle from the Institute of Pathology (Saarland University, Campus Homburg), and Dr. Vincent Zimmer and Prof. Dr. Frank Lammert from the Department of Medicine II (Saarland University Medical Center, Saarland University, Campus Homburg).

11. Microdissection and RT-PCR

Tissue sections of paraffin-embedded (FFPE) tissues were mounted on nuclease and human nucleic acid free glass membrane slides, deparaffinized and stained with haemalaun. Laser microdissection was performed as described previously (Fink et al., 2000, Fink et al., 1999) using a Leica LMD6000 microscope (Leica Microsystems CMS). Laser-microdissected cells were transferred into a reaction tube containing PKD buffer. RNA was isolated according to the manufacturer's protocol "Purification of total RNA from microdissected FFPE tissue sections" using the RNeasy FFPE Kit. 28 ng RNA were reverse transcribed using random primers as described (Kessler et al., 2013).

Microdissection and RT-PCR were performed by Dr. Sonja M. Kessler from the Department of Pharmacy (Pharmaceutical Biology, Saarland University) and Prof. Dr. Rainer M. Bohle from the Institute of Pathology (Saarland University, Campus Homburg).

12. *H19* RNA immunoprecipitation

Immunoprecipitation (IP) of HuR-associated RNAs from Huh7 cells, validation of IP by western blot, and qPCR for the negative control *GAPDH* and the positive control *Cyclin B1* (*CCNB1)* were performed as described previously (Hachenthal, 2017, Hoppstädter et al., 2016). The magnetic SureBeads system (Bio-Rad, Munich, Germany) was used according to the manufacturer`s protocol. All buffers were supplemented with RNaseOUT and 7x Complete protease inhibitor. Primer sequences (*hu GAPDH IP, hu CCNB1* and *hu H19 IP*) and conditions for qPCR can be found in **Table 4**.

For the generation of four samples, 4.5 x 10^7 Huh7 cells in medium were centrifuged for 5 min at 500 *x g* and 4°C. The cell pellet was washed with 1 ml ice cold PBS and lysed in 2 ml of radioimmune precipitation assay (RIPA) buffer (50 mM Tris-HCl, pH 7.5, 1% Nonidet P-40, 0.5% sodium deoxycholate, 0.05% sodium dodecyl sulfate, 1 mM EDTA, 150 mM NaCl). After centrifugation for 10 min at 16,000 *x g* and 4°C, the pellet was discarded and 500 µl of the supernatant were added to the prepared beads. After incubation under slight rotation for 1 h at room temperature, the samples were washed as described by the manufacturer, resuspended in 0.5 ml QIAzol and frozen at -80°C for at least 1 h. RNA isolation and qPCR were performed as described in chapter 4 with one modification: 6 µl of Ambion linear acrylamide (5 mg/ml), 60 µl of 5 M ammonium acetate, and 600 µl of isopropyl alcohol per sample were used for the mRNA precipitation at -80°C overnight.

H19 RNA immunoprecipitation was carried out by Dr. Nina Hachenthal from the Department of Pharmacy (Pharmaceutical Biology, Saarland University).

13. RFLP (restriction fragment length polymorphism) analysis

Genomic DNA (gDNA) was isolated from paraffin-embedded tissues using the QIAamp DNA FFPE Tissue Kit according to the manufacturer's instructions. Genomic DNA was amplified to screen liver tissue samples for heterozygosity at a known AluI polymorphism at the *H19* gene (Zhang & Tycko, 1992). 9 of the 32 samples (Kessler et al., 2013) were heterozygous and therefore corresponding cDNA was tested for biallelic expression. Primer sequences used were the following: 5'-TACAACCACTGCACTACCTG-3' (sense), 5'-TGGCCATGAAGATGGAGTCG-3' (antisense). The PCR reaction was performed using the DyNAmo Flash SYBR Green Master mix containing 400 nM primer, each. Amplification was performed in a Thermal Cycler (Px2 Thermal Cycler, Thermo Electron Corporation, Schwerte, Germany). PCR products were digested for 2 h at 37°C with AluI. Detection of existence of polymorphisms and expression status were done by agarose gel electrophoresis showing three bands (228 bp, 128 bp, and 100 bp) in gDNA after digestion. In case of monoallelic expression, cDNA was expected to show one 148 bp

band and three bands (48 bp, 100 bp, and 148 bp) in case of biallelic expression. Due to the high agarose concentration (3%), the 48 bp band was not detectable.

RFLP analysis was performed by Dr. Sonja M. Kessler from the Department of Pharmacy (Pharmaceutical Biology, Saarland University).

14. Ki67 staining

Cells were detached from the plates using trypsin (Sigma-Aldrich, Taufkirchen, Germany) and cell staining was performed as described previously (Hoppstädter et al., 2016). For intracellular staining of Ki67, cells were washed with flow cytometry buffer (FCB; PBS containing 2.5% (v/v) bovine calf serum and 0.05% (w/v) NaN_3) and fixed for 10 min in 1% (w/v) paraformaldehyde in PBS, pH 7.6, followed by permeabilization in SAP (FCB with 0.2% (w/v) saponin), and blocking for 30 min in 20% FCS (v/v, diluted in SAP). Cells were incubated with Ki67 or isotype control antibody (10 µl in 50 µl of FCB) for 15 min on ice. The cells were washed in FCB and resuspended in 1% (w/v) cold paraformaldehyde in PBS, pH 7.6. The stained cells were examined on a BD LSRFortess cell analyzer and results were analyzed using the FACS Diva software (BD Biosciences, Heidelberg, Germany).

Ki67 staining was realized by Dr. Kevan Hosseini from the Department of Pharmacy (Pharmaceutical Biology, Saarland University).

15. Chromogenic *in situ* hybridization (CISH)

Eight paraffin-embedded samples from HCC patients were investigated. The reseach project was authorized by the ethical committee of the Medical University of Graz (Ref. Nr. 20-119 ex 08/09). CISH was performed using the miCURY LNA microRNA ISH Optimization Kit (FFPE) according to manufacturer's instruction. A biotin-labeled probe was used for the detection of *H19* RNA (/5BioTEG/GTCCTGTAACCAAAAGTG ACCG).

A digoxin-labeled probe of scrambled RNA served as negative control (/5DigN/GTGTAACACGTCTATACGCCCA) and a digoxin-labeled *actin beta* probe was used as positive control (/5DigN/CTCATTGTAGAAGGTGTGGTGCCA). All probes were used in a concentration of 40 nM. Proteinase K digestion was done for 10 min at 37°C with 15 µg/ml Proteinase K. The hybridization step was performed at 56°C for 1 h in a slide hybridizer DakoCytomation (Dako, Hamburg, Germany). Nuclei were counterstained with Nuclear Fast Red Counterstain.

CISH was performed by Dr. Sonja M. Kessler from the Department of Pharmacy (Pharmaceutical Biology, Saarland University) and samples were examined together with Prof. Dr. Dr. Johannes Haybaeck from the Institute of Pathology (Medical University of Graz) and the Department of Pathology (Medical Faculty, Otto-von-Guericke University Magdeburg).

16. Statistics

Data analysis and statistics were performed with Microsoft Office Excel 2013 and OriginPro 8.6G (OriginLab Corporation, Northampton, USA). Values were expressed as mean ± SEM or as box plots with 25^{th}/75^{th} percentile boxes, geometric medians (EASL-Clinical-Practice-Guidelines), means (square), and 10^{th}/90^{th} percentile as whiskers. Statistical differences were calculated using an independent two-sample t-test, ANOVA combined with Bonferroni *post hoc* test, Mann-Whitney *U* test, or Kolmogorov-Smirnov test as indicated depending on whether the data were normally distributed. A Chi-square test was used for the statistical analysis of tumor development and characterization, apoptosis, and inflammation in mouse livers.

Part of the methods were published in: **Schultheiss C.S.**, Laggai S., Czepukojc B., Hussein U.K., List M., Barghash A., Tierling S., Hosseini K., Golob-Schwarzl N., Pokorny J., Hachenthal N., Schulz M., Helms V., Walter J., Zimmer V., Lammert F., Bohle R.M., Dandolo L., Haybaeck J., Kiemer A.K., and Kessler S.M. (2017) The long non-coding RNA *H19* suppresses carcinogenesis and chemoresistance in hepatocellular carcinoma. *Cell Stress*. 1(1), 37-54.

Supplemental information

A

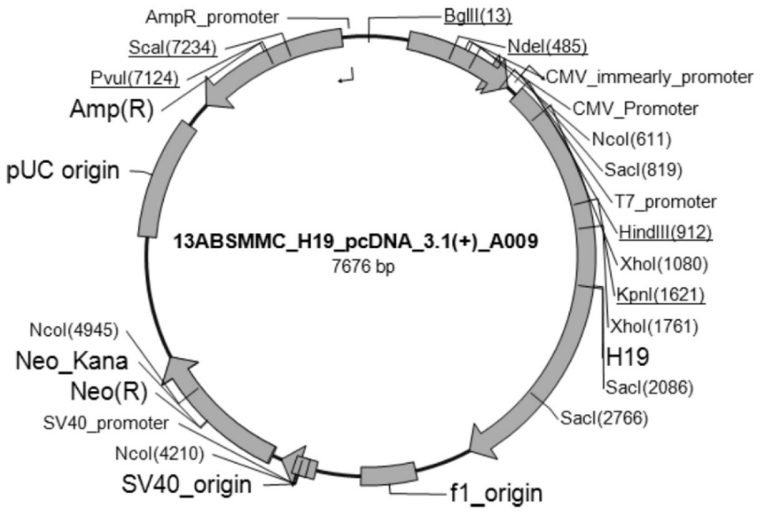

B

AAGCTTGGGAGGGGGTGGGATGGGTGGGGGGTAACGGGGGAAACTGGGGAAGTGGGGAACCGAGGGGCAACCAGGGGA
AGATGGGGTGCTGGAGGAGAGCTTGTGGGAGCCAAGGAGCACCTTGGACATCTGGAGTCTGGCAGGAGTGATGACGGG
TGGAGGGGCTAGCTCGAGGCAGGGCTGGTGGGGCCTGAGGCCAGTGAGGAGTGTGGAGTAGGCGCCCAGGCATCGTGC
AGACAGGGCGACATCAGCTGGGGACGATGGGCCTGAGCTAGGGCTGGAAAGAAGGGGGAGCCAGGCATTCATCCCGGT
CACTTTTGGTTACAGGACGTGGCAGCTGGTTGGACGAGGGGAGCTGGTGGGCAGGGTTTGATCCCAGGGCCTGGGCAA
CGGAGGTGTAGCTGGCAGCAGCGGGCAGGTGAGGACCCCATCTGCCGGGCAGGTGAGTCCCTTCCCTCCCCAGGCCTC
GCTTCCCCAGCCTTCTGAAAGAAGGAGGTTTAGGGGATCGAGGGCTGGCGGGGAGAAGCAGACACCCTCCCAGCAGAG
GGGCAGGATGGGGGCAGGAGAGTTAGCAAAGGTGACATCTTCTCGGGGGGAGCCGAGACTGCGCAAGGCTGGGGGGTT
ATGGGCCCGTTCCAGGCAGAAAGAGCAAGAGGGCAGGGAGGGAGCACAGGGGTGGCCAGCGTAGGGTCCAGCACGTGG
GGTGGTACCCCAGGCCTGGGTCAGACAGGGACATGGCAGGGGACACAGGACAGAGGGGTCCCCAGCTGCCACCTCACC
CACCGCAATTCATTTAGTAGCAGGCACAGGGGCAGCTCCGGCACGGCTTTCTCAGGCCTATGCCGGAGCCTCGAGGGC
TGGAGAGCGGGAAGACAGGCAGTGCTCGGGGAGTTGCAGCAGGACGTCACCAGGAGGGCGAAGCGGCCACGGGAGGGG
GGCCCCGGGACATTGCGCAGCAAGGAGGCTGCAGGGGCTCGGCCTGCGGGCGCCGGTCCCACGAGGCACTGCGGCCCA
GGGTCTGGTGCGGAGAGGGCCCACAGTGGACTTGGTGACGCTGTATGCCCTCACCGCTCAGCCCCTGGGGCTGGCTTG
GCAGACAGTACAGCATCCAGGGGAGTCAAGGGCATGGGGCGAGACCAGACTAGGCGAGGCGGGCGGGGCGGAGTGAAT
GAGCTCTCAGGAGGGAGGATGGTGCAGGCAGGGGTGAGGAGCGCAGCGGGCGGCGAGCGGGAGGCACTGGCCTCCAGA
GCCCGTGGCCAAGGCGGGCCTCGCGGGCGGCGACGGAGCCGGGATCGGTGCCTCAGCGTTCGGGCTGGAGACGAGGCC
AGGTCTCCAGCTGGGGTGGACGTGCCCACCAGCTGCCGAAGGCCAAGACGCCAGGTCCGGTGGACGTGACAAGCAGGA
CATGACATGGTCCGGTGTGACGGCGAGGACAGAGGAGGCGCGTCCGGCCTTCCTGAACACCTTAGGCTGGTGGGGCTG
CGGCAAGAAGCGGGTCTGTTTCTTTACTTCCTCCACGGAGTCGGCACACTATGGCTGCCCTCTGGGCTCCCAGAACCC
ACAACATGAAAGAAATGGTGCTACCCAGCTCAAGCCTGGGCCTTTGAATCCGGACACAAAACCCTCTAGCTTGGAAAT
GAATATGCTGCACTTTACAACCACTGCACTACCTGACTCAGGAATCGGCTCTGGAAGGTGAAGCTAGAGGAACCAGAC
CTCATCAGCCCAACATCAAAGACACCATCGGAACAGCAGCGCCCGCAGCACCCACCCCGCACCGGCGACTCCATCTTC
ATGGCCACCCCCTGCGGCGGACGGTTGACCACCAGCCACCACATCATCCCAGAGCTGAGCTCCTCCAGCGGGATGACG
CCGTCCCCACCACCTCCCTCTTCTTCTTTTTCATCCTTCTGTCTCTTTGTTTCTGAGCTTTCCTGTCTTTCCTTTTTT
CTGAGAGATTCAAAGCCTCCACGACTCTGTTTCCCCCGTCCCTTCTGAATTTAATTTGCACTAAGTCATTTGCACTGG
TTGGAGTTGTGGAGACGGCCTTGAGTCTCAGTACGAGTGTGCGTGAGTGTGAGCCACCTTGGCAAGTGCCTGTGCAGG
GCCCGGCCGCCCTCCATCTGGGCCGGGTGACTGGGCGCCGGCTGTGTGCCCGAGGCCTCACCCTGCCCTCGCCTAGTC
TGGAAGCTCCGACCGACATCACGGAGCAGCCTTCAAGCATTCCATTACGCCCCATCTCGCTCTGTGCCCCTCCCCACC
AGGGCTTCAGCAGGAGCCCTGGACTCATCATCAATAAACACTGTTACAGCAAAAAAAAAAAAAAAATCTAGA

Supplemental Figure S1: (**A**) **Plasmid map** (pcDNA3.1(+)_A009) **and** (**B**) ***H19*-sequence** (2,334 bp) (Ref. No.: 1381790).

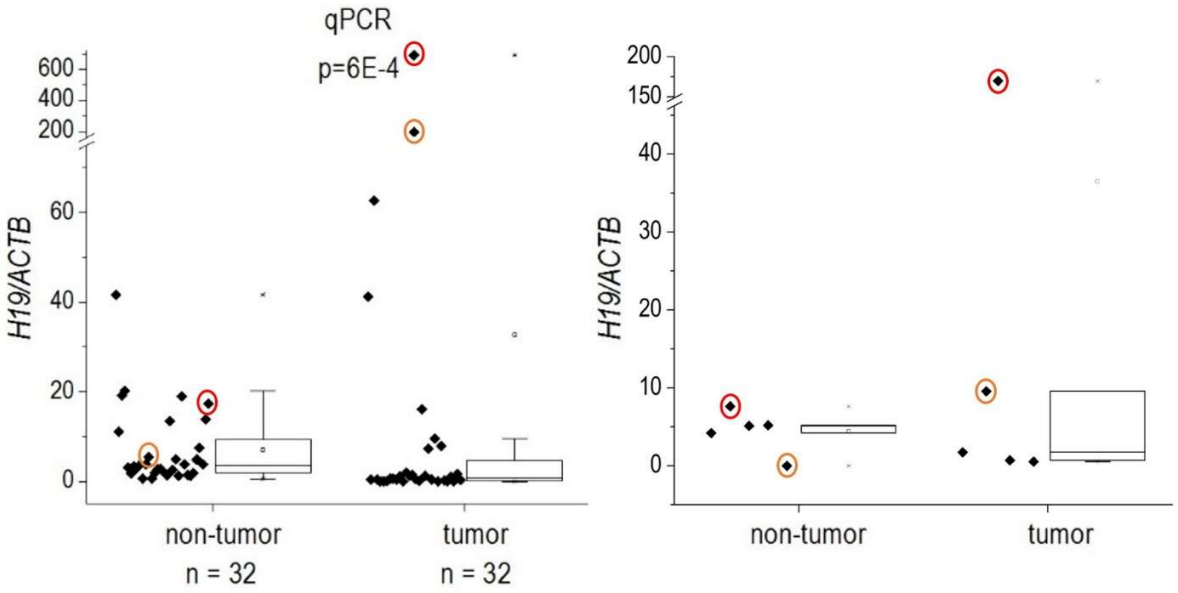

Supplemental Figure S2: ***H19*** **expression in HCC** tissues from Saarland University Medical Center determined by qPCR (each, n=32, Mann-Whitney U test; see **Figure 1D**). Highlighted are the two highest expressing HCC tissues and corresponding normal tissues, from which hepatocytes were microdissected and compared with hepatocytes from three low expressing HCC tissues.

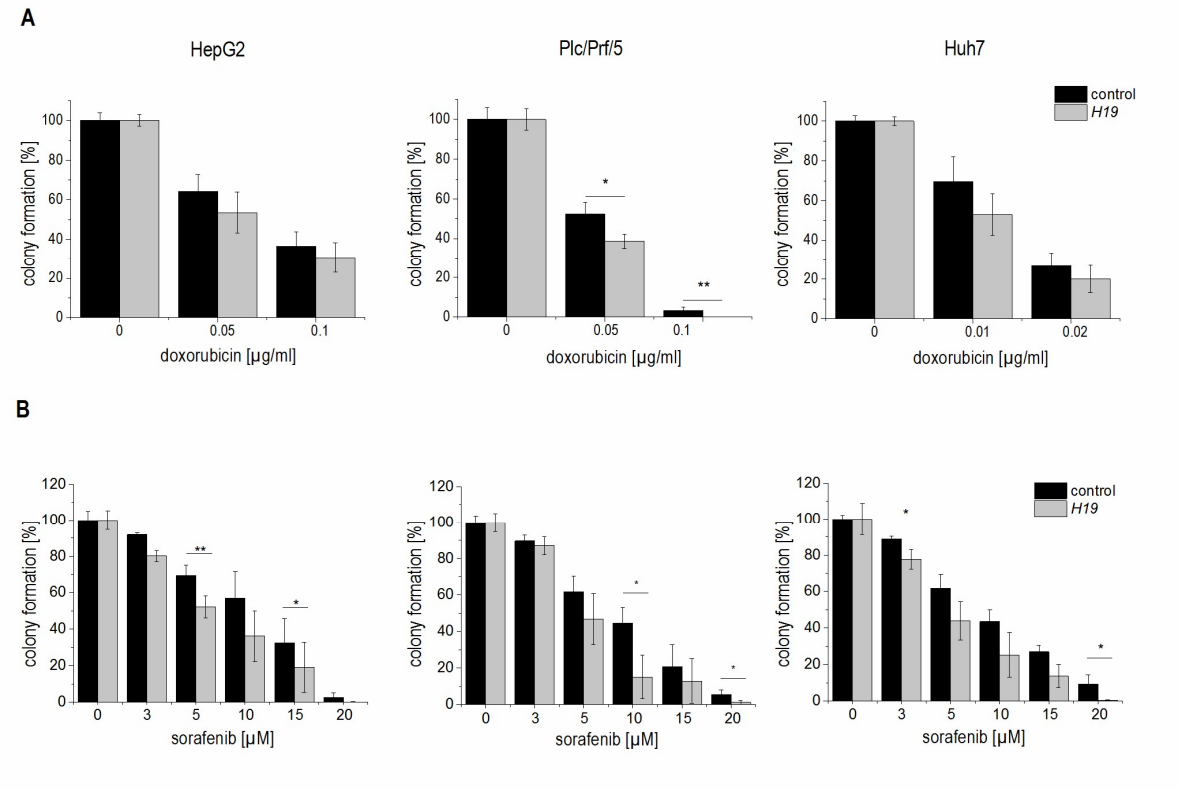

Supplemental Figure S3: **Effect of *H19* overexpression on colony formation ability** in stably *H19* overexpressing (*H19*) and vector control (control, co) HepG2 (left panels), Plc/Prf/5 (middle panels), and Huh7 (right panels) cells. (**A, B**) Colony formation ability of control or *H19* cells normalized to their respective untreated controls after (**A**) doxorubicin (n≥3, duplicates) or (**B**) sorafenib (n=3, triplicates) treatment. The p values were calculated by two-sample t-test or Mann-Whitney *U* test depending on the data distribution. * $p < 0.05$, ** $p < 0.01$, *** $p < 0.001$.

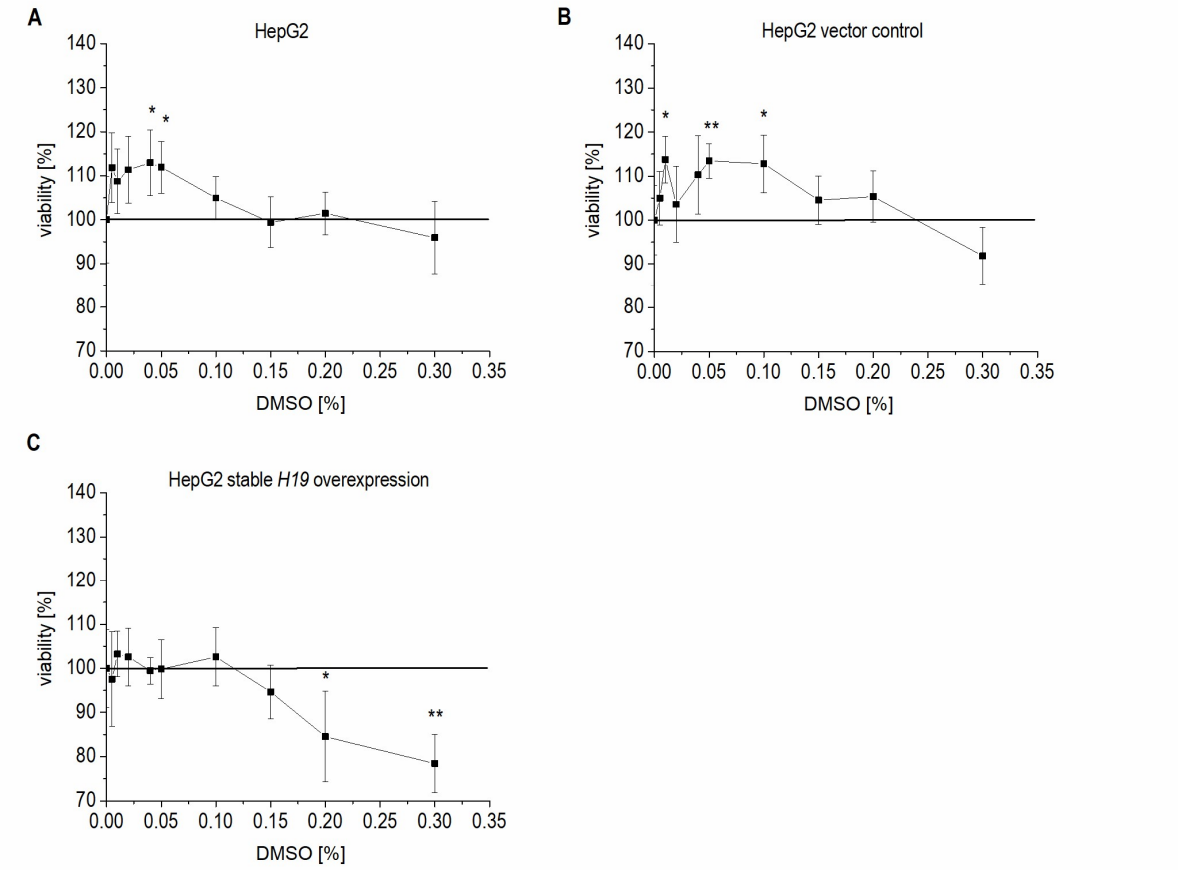

Supplemental Figure S4: **Cytotoxicity estimated by MTT assay after treatment with DMSO** in (**A**) HepG2, (**B**) vector control transfected HepG2, or (**C**) stably *H19* overexpressing HepG2 cells normalized to the respective untreated control (n=1, octuplicates).

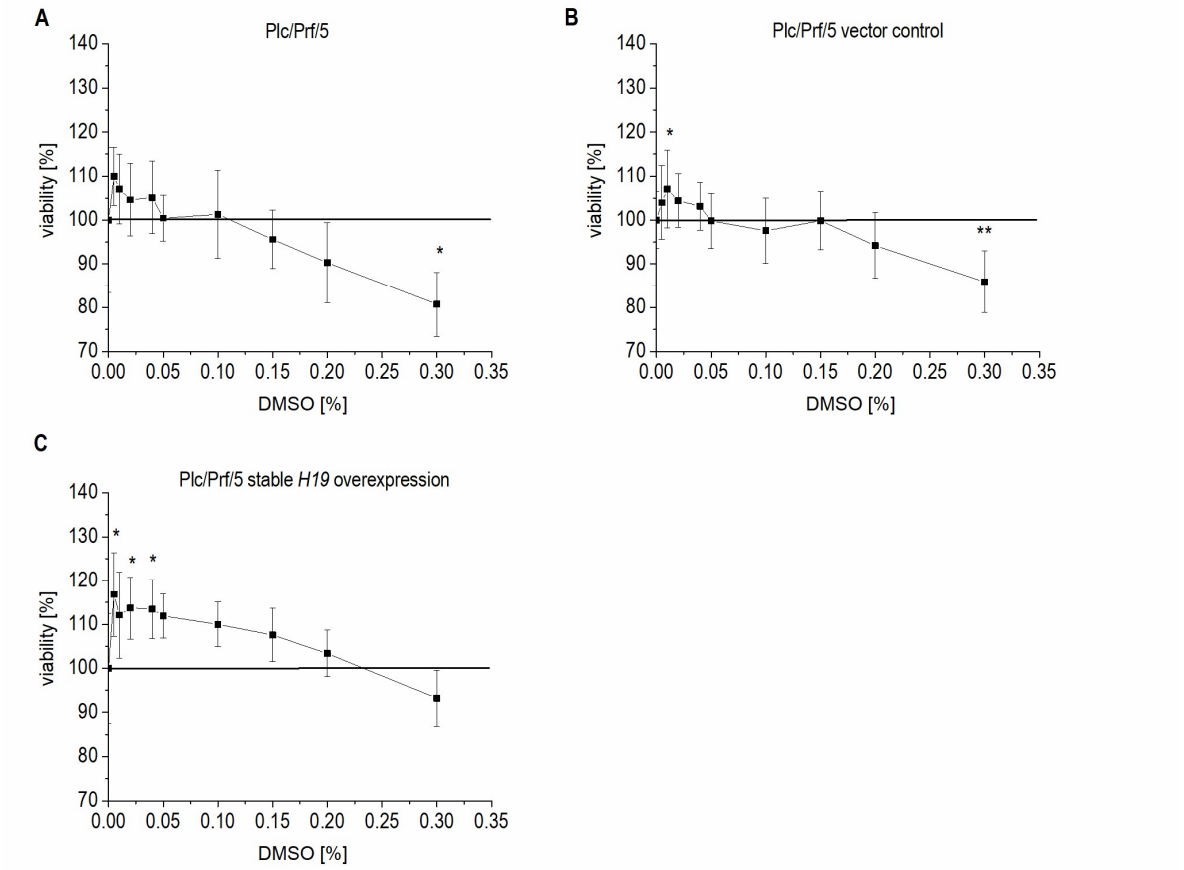

Supplemental Figure S5: **Cytotoxicity estimated by MTT assay after treatment with DMSO** in (**A**) Plc/Prf/5, (**B**) vector control transfected Plc/Prf/5, or (**C**) stably *H19* overexpressing Plc/Prf/5 cells normalized to the respective untreated control (n=1, octuplicates).

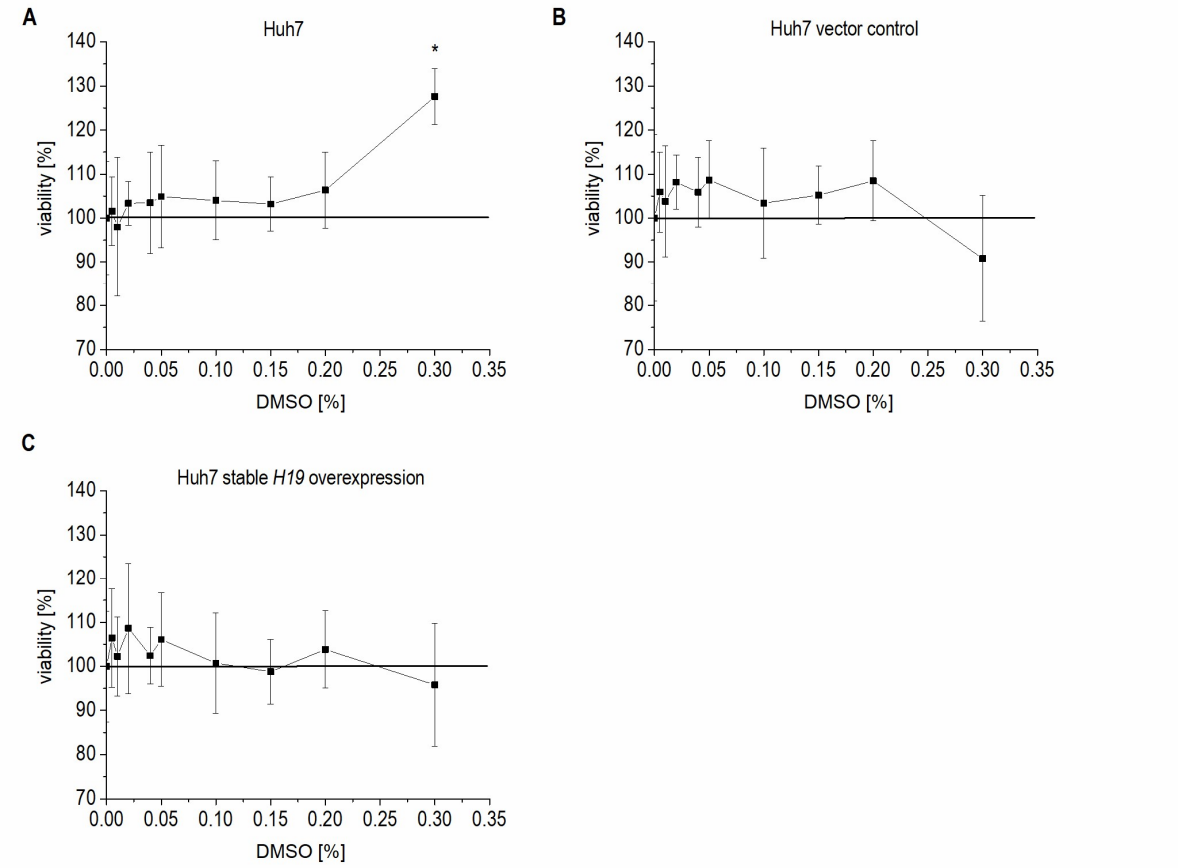

Supplemental Figure S6: **Cytotoxicity estimated by MTT assay after treatment with DMSO** in (**A**) Huh7, (**B**) vector control transfected Huh7, or (**C**) stably *H19* overexpressing Huh7 cells normalized to the respective untreated control (n=1, octuplicates).

References

Ambros V (2004) The functions of animal microRNAs. Nature 431: 350-5

Ariel I, Miao HQ, Ji XR, Schneider T, Roll D, de Groot N, Hochberg A, Ayesh S (1998) Imprinted H19 oncofetal RNA is a candidate tumour marker for hepatocellular carcinoma. Mol Pathol 51: 21-5

Barsyte-Lovejoy D, Lau SK, Boutros PC, Khosravi F, Jurisica I, Andrulis IL, Tsao MS, Penn LZ (2006) The c-Myc oncogene directly induces the H19 noncoding RNA by allele-specific binding to potentiate tumorigenesis. Cancer Res 66: 5330-7

Bartolomei MS, Zemel S, Tilghman SM (1991) Parental imprinting of the mouse H19 gene. Nature 351: 153-5

Batista PJ, Chang HY (2013) Long noncoding RNAs: cellular address codes in development and disease. Cell 152: 1298-307

Berteaux N, Lottin S, Monte D, Pinte S, Quatannens B, Coll J, Hondermarck H, Curgy JJ, Dugimont T, Adriaenssens E (2005) H19 mRNA-like noncoding RNA promotes breast cancer cell proliferation through positive control by E2F1. J Biol Chem 280: 29625-36

Blackburn EH, Collins K (2011) Telomerase: an RNP enzyme synthesizes DNA. Cold Spring Harb Perspect Biol 3: 1-10

Block K, Gorin Y (2012) Aiding and abetting roles of NOX oxidases in cellular transformation. Nat Rev Cancer 12: 627-37

Bochar DA, Wang L, Beniya H, Kinev A, Xue Y, Lane WS, Wang W, Kashanchi F, Shiekhattar R (2000) BRCA1 is associated with a human SWI/SNF-related complex: linking chromatin remodeling to breast cancer. Cell 102: 257-65

Bosch FX, Ribes J, Diaz M, Cleries R (2004) Primary liver cancer: worldwide incidence and trends. Gastroenterology 127: S5-S16

Brannan CI, Dees EC, Ingram RS, Tilghman SM (1990) The product of the H19 gene may function as an RNA. Mol Cell Biol 10: 28-36

Cai X, Cullen BR (2007) The imprinted H19 noncoding RNA is a primary microRNA precursor. RNA 13: 313-6

Cantarino N, Douet J, Buschbeck M (2013) MacroH2A--an epigenetic regulator of cancer. Cancer Lett 336: 247-52

Castello G, Scala S, Palmieri G, Curley SA, Izzo F (2010) HCV-related hepatocellular carcinoma: From chronic inflammation to cancer. Clin Immunol 134: 237-50

Chen S, Bu D, Ma Y, Zhu J, Chen G, Sun L, Zuo S, Li T, Pan Y, Wang X, Liu Y, Wang P (2017) H19 Overexpression Induces Resistance to 1,25(OH)2D3 by Targeting VDR Through miR-675-5p in Colon Cancer Cells. Neoplasia 19: 226-236

Chen SW, Wang PY, Liu YC, Sun L, Zhu J, Zuo S, Ma J, Li TY, Zhang JL, Chen GW, Wang X, Zhu QR, Zheng YW, Chen ZY, Yao ZH, Pan YS (2016) Effect of Long Noncoding RNA H19 Overexpression on Intestinal Barrier Function and Its Potential Role in the Pathogenesis of Ulcerative Colitis. Inflamm Bowel Dis 22: 2582-2592

Cho RW, Clarke MF (2008) Recent advances in cancer stem cells. Curr Opin Genet Dev 18: 48-53

Colaprico A, Silva TC, Olsen C, Garofano L, Cava C, Garolini D, Sabedot TS, Malta TM, Pagnotta SM, Castiglioni I, Ceccarelli M, Bontempi G, Noushmehr H (2016) TCGAbiolinks: an R/Bioconductor package for integrative analysis of TCGA data. Nucleic Acids Res 44: e71

Conway AE, Van Nostrand EL, Pratt GA, Aigner S, Wilbert ML, Sundararaman B, Freese P, Lambert NJ, Sathe S, Liang TY, Essex A, Landais S, Burge CB, Jones DL, Yeo GW (2016) Enhanced CLIP Uncovers IMP Protein-RNA Targets in Human Pluripotent Stem Cells Important for Cell Adhesion and Survival. Cell Rep 15: 666-679

Cutts SM, Nudelman A, Rephaeli A, Phillips DR (2005) The power and potential of doxorubicin-DNA adducts. IUBMB Life 57: 73-81

Czech B, Hannon GJ (2011) Small RNA sorting: matchmaking for Argonautes. Nat Rev Genet 12: 19-31

Dai N, Ji F, Wright J, Minichiello L, Sadreyev R, Avruch J (2017) IGF2 mRNA binding protein-2 is a tumor promoter that drives cancer proliferation through its client mRNAs IGF2 and HMGA1. Elife 6

Day CP, James OF (1998) Steatohepatitis: a tale of two "hits"? Gastroenterology 114: 842-5

Degrauwe N, Schlumpf TB, Janiszewska M, Martin P, Cauderay A, Provero P, Riggi N, Suva ML, Paro R, Stamenkovic I (2016) The RNA Binding Protein IMP2 Preserves Glioblastoma Stem Cells by Preventing let-7 Target Gene Silencing. Cell Rep 15: 1634-47

Degrauwe N, Suva ML, Janiszewska M, Riggi N, Stamenkovic I (2018) IMPs: an RNA-binding protein family that provides a link between stem cell maintenance in normal development and cancer. Genes Dev 30: 2459-2474

Diesel B, Hoppstadter J, Hachenthal N, Zarbock R, Cavelius C, Wahl B, Thewes N, Jacobs K, Kraegeloh A, Kiemer AK (2013) Activation of Rac1 GTPase by nanoparticulate structures in human macrophages. Eur J Pharm Biopharm 84: 315-24

Diesel B, Ripoche N, Risch RT, Tierling S, Walter J, Kiemer AK (2012) Inflammation-induced up-regulation of TLR2 expression in human endothelial cells is independent of differential methylation in the TLR2 promoter CpG island. Innate Immun 18: 112-23

Ding Z, Qian YB, Zhu LX, Xiong QR (2009) Promoter methylation and mRNA expression of DKK-3 and WIF-1 in hepatocellular carcinoma. World J Gastroenterol 15: 2595-601

Djebali S, Davis CA, Merkel A, Dobin A, Lassmann T, Mortazavi A, Tanzer A, Lagarde J, Lin W, Schlesinger F, Xue C, Marinov GK, Khatun J, Williams BA, Zaleski C, Rozowsky J, Roder M, Kokocinski F, Abdelhamid RF, Alioto T et al. (2012) Landscape of transcription in human cells. Nature 489: 101-8

EASL-Clinical-Practice-Guidelines (2018) EASL Clinical Practice Guidelines: Management of hepatocellular carcinoma. J Hepatol 69: 182-236

El-Serag HB, Rudolph KL (2007) Hepatocellular carcinoma: epidemiology and molecular carcinogenesis. Gastroenterology 132: 2557-76

Eng FJ, Friedman SL (2000) Fibrogenesis I. New insights into hepatic stellate cell activation: the simple becomes complex. Am J Physiol Gastrointest Liver Physiol 279: G7-G11

Farina KL, Huttelmaier S, Musunuru K, Darnell R, Singer RH (2003) Two ZBP1 KH domains facilitate beta-actin mRNA localization, granule formation, and cytoskeletal attachment. J Cell Biol 160: 77-87

Fellig Y, Ariel I, Ohana P, Schachter P, Sinelnikov I, Birman T, Ayesh S, Schneider T, de Groot N, Czerniak A, Hochberg A (2005) H19 expression in hepatic metastases from a range of human carcinomas. J Clin Pathol 58: 1064-8

Festuccia C, Gravina GL, D'Alessandro AM, Muzi P, Millimaggi D, Dolo V, Ricevuto E, Vicentini C, Bologna M (2009) Azacitidine improves antitumor effects of docetaxel and cisplatin in aggressive prostate cancer models. Endocr Relat Cancer 16: 401-13

Feuerhahn S, Iglesias N, Panza A, Porro A, Lingner J (2010) TERRA biogenesis, turnover and implications for function. FEBS Lett 584: 3812-8

Fink L, Kinfe T, Stein MM, Ermert L, Hanze J, Kummer W, Seeger W, Bohle RM (2000) Immunostaining and laser-assisted cell picking for mRNA analysis. Lab Invest 80: 327-33

Fink L, Stahl U, Ermert L, Kummer W, Seeger W, Bohle RM (1999) Rat porphobilinogen deaminase gene: a pseudogene-free internal standard for laser-assisted cell picking. Biotechniques 26: 510-6

Franken NA, Rodermond HM, Stap J, Haveman J, van Bree C (2006) Clonogenic assay of cells in vitro. Nat Protoc 1: 2315-9

Friedman SL (2003) Liver fibrosis -- from bench to bedside. J Hepatol 38 Suppl 1: S38-53

Fürst R, Brueckl C, Kuebler WM, Zahler S, Krotz F, Görlach A, Vollmar AM, Kiemer AK (2005) Atrial natriuretic peptide induces mitogen-activated protein kinase phosphatase-1 in human endothelial cells via Rac1 and NAD(P)H oxidase/Nox2-activation. Circ Res 96: 43-53

Gabory A, Jammes H, Dandolo L (2010) The H19 locus: role of an imprinted non-coding RNA in growth and development. Bioessays 32: 473-80

Gabory A, Ripoche MA, Le Digarcher A, Watrin F, Ziyyat A, Forne T, Jammes H, Ainscough JF, Surani MA, Journot L, Dandolo L (2009) H19 acts as a trans regulator of the imprinted gene network controlling growth in mice. Development 136: 3413-21

Gabory A, Ripoche MA, Yoshimizu T, Dandolo L (2006) The H19 gene: regulation and function of a non-coding RNA. Cytogenet Genome Res 113: 188-93

Gao ZH, Suppola S, Liu J, Heikkila P, Janne J, Voutilainen R (2002) Association of H19 promoter methylation with the expression of H19 and IGF-II genes in adrenocortical tumors. J Clin Endocrinol Metab 87: 1170-6

Gascoigne DK, Cheetham SW, Cattenoz PB, Clark MB, Amaral PP, Taft RJ, Wilhelm D, Dinger ME, Mattick JS (2012) Pinstripe: a suite of programs for integrating transcriptomic and proteomic datasets identifies novel proteins and improves differentiation of protein-coding and non-coding genes. Bioinformatics 28: 3042-50

Germano D, Daniele B (2014) Systemic therapy of hepatocellular carcinoma: current status and future perspectives. World J Gastroenterol 20: 3087-99

Gerstberger S, Hafner M, Tuschl T (2014) A census of human RNA-binding proteins. Nat Rev Genet 15: 829-45

Giovarelli M, Bucci G, Ramos A, Bordo D, Wilusz CJ, Chen CY, Puppo M, Briata P, Gherzi R (2014) H19 long noncoding RNA controls the mRNA decay promoting function of KSRP. Proc Natl Acad Sci U S A 111: E5023-8

Gries J, Schumacher D, Arand J, Lutsik P, Markelova MR, Fichtner I, Walter J, Sers C, Tierling S (2013) Bi-PROF: bisulfite profiling of target regions using 454 GS FLX Titanium technology. Epigenetics 8: 765-71

Guicciardi ME, Gores GJ (2005) Apoptosis: a mechanism of acute and chronic liver injury. Gut 54: 1024-33

Guo Z, Li LQ, Jiang JH, Ou C, Zeng LX, Xiang BD (2014) Cancer stem cell markers correlate with early recurrence and survival in hepatocellular carcinoma. World J Gastroenterol 20: 2098-106

Guttman M, Rinn JL (2012) Modular regulatory principles of large non-coding RNAs. Nature 482: 339-46

Hachenthal N (2017) Regulation des Glucocorticoid-induced leucine zipper (GILZ) in Entzündungsprozessen: Mechanismen und funktionelle Bedeutung. PhD Thesis Department of Pharmacy, Pharmaceutical Biology, Saarland University

Hadji F, Boulanger MC, Guay SP, Gaudreault N, Amellah S, Mkannez G, Bouchareb R, Marchand JT, Nsaibia MJ, Guauque-Olarte S, Pibarot P, Bouchard L, Bosse Y, Mathieu P (2016) Altered DNA Methylation of Long Noncoding RNA H19 in Calcific Aortic Valve Disease Promotes Mineralization by Silencing NOTCH1. Circulation 134: 1848-1862

Hafner M, Landthaler M, Burger L, Khorshid M, Hausser J, Berninger P, Rothballer A, Ascano M, Jr., Jungkamp AC, Munschauer M, Ulrich A, Wardle GS, Dewell S, Zavolan M, Tuschl T (2010) Transcriptome-wide identification of RNA-binding protein and microRNA target sites by PAR-CLIP. Cell 141: 129-41

Hamamoto R, Furukawa Y, Morita M, Iimura Y, Silva FP, Li M, Yagyu R, Nakamura Y (2004) SMYD3 encodes a histone methyltransferase involved in the proliferation of cancer cells. Nat Cell Biol 6: 731-40

Hanahan D, Weinberg RA (2011) Hallmarks of cancer: the next generation. Cell 144: 646-74

Hediger MA, Romero MF, Peng JB, Rolfs A, Takanaga H, Bruford EA (2004) The ABCs of solute carriers: physiological, pathological and therapeutic implications of human membrane transport proteinsIntroduction. Pflugers Arch 447: 465-8

Heindryckx F, Colle I, Van Vlierberghe H (2009) Experimental mouse models for hepatocellular carcinoma research. Int J Exp Pathol 90: 367-86

Henras AK, Dez C, Henry Y (2004) RNA structure and function in C/D and H/ACA s(no)RNPs. Curr Opin Struct Biol 14: 335-43

Hoppstädter J, Hachenthal N, Valbuena-Perez JV, Lampe S, Astanina K, Kunze MM, Bruscoli S, Riccardi C, Schmid T, Diesel B, Kiemer AK (2016) Induction of Glucocorticoid-induced Leucine Zipper (GILZ) Contributes to Anti-inflammatory Effects of the Natural Product Curcumin in Macrophages. J Biol Chem 291: 22949-22960

Huang J, Zhang X, Zhang M, Zhu JD, Zhang YL, Lin Y, Wang KS, Qi XF, Zhang Q, Liu GZ, Yu J, Cui Y, Yang PY, Wang ZQ, Han ZG (2007) Up-regulation of DLK1 as an imprinted gene could contribute to human hepatocellular carcinoma. Carcinogenesis 28: 1094-103

Hussain SP, Schwank J, Staib F, Wang XW, Harris CC (2007) TP53 mutations and hepatocellular carcinoma: insights into the etiology and pathogenesis of liver cancer. Oncogene 26: 2166-76

IHGS-Consortium (2004) Finishing the euchromatic sequence of the human genome. Nature 431: 931-45

Jeng YM, Chang CC, Hu FC, Chou HY, Kao HL, Wang TH, Hsu HC (2008) RNA-binding protein insulin-like growth factor II mRNA-binding protein 3 expression promotes tumor invasion and predicts early recurrence and poor prognosis in hepatocellular carcinoma. Hepatology 48: 1118-27

Jin ZH, Yang RJ, Dong B, Xing BC (2008) Progenitor gene DLK1 might be an independent prognostic factor of liver cancer. Expert Opin Biol Ther 8: 371-7

Kallen AN, Zhou XB, Xu J, Qiao C, Ma J, Yan L, Lu L, Liu C, Yi JS, Zhang H, Min W, Bennett AM, Gregory RI, Ding Y, Huang Y (2013) The imprinted H19 lncRNA antagonizes let-7 microRNAs. Mol Cell 52: 101-12

Keniry A, Oxley D, Monnier P, Kyba M, Dandolo L, Smits G, Reik W (2012) The H19 lincRNA is a developmental reservoir of miR-675 that suppresses growth and Igf1r. Nat Cell Biol 14: 659

Kessler SM, Laggai S, Barghash A, Schultheiss CS, Lederer E, Artl M, Helms V, Haybaeck J, Kiemer AK (2015) IMP2/p62 induces genomic instability and an aggressive hepatocellular carcinoma phenotype. Cell Death Dis 6: e1894

Kessler SM, Lederer E, Laggai S, Golob-Schwarzl N, Hosseini K, Petzold J, Schweiger C, Reihs R, Keil M, Hoffmann J, Mayr C, Kiesslich T, Pichler M, Kim KS, Rhee H, Park YN, Lax S, Obrist P, Kiemer AK, Haybaeck J (2017) IMP2/IGF2BP2 expression, but not IMP1 and IMP3, predicts poor outcome in patients and high tumor growth rate in xenograft models of gallbladder cancer. Oncotarget 8: 89736-89745

Kessler SM, Pokorny J, Zimmer V, Laggai S, Lammert F, Bohle RM, Kiemer AK (2013) IGF2 mRNA binding protein p62/IMP2-2 in hepatocellular carcinoma: antiapoptotic action is independent of IGF2/PI3K signaling. Am J Physiol Gastrointest Liver Physiol 304: G328-36

Kessler SM, Simon Y, Gemperlein K, Gianmoena K, Cadenas C, Zimmer V, Pokorny J, Barghash A, Helms V, van Rooijen N, Bohle RM, Lammert F, Hengstler JG, Mueller R, Haybaeck J, Kiemer AK (2014) Fatty acid elongation in non-alcoholic steatohepatitis and hepatocellular carcinoma. Int J Mol Sci 15: 5762-73

Kim KS, Lee YI (1997) Biallelic expression of the H19 and IGF2 genes in hepatocellular carcinoma. Cancer Lett 119: 143-8

Kim VN, Han J, Siomi MC (2009) Biogenesis of small RNAs in animals. Nat Rev Mol Cell Biol 10: 126-39

Kim YI, Giuliano A, Hatch KD, Schneider A, Nour MA, Dallal GE, Selhub J, Mason JB (1994) Global DNA hypomethylation increases progressively in cervical dysplasia and carcinoma. Cancer 74: 893-9

Kohno T, Tsuge M, Murakami E, Hiraga N, Abe H, Miki D, Imamura M, Ochi H, Hayes CN, Chayama K (2014) Human microRNA hsa-miR-1231 suppresses hepatitis B virus replication by targeting core mRNA. J Viral Hepat 21: e89-97

Kong LM, Liao CG, Chen L, Yang HS, Zhang SH, Zhang Z, Bian HJ, Xing JL, Chen ZN (2011) Promoter hypomethylation up-regulates CD147 expression through increasing Sp1

binding and associates with poor prognosis in human hepatocellular carcinoma. J Cell Mol Med 15: 1415-28

Koyama Y, Brenner DA (2017) Liver inflammation and fibrosis. J Clin Invest 127: 55-64

Laggai S (2014) Hepatic steatosis and cancer development: Role of insulin-like growth factor2 mRNA binding protein p62/IGF2BP2-2/IMP2-2 and fatty acid elongase ELOVL6. PhD Thesis Department of Pharmacy, Pharmaceutical Biology, Saarland University

Laggai S, Kessler SM, Boettcher S, Lebrun V, Gemperlein K, Lederer E, Leclercq IA, Mueller R, Hartmann RW, Haybaeck J, Kiemer AK (2014) The IGF2 mRNA binding protein p62/IGF2BP2-2 induces fatty acid elongation as a critical feature of steatosis. J Lipid Res 55: 1087-97

Lau WY, Lai EC (2008) Hepatocellular carcinoma: current management and recent advances. Hepatobiliary Pancreat Dis Int 7: 237-57

Lee TK, Poon RT, Yuen AP, Man K, Yang ZF, Guan XY, Fan ST (2006) Rac activation is associated with hepatocellular carcinoma metastasis by up-regulation of vascular endothelial growth factor expression. Clin Cancer Res 12: 5082-9

Leighton PA, Ingram RS, Eggenschwiler J, Efstratiadis A, Tilghman SM (1995) Disruption of imprinting caused by deletion of the H19 gene region in mice. Nature 375: 34-9

Lencioni R, Llovet JM, Han G, Tak WY, Yang J, Guglielmi A, Paik SW, Reig M, Kim DY, Chau GY, Luca A, Del Arbol LR, Leberre MA, Niu W, Nicholson K, Meinhardt G, Bruix J (2016) Sorafenib or placebo plus TACE with doxorubicin-eluting beads for intermediate stage HCC: The SPACE trial. J Hepatol 64: 1090-1098

Li B, Dewey CN (2011) RSEM: accurate transcript quantification from RNA-Seq data with or without a reference genome. BMC Bioinformatics 12: 323)

Li X, Wang H, Yao B, Xu W, Chen J, Zhou X (2016) lncRNA H19/miR-675 axis regulates cardiomyocyte apoptosis by targeting VDAC1 in diabetic cardiomyopathy. Sci Rep 6: 36340

Liang WC, Fu WM, Wong CW, Wang Y, Wang WM, Hu GX, Zhang L, Xiao LJ, Wan DC, Zhang JF, Waye MM (2015) The lncRNA H19 promotes epithelial to mesenchymal transition by functioning as miRNA sponges in colorectal cancer. Oncotarget 6: 22513-25

Liao B, Hu Y, Herrick DJ, Brewer G (2005) The RNA-binding protein IMP-3 is a translational activator of insulin-like growth factor II leader-3 mRNA during proliferation of human K562 leukemia cells. J Biol Chem 280: 18517-24

Lim SO, Gu JM, Kim MS, Kim HS, Park YN, Park CK, Cho JW, Park YM, Jung G (2008) Epigenetic changes induced by reactive oxygen species in hepatocellular carcinoma: methylation of the E-cadherin promoter. Gastroenterology 135: 2128-40, 2140 e1-8

Lin CH, Hsieh SY, Sheen IS, Lee WC, Chen TC, Shyu WC, Liaw YF (2001) Genome-wide hypomethylation in hepatocellular carcinogenesis. Cancer Res 61: 4238-43

List M, Amirabad AD, Laggai S, Kessler SM, Schultheiss CS, Kostka D, Kiemer AK, Schulz MH (2017) Genome-wide competing endogenous RNA networks highlight biomarkers in cancer. Conference Proceedings: Intelligent Systems for Molecular Biology (ISMB 2017)

Liu L, Cao Y, Chen C, Zhang X, McNabola A, Wilkie D, Wilhelm S, Lynch M, Carter C (2006) Sorafenib blocks the RAF/MEK/ERK pathway, inhibits tumor angiogenesis, and induces tumor cell apoptosis in hepatocellular carcinoma model PLC/PRF/5. Cancer Res 66: 11851-8

Liu W, Li Z, Xu W, Wang Q, Yang S (2013) Humoral autoimmune response to IGF2 mRNA-binding protein (IMP2/p62) and its tissue-specific expression in colon cancer. Scand J Immunol 77: 255-60

Llovet JM, Bru C, Bruix J (1999) Prognosis of hepatocellular carcinoma: the BCLC staging classification. Semin Liver Dis 19: 329-38

Llovet JM, Zucman-Rossi J, Pikarsky E, Sangro B, Schwartz M, Sherman M, Gores G (2016) Hepatocellular carcinoma. Nat Rev Dis Primers 2: 16018

Lu M, Nakamura RM, Dent ED, Zhang JY, Nielsen FC, Christiansen J, Chan EK, Tan EM (2001) Aberrant expression of fetal RNA-binding protein p62 in liver cancer and liver cirrhosis. Am J Pathol 159: 945-53

Lu TX, Sherrill JD, Wen T, Plassard AJ, Besse JA, Abonia JP, Franciosi JP, Putnam PE, Eby M, Martin LJ, Aronow BJ, Rothenberg ME (2012) MicroRNA signature in patients with eosinophilic esophagitis, reversibility with glucocorticoids, and assessment as disease biomarkers. J Allergy Clin Immunol 129: 1064-75 e9

Lu ZL, Luo DZ, Wen JM (2005) Expression and significance of tumor-related genes in HCC. World J Gastroenterol 11: 3850-4

Luo M, Li Z, Wang W, Zeng Y, Liu Z, Qiu J (2013) Long non-coding RNA H19 increases bladder cancer metastasis by associating with EZH2 and inhibiting E-cadherin expression. Cancer Lett 333: 213-21

Martinet C, Monnier P, Louault Y, Benard M, Gabory A, Dandolo L (2016) H19 controls reactivation of the imprinted gene network during muscle regeneration. Development 143: 962-71

Matouk I, Raveh E, Ohana P, Lail RA, Gershtain E, Gilon M, De Groot N, Czerniak A, Hochberg A (2013) The increasing complexity of the oncofetal H19 gene locus: functional dissection and therapeutic intervention. Int J Mol Sci 14: 4298-316

Matouk IJ, DeGroot N, Mezan S, Ayesh S, Abu-lail R, Hochberg A, Galun E (2007) The H19 non-coding RNA is essential for human tumor growth. PLoS One 2: e845

Miki Y, Swensen J, Shattuck-Eidens D, Futreal PA, Harshman K, Tavtigian S, Liu Q, Cochran C, Bennett LM, Ding W, et al. (1994) A strong candidate for the breast and ovarian cancer susceptibility gene BRCA1. Science 266: 66-71

Monnier P, Martinet C, Pontis J, Stancheva I, Ait-Si-Ali S, Dandolo L (2014) H19 lncRNA controls gene expression of the Imprinted Gene Network by recruiting MBD1. Proc Natl Acad Sci U S A 110: 20693-8

Moore T, Haig D (1991) Genomic imprinting in mammalian development: a parental tug-of-war. Trends Genet 7: 45-9

Nakatani T, Roy G, Fujimoto N, Asahara T, Ito A (2001) Sex hormone dependency of diethylnitrosamine-induced liver tumors in mice and chemoprevention by leuprorelin. Jpn J Cancer Res 92: 249-56

Naugler WE, Sakurai T, Kim S, Maeda S, Kim K, Elsharkawy AM, Karin M (2007) Gender disparity in liver cancer due to sex differences in MyD88-dependent IL-6 production. Science 317: 121-4

Newman R, McHugh J, Turner M (2015) RNA binding proteins as regulators of immune cell biology. Clin Exp Immunol 183: 37-49

Nielsen FC (1992) The molecular and cellular biology of insulin-like growth factor II. Prog Growth Factor Res 4: 257-90

Nielsen J, Christiansen J, Lykke-Andersen J, Johnsen AH, Wewer UM, Nielsen FC (1999) A family of insulin-like growth factor II mRNA-binding proteins represses translation in late development. Mol Cell Biol 19: 1262-70

Niyazi M, Niyazi I, Belka C (2007) Counting colonies of clonogenic assays by using densitometric software. Radiat Oncol 2: 4

Ohtsuka M, Ling H, Ivan C, Pichler M, Matsushita D, Goblirsch M, Stiegelbauer V, Shigeyasu K, Zhang X, Chen M, Vidhu F, Bartholomeusz GA, Toiyama Y, Kusunoki M, Doki Y, Mori M, Song S, Gunther JR, Krishnan S, Slaby O et al. (2016) H19 Noncoding RNA, an Independent Prognostic Factor, Regulates Essential Rb-E2F and CDK8-beta-Catenin Signaling in Colorectal Cancer. EBioMedicine 13: 113-124

Okada H, Kimura MT, Tan D, Fujiwara K, Igarashi J, Makuuchi M, Hui AM, Tsurumaru M, Nagase H (2005) Frequent trefoil factor 3 (TFF3) overexpression and promoter hypomethylation in mouse and human hepatocellular carcinomas. Int J Oncol 26: 369-77

Okamura K, Lai EC (2008) Endogenous small interfering RNAs in animals. Nat Rev Mol Cell Biol 9: 673-8

Onyango P, Feinberg AP (2011) A nucleolar protein, H19 opposite tumor suppressor (HOTS), is a tumor growth inhibitor encoded by a human imprinted H19 antisense transcript. Proc Natl Acad Sci U S A 108: 16759-64

Ozakyol A (2017) Global Epidemiology of Hepatocellular Carcinoma (HCC Epidemiology). J Gastrointest Cancer

Pachnis V, Belayew A, Tilghman SM (1984) Locus unlinked to alpha-fetoprotein under the control of the murine raf and Rif genes. Proc Natl Acad Sci U S A 81: 5523-7

Park EJ, Lee JH, Yu GY, He G, Ali SR, Holzer RG, Osterreicher CH, Takahashi H, Karin M (2010) Dietary and genetic obesity promote liver inflammation and tumorigenesis by enhancing IL-6 and TNF expression. Cell 140: 197-208

Park JG, Lee SK, Hong IG, Kim HS, Lim KH, Choe KJ, Kim WH, Kim YI, Tsuruo T, Gottesman MM (1994) MDR1 gene expression: its effect on drug resistance to doxorubicin in human hepatocellular carcinoma cell lines. J Natl Cancer Inst 86: 700-5

Park YN (2011) Update on precursor and early lesions of hepatocellular carcinomas. Arch Pathol Lab Med 135: 704-15

Peculis BA (2000) RNA-binding proteins: if it looks like a sn(o)RNA. Curr Biol 10: R916-8

Petta S, Craxi A (2010) Hepatocellular carcinoma and non-alcoholic fatty liver disease: from a clinical to a molecular association. Curr Pharm Des 16: 741-52

Poliseno L, Salmena L, Zhang J, Carver B, Haveman WJ, Pandolfi PP (2010) A coding-independent function of gene and pseudogene mRNAs regulates tumour biology. Nature 465: 1033-8

Qian HL, Peng XX, Chen SH, Ye HM, Qiu JH (2005) p62 Expression in primary carcinomas of the digestive system. World J Gastroenterol 11: 1788-92

Rachmilewitz J, Goshen R, Ariel I, Schneider T, de Groot N, Hochberg A (1992) Parental imprinting of the human H19 gene. FEBS Lett 309: 25-8

Ransohoff JD, Wei Y, Khavari PA (2018) The functions and unique features of long intergenic non-coding RNA. Nat Rev Mol Cell Biol 19: 143-157

Raveh E, Matouk IJ, Gilon M, Hochberg A (2015) The H19 Long non-coding RNA in cancer initiation, progression and metastasis - a proposed unifying theory. Mol Cancer 14: 184)

Raymond E, Roskams T, Bruix J, Colombo M, Zhu A (2012) EASL-EORTC clinical practice guidelines: management of hepatocellular carcinoma. J Hepatol 56: 908-43

Resnicoff M, Abraham D, Yutanawiboonchai W, Rotman HL, Kajstura J, Rubin R, Zoltick P, Baserga R (1995) The insulin-like growth factor I receptor protects tumor cells from apoptosis in vivo. Cancer Res 55: 2463-9

Rinn JL, Chang HY (2012) Genome regulation by long noncoding RNAs. Annu Rev Biochem 81: 145-66

Ripoche MA, Kress C, Poirier F, Dandolo L (1997) Deletion of the H19 transcription unit reveals the existence of a putative imprinting control element. Genes Dev 11: 1596-604

Runge S, Nielsen FC, Nielsen J, Lykke-Andersen J, Wewer UM, Christiansen J (2000) H19 RNA binds four molecules of insulin-like growth factor II mRNA-binding protein. J Biol Chem 275: 29562-9

Schmitt AM, Chang HY (2016) Long Noncoding RNAs in Cancer Pathways. Cancer Cell 29: 452-463

Shen L, Fang J, Qiu D, Zhang T, Yang J, Chen S, Xiao S (1998) Correlation between DNA methylation and pathological changes in human hepatocellular carcinoma. Hepatogastroenterology 45: 1753-9

Sia D, Villanueva A, Friedman SL, Llovet JM (2017) Liver Cancer Cell of Origin, Molecular Class, and Effects on Patient Prognosis. Gastroenterology 152: 745-761

Simon Y, Kessler SM, Bohle RM, Haybaeck J, Kiemer AK (2014a) The insulin-like growth factor 2 (IGF2) mRNA-binding protein p62/IGF2BP2-2 as a promoter of NAFLD and HCC? Gut 63: 861-3

Simon Y, Kessler SM, Gemperlein K, Bohle RM, Muller R, Haybaeck J, Kiemer AK (2014b) Elevated free cholesterol in a p62 overexpression model of non-alcoholic steatohepatitis. World J Gastroenterol 20: 17839-50

Siomi MC, Sato K, Pezic D, Aravin AA (2011) PIWI-interacting small RNAs: the vanguard of genome defence. Nat Rev Mol Cell Biol 12: 246-58

Sohda T, Iwata K, Soejima H, Kamimura S, Shijo H, Yun K (1998) In situ detection of insulin-like growth factor II (IGF2) and H19 gene expression in hepatocellular carcinoma. J Hum Genet 43: 49-53

Stewart BW, Wild CP (2014) World cancer report 2014. International Agency for Research on Cancer

Takeda S, Kondo M, Kumada T, Koshikawa T, Ueda R, Nishio M, Osada H, Suzuki H, Nagatake M, Washimi O, Takagi K, Takahashi T, Nakao A, Takahashi T (1996) Allelic-expression imbalance of the insulin-like growth factor 2 gene in hepatocellular carcinoma and underlying disease. Oncogene 12: 1589-92

Tilghman SM, Bartolomei MS, Webber AL, Brunkow ME, Saam J, Leighton PA, Pfeifer K, Zemel S (1993) Parental imprinting of the H19 and Igf2 genes in the mouse. Cold Spring Harb Symp Quant Biol 58: 287-295

Tripathi K, Hussein UK, Anupalli R, Barnett R, Bachaboina L, Scalici J, Rocconi RP, Owen LB, Piazza GA, Palle K (2015) Allyl isothiocyanate induces replication-associated DNA damage response in NSCLC cells and sensitizes to ionizing radiation. Oncotarget 6: 5237-52

Tsai MC, Spitale RC, Chang HY (2011) Long intergenic noncoding RNAs: new links in cancer progression. Cancer Res 71: 3-7

Tsang WP, Kwok TT (2007) Riboregulator H19 induction of MDR1-associated drug resistance in human hepatocellular carcinoma cells. Oncogene 26: 4877-81

Tsang WP, Ng EK, Ng SS, Jin H, Yu J, Sung JJ, Kwok TT (2010) Oncofetal H19-derived miR-675 regulates tumor suppressor RB in human colorectal cancer. Carcinogenesis 31: 350-8

Tybl E, Shi FD, Kessler SM, Tierling S, Walter J, Bohle RM, Wieland S, Zhang J, Tan EM, Kiemer AK (2011) Overexpression of the IGF2-mRNA binding protein p62 in transgenic mice induces a steatotic phenotype. J Hepatol 54: 994-1001

Vandesompele J, De Preter K, Pattyn F, Poppe B, Van Roy N, De Paepe A, Speleman F (2002) Accurate normalization of real-time quantitative RT-PCR data by geometric averaging of multiple internal control genes. Genome Biol 3: RESEARCH0034

Varrault A, Gueydan C, Delalbre A, Bellmann A, Houssami S, Aknin C, Severac D, Chotard L, Kahli M, Le Digarcher A, Pavlidis P, Journot L (2006) Zac1 regulates an imprinted gene network critically involved in the control of embryonic growth. Dev Cell 11: 711-22

Vazquez-Chantada M, Fernandez-Ramos D, Embade N, Martinez-Lopez N, Varela-Rey M, Woodhoo A, Luka Z, Wagner C, Anglim PP, Finnell RH, Caballeria J, Laird-Offringa IA, Gorospe M, Lu SC, Mato JM, Martinez-Chantar ML (2010) HuR/methyl-HuR and AUF1 regulate the MAT expressed during liver proliferation, differentiation, and carcinogenesis. Gastroenterology 138: 1943-53

Vennin C, Spruyt N, Dahmani F, Julien S, Bertucci F, Finetti P, Chassat T, Bourette RP, Le Bourhis X, Adriaenssens E (2015) H19 non coding RNA-derived miR-675 enhances tumorigenesis and metastasis of breast cancer cells by downregulating c-Cbl and Cbl-b. Oncotarget 6: 29209-23

Vrijens K, Bollati V, Nawrot TS (2015) MicroRNAs as potential signatures of environmental exposure or effect: a systematic review. Environ Health Perspect 123: 399-411

Wagner JR, Busche S, Ge B, Kwan T, Pastinen T, Blanchette M (2014) The relationship between DNA methylation, genetic and expression inter-individual variation in untransformed human fibroblasts. Genome Biol 15: R37

Wang H, Ding N, Guo J, Xia J, Ruan Y (2016a) Dysregulation of TTP and HuR plays an important role in cancers. Tumour Biol 37: 14451-14461

Wang SH, Wu XC, Zhang MD, Weng MZ, Zhou D, Quan ZW (2016b) Long noncoding RNA H19 contributes to gallbladder cancer cell proliferation by modulated miR-194-5p targeting AKT2. Tumour Biol 37: 9721-30

Wang WT, Ye H, Wei PP, Han BW, He B, Chen ZH, Chen YQ (2016c) LncRNAs H19 and HULC, activated by oxidative stress, promote cell migration and invasion in cholangiocarcinoma through a ceRNA manner. J Hematol Oncol 9: 117

Wang Y, Zhao L, Smas C, Sul HS (2010) Pref-1 interacts with fibronectin to inhibit adipocyte differentiation. Mol Cell Biol 30: 3480-92

Wapinski O, Chang HY (2011) Long noncoding RNAs and human disease. Trends Cell Biol 21: 354-61

Watanuki A, Ohwada S, Fukusato T, Makita F, Yamada T, Kikuchi A, Morishita Y (2002) Prognostic significance of DNA topoisomerase IIalpha expression in human hepatocellular carcinoma. Anticancer Res 22: 1113-9

Wilhelm SM, Carter C, Tang L, Wilkie D, McNabola A, Rong H, Chen C, Zhang X, Vincent P, McHugh M, Cao Y, Shujath J, Gawlak S, Eveleigh D, Rowley B, Liu L, Adnane L, Lynch M, Auclair D, Taylor I et al. (2004) BAY 43-9006 exhibits broad spectrum oral antitumor activity and targets the RAF/MEK/ERK pathway and receptor tyrosine kinases involved in tumor progression and angiogenesis. Cancer Res 64: 7099-109

World-Health-Organization (2008) The Global Burden of Disease: 2004 Update. Geneva: World Health Organization; 2008

Wörns MA, Weinmann A, Schuchmann M, Galle PR (2009) Systemic therapies in hepatocellular carcinoma. Dig Dis 27: 175-88

Wu J, Qin Y, Li B, He WZ, Sun ZL (2008) Hypomethylated and hypermethylated profiles of H19DMR are associated with the aberrant imprinting of IGF2 and H19 in human hepatocellular carcinoma. Genomics 91: 443-50

Xiao S, Scott F, Fierke CA, Engelke DR (2002) Eukaryotic ribonuclease P: a plurality of ribonucleoprotein enzymes. Annu Rev Biochem 71: 165-89

Yan J, Caviglia JM, Schwabe RF (2018) Animal models of HCC - When injury meets mutation. J Hepatol: 193–194

Yan J, Zhang Y, She Q, Li X, Peng L, Wang X, Liu S, Shen X, Zhang W, Dong Y, Lu J, Zhang G (2017) Long Noncoding RNA H19/miR-675 Axis Promotes Gastric Cancer via FADD/Caspase 8/Caspase 3 Signaling Pathway. Cell Physiol Biochem 42: 2364-2376

Yang B, Liu Y, Zhao J, Hei K, Zhuang H, Li Q, Wei W, Chen R, Zhang N, Li Y (2017) Ectopic overexpression of filamin C scaffolds MEK1/2 and ERK1/2 to promote the progression of human hepatocellular carcinoma. Cancer Lett 388: 167-176

Yang F, Bi J, Xue X, Zheng L, Zhi K, Hua J, Fang G (2012) Up-regulated long non-coding RNA H19 contributes to proliferation of gastric cancer cells. Febs J 279: 3159-65

Yoshimizu T, Miroglio A, Ripoche MA, Gabory A, Vernucci M, Riccio A, Colnot S, Godard C, Terris B, Jammes H, Dandolo L (2008) The H19 locus acts in vivo as a tumor suppressor. Proc Natl Acad Sci U S A 105: 12417-22

Yu LL, Chang K, Lu LS, Zhao D, Han J, Zheng YR, Yan YH, Yi P, Guo JX, Zhou YG, Chen M, Li L (2013) Lentivirus-mediated RNA interference targeting the H19 gene inhibits cell proliferation and apoptosis in human choriocarcinoma cell line JAR. BMC Cell Biol 14: 26

Yu YQ, Weng J, Li SQ, Li B, Lv J (2016) MiR-675 Promotes the Growth of Hepatocellular Carcinoma Cells Through the Cdc25A Pathway. Asian Pac J Cancer Prev 17: 3881-5

Zeisel MB, Baumert TF (2016) Translation and protein expression of lncRNAs: Impact for liver disease and hepatocellular carcinoma. Hepatology 64: 671-4

Zhang JY, Chan EK, Peng XX, Tan EM (1999) A novel cytoplasmic protein with RNA-binding motifs is an autoantigen in human hepatocellular carcinoma. J Exp Med 189: 1101-10

Zhang L, Yang F, Yuan JH, Yuan SX, Zhou WP, Huo XS, Xu D, Bi HS, Wang F, Sun SH (2013) Epigenetic activation of the MiR-200 family contributes to H19-mediated metastasis suppression in hepatocellular carcinoma. Carcinogenesis 34: 577-86

Zhang LF, Lou JT, Lu MH, Gao C, Zhao S, Li B, Liang S, Li Y, Li D, Liu MF (2015) Suppression of miR-199a maturation by HuR is crucial for hypoxia-induced glycolytic switch in hepatocellular carcinoma. EMBO J 34: 2671-85

Zhang Y, Tycko B (1992) Monoallelic expression of the human H19 gene. Nat Genet 1: 40-4

Zhou J, Yang L, Zhong T, Mueller M, Men Y, Zhang N, Xie J, Giang K, Chung H, Sun X, Lu L, Carmichael GG, Taylor HS, Huang Y (2015a) H19 lncRNA alters DNA methylation genome wide by regulating S-adenosylhomocysteine hydrolase. Nat Commun 6: 10221

Zhou W, Ye XL, Xu J, Cao MG, Fang ZY, Li LY, Guan GH, Liu Q, Qian YH, Xie D (2017) The lncRNA H19 mediates breast cancer cell plasticity during EMT and MET plasticity by differentially sponging miR-200b/c and let-7b. Sci Signal 10

Zhou X, Ye F, Yin C, Zhuang Y, Yue G, Zhang G (2015b) The Interaction Between MiR-141 and lncRNA-H19 in Regulating Cell Proliferation and Migration in Gastric Cancer. Cell Physiol Biochem 36: 1440-52

Zhu H, Berkova Z, Mathur R, Sehgal L, Khashab T, Tao RH, Ao X, Feng L, Sabichi AL, Blechacz B, Rashid A, Samaniego F (2015) HuR Suppresses Fas Expression and Correlates with Patient Outcome in Liver Cancer. Mol Cancer Res 13: 809-18

Zhu M, Chen Q, Liu X, Sun Q, Zhao X, Deng R, Wang Y, Huang J, Xu M, Yan J, Yu J (2014) lncRNA H19/miR-675 axis represses prostate cancer metastasis by targeting TGFBI. Febs J 281: 3766-75

Abbreviations

°C	degree Celsius
3‘-UTR	3‘-untranslated region
ABCB1	ATP binding cassette subfamily B member 1
ACTB	actin beta
AFLD	alcoholic fatty liver disease
AFP	alpha-fetoprotein
ANOVA	analysis of variance
ARE	AU-rich elements
AT	annealing temperature
atto	10^{-18}
b	bases
BCL2	B-cell CLL/lymphoma 2
BCLC	Barcelona Clinic Liver Cancer
bp	base pair
BRCA1	breast cancer 1
C57BL/6J	C57 black 6 J
CALN1	calneuron 1
CCNB1	cyclin B1
CDC6	cell division cycle 6
CDH-11	cadherin 11
CDH-13	cadherin 13
cDNA	complementary DNA
ceRNA	competing endogenous RNAs
CISH	chromogenic *in situ* hybridization
cm^2	square centimetre
CSNK2A2	casein kinase 2 alpha 2
CTSV	cathepsin V
Da	Dalton
DCDHF	dichlorodihydrofluorescein diacetate

ddCTP	dideoxycytidine triphosphate
ddTTP	dideoxythymidine triphosphate
DEN	diethylnitrosamine
DLK1	delta-like 1 homolog
DMSO	dimethyl sulfoxide
DNA	deoxyribonucleic acid
DNase	deoxyribonuclease
DNMT3B	DNA methyltransferase 3 beta
dNTP	deoxyribonucleoside triphosphate
DSMZ	Deutsche Sammlung von Mikroorganismen und Zellkulturen
GmbH	Gesellschaft mit beschränkter Haftung
DTT	dithiothreitol
E2F8	E2F transcription factor 8
EDTA	ethylenediaminetetraacetic acid
ELAVL1	ELAV-like RNA-binding protein 1
EMT	epithelial to mesenchymal transition
ExoSAP	exonuclease shrimp alkaline phosphatase
FACS	fluorescence-activated cell sorting
FADD	anti-apoptotic Fas-associated via death domain
FCB	flow cytometry buffer
FCS	fetal calf serum
g	gram
g	gravitational force
GAPDH	glyceraldehyde-3-phosphate dehydrogenase
gDNA	genomic DNA
GDP	guanosine diphosphate
GEO	gene expression omnibus
Gp73	Golgi membrane protein 73
GS	glutamine synthetase
GST	glutathione S-tranferase
GTP	guanosine triphosphate
h	hour

H&E	haematoxylin-eosin
H2AFY2	H2A histone family member Y2
HBV	hepatitis B virus
HCC	hepatocellular carcinoma
HCV	hepatitis C virus
HOTS	*H19* opposite tumor suppressor
HPLC	high performance liquid chromatography
hu	human
IGF	insulin-like growth factor
IGF1R	IGF1 receptor
IGF2BP1	*IGF2* mRNA-binding protein 1
IGF2R	IGF2 receptor
IKBKAP	inhibitor of kappa light polypeptide gene
IMP	*IGF2* mRNA-binding proteins
IP	immunoprecipitation
IP/RP-HPLC	ion pair reversed phase HPLC
k	kilo
KDELC1	KDEL motif containing 1
ko	knockout
KSRP	K homology-type splicing regulatory protein
l	litre
LAP	liver-enriched activator protein
LCC	large cell changes
LNA	locked nucleic acid
lncRNA	long non-coding RNA
LOI	loss of imprinting
m	metre or milli (10^{-3})
M	molar
MBD1	methyl-CpG-binding protein domain 1
MDR1	multi-drug resistance protein 1
$MgCl_2$	magnesium chloride
min	minute

miRNA	microRNA
MITF	melanogenesis-associated transcription factor
MPI-I	Max Planck Institut for Informatics
mRNA	messenger ribonucleic acid
MTT	thiazolyl blue tetrazolium bromide
mu	murine
MYBL2	MYB proto-oncogene like 2
n	nano (10^{-9}) or size of a statistical sample or number of experiments
NaCl	sodium chloride
NAFLD	non-alcoholic fatty liver disease
NaN_3	sodium azide
NASH	non-alcoholic steatohepatitis
ncRNA	non-coding RNA
Neo (R)	neomycin resistance gene
NINL	ninein like
NOMO 1	nodal modulator 1
ORF	open reading frame
p	probability (value)
PAGE	polyacrylamide gel electrophoresis
PBD	p21 binding domain
PBS	phosphate buffered saline
PCR	polymerase chain reaction
piRNA	Piwi-associated RNA
PKD	digestion buffer
PMSF	phenylmethylsulfonyl fluoride
qPCR	real-time quantitative polymerase chain reaction
RAC1	ras-related C3 botulinum toxin substrate 1
RB	retinoblastoma
RBB	Rockland Blocking Buffer
RBP	mRNA-binding protein
Ref. No.	reference number
RFLP	restriction fragment length polymorphism

RIPA	radioimmune precipitation assay
RNA	ribonucleic acid
RNA18S5	18S ribosomal 5
RNAse	ribonuclease
RNU6B	RNA U6 small nuclear 6 pseudogene
ROS	reactive oxygen species
RPMI	Roswell Park Memorial Institute
rRNA	ribosomal RNA
RSEM	RNA-Seq by Expectation Maximization
RUNX1	runt related transcription factor 1
SCC	small cell changes
SDS	sodium dodecyl sulfate
sec	second
SEM	standard error of mean
seq	sequencing
siRNA	small interfering RNA
SLC15A1	solute carrier family 15 member 1
SMAD1	SMAD family member 1
SMAD5	SMAD family member 5
SMYD3	SET and MYND domain containing 3
snoRNA	small nucleolar RNA
snRNA	small nuclear RNA
SNuPE	single nucleotide primer extension
SOAT2	sterol O-acyltransferase 2
SPONGE	sparse partial correlation on gene expression
SV40	simian virus 40
TA	transactivator
TBARS	thiobarbituric acid reactive substances
TCGA	The Cancer Genome Atlas
tg	transgene
TGFBI	transforming growth factor beta induced protein
TRE-CMV	transrepressive responsive element cytomegaly virus

tRNA	transfer RNA
tTA	tetracycline transactivator
v/v	volume per volume
VDR	vitamin D receptor
w/v	weight per volume
WASF1	WAS protein family member 1
wt	wild-type
µ	micro (10^{-6})

Publications

Original publications

Kessler S. M., Laggai S., Barghash A., **Schultheiss C. S.**, Lederer E., Artl M., Helms V., Haybaeck J., and Kiemer A. K. (2015) IMP2/p62 induces genomic instability and an aggressive hepatocellular carcinoma phenotype. *Cell Death and Disease,* 6, e1894.

Schultheiss C.S., Laggai S., Czepukojc B., Hussein U. K., List M., Barghash A., Tierling S., Hosseini K., Golob-Schwarzl N., Pokorny J., Hachenthal N., Schulz M., Helms V., Walter J., Zimmer V., Lammert F., Bohle R. M., Dandolo L., Haybaeck J., Kiemer A. K., and Kessler S. M. (2017) The long non-coding RNA *H19* suppresses carcinogenesis and chemoresistance in hepatocellular carcinoma. *Cell Stress*. 1, 37-54.

Kessler S. M., Hosseini K., Hussein U. K., Kim K. M., List M., **Schultheiss C.S.**, Schulz M. H., Laggai S., Jang K. Y., and Kiemer A. K. (2018) Hepatocellular carcinoma and nuclear paraspeckles: induction in chemoresistance and prediction for poor survival. *submitted*.

Abstracts and poster presentations

Schultheiss C. S., Tierling S., Walter J., Kiemer A. K., and Kessler S. M. (2012) Expression of the non-coding RNA *H19* is suppressed by DNA methylation in human hepatocellular carcinoma. Conference Proceedings: Liver Cancer - from molecular pathogenesis to targeted therapies, Heidelberg, Germany.

Schultheiss C. S., Kessler S. M., Hussein U. K., Golob-Schwarzl N., Zimmer V., Pokorny J., Bohle R. M., Lammert F., Dandolo L., Haybaeck J., Kiemer A. K. (2016) The role of long non-coding RNA *H19* in hepatocarcinogenesis and chemoresistance of hepatocellular carcinoma. Poster presentation at the annual meeting of the German Pharmaceutical Society (DPhG), Aachen, Germany.

List M., Amirabad A. D., Laggai S., Kessler S. M., **Schultheiss C. S.**, Kostka D., Kiemer A. K., and Schulz M. H. (2017). Genome-wide competing endogenous RNA networks highlight biomarkers in cancer. Conference Proceedings: Intelligent Systems for Molecular Biology (ISMB).

Hosseini K., Kessler S. M., **Schultheiss C. S.**, List M., Schulz M. H., Kiemer A. K., and Laggai S. (2017) Paraspeckle formation and induction of lncRNA *NEAT1* in hepatocellular carcinoma chemoresistance. Poster presentation at the annual meeting of the German Pharmaceutical Society (DPhG), Saarbrücken, Germany.

Danksagung

An erster Stelle möchte ich mich bei **Prof. Dr. Alexandra K. Kiemer** für die Möglichkeit bedanken, sowohl meine Diplomarbeit als auch meine Doktorarbeit in ihrem Arbeitskreis anfertigen zu dürfen. Es hat mich sehr gefreut das interessante Thema meiner Diplomarbeit im Zuge der Promotion weiter verfolgen zu können. Danke für die Unterstützung, die Geduld und das entgegengebrachte Vertrauen, aber auch für die konstruktive Kritik und die vielen Besprechungen, die diese Arbeit entscheidend vorangebracht haben.

Prof. Dr. Claus-Michael Lehr danke ich dafür, dass er sowohl die Rolle des wissenschaftlichen Begleiters meiner Promotion als auch die Anfertigung des Zweitgutachtens meiner Arbeit übernommen hat.

Bei **Dr. Sonja M. Kessler** möchte ich mich für die Betreuung meiner Diplom- und Doktorarbeit bedanken. Sie hat mich mit dem Forschungsthema und der Laborarbeit vertraut gemacht und mir stets freundlich und mit viel fachlicher Kompetenz zur Seite gestanden. Sie sorgte mit ihrer positiven Art immer für ein angenehmes Arbeitsklima und strahlte auch in schwierigen Phasen Ruhe und Zuversicht aus. Danke auch an **Dr. Stephan Laggai** für die sehr gute Vertretung von Dr. Kessler während ihrer Schwangerschaft und Elternzeit.
Insgesamt kann ich sagen: Eine bessere Betreuung hätte ich mir nicht wünschen können!

Mein Dank geht weiterhin an **Prof. Dr. Dr. Johannes Haybäck**, der mir einen einmonatigen Aufenthalt an der medizinischen Universität in Graz ermöglicht und mit mir die histologischen Untersuchungen der murinen Lebern durchgeführt hat. Er und seine gesamte Arbeitsgruppe haben mich sehr herzlich aufgenommen und mir einen Einblick in ihre Forchungsprojekte gegeben. In diesem Sinne möchte ich mich auch bei Böhringer Ingelheim Fonds für die Finanzierung des Auslandsaufenthalts in Graz bedanken.

Aus der Arbeitsgruppe von **Prof. Dr. Jörn Walter** danke ich **Dr. Sascha Tierling** für die freundliche Zusammenarbeit und die Hilfe bei der Durchführung der epigenetischen Analysen. Danke auch an die Tierpflegerin **Eva Dilly** für die Unterstützung in der Mauszucht.

Dr. Marcel H. Schulz und **Dr. Markus List** danke ich für die bioinformatischen Analysen und die freundliche Kooperation im *H19*-Sponge Projekt.

Danke auch an alle (zum Teil ehemaligen) **Mitarbeiter der Arbeitsgruppe** von Frau Prof. Dr. Alexandra K. Kiemer für die kollegiale Zusammenarbeit und die schöne gemeinsame Zeit. Insbesondere bedanke ich mich für die experimentelle Unterstützung in der Zeit meiner Schwangerschaft. **Astrid Decker** danke ich für die freundliche Hilfe in allen bürokratischen Angelegenheiten. Ein herzlicher Dank geht an **Theo Ranßweiler** für das stets offene Ohr und die erfrischenden Gespräche in kleinen Kaffeepausen.

Ein ganz besonderer Dank geht an **Dr. Nina Hachenthal** - meine Arbeitskollegin, liebste Arbeitsplatznachbarin und sehr gute Freundin. Wir haben die Doktorandenzeit mit allen Höhen und Tiefen gemeinsam durchlebt und uns in schweren Zeiten gegenseitig Trost, aber auch neue Motivation gespendet. Nina ohne dich wäre die Zeit nur halb so schön gewesen!

Das Wichtigste kommt bekanntlich zum Schluss, deshalb möchte ich an dieser Stelle von ganzem Herzen meiner **Familie** danken! Meinen Eltern danke ich für die langjährige Unterstützung und Motivation. Ihr habt mich gelehrt immer positiv zu denken und niemals aufzugeben. Dadurch habt ihr meine berufliche Laufbahn maßgeblich beeinflusst. Ein herzliches Dankeschön geht auch an meinen Ehemann! Er ist der Ruhepol in meinem Leben und in vielerlei Hinsicht meine bessere Hälfte. Ich danke euch dafür, dass ihr die Betreuung meines Sohnes oft übernommen habt, sodass ich genug Zeit hatte um diese Arbeit zu schreiben.
Meinem Sohn danke ich für das strahlende Lächeln an jedem Morgen! Er hat mein Leben in einer Art und Weise bereichert, wie es nur ein Kind zu tun vermag und zeigt mir jeden Tag aufs Neue, wie sehr man sich auch über die kleinen Dinge im Leben freuen kann ☺!